Aus dem Zentrum für Innere Medizin der Universität zu Köln
Klinik und Poliklinik für Innere Medizin I
Direktor: Universitätsprofessor Dr. med. M. Hallek

Macrophages are activated toward phagocytic lymphoma cell clearance by pentose phosphate pathway inhibition

Inaugural-Dissertation zur Erlangung der Doktorwürde
der Medizinischen Fakultät
der Universität zu Köln

vorgelegt von
Anna Christina Beielstein
aus Wuppertal

promoviert am 30. Oktober 2025

Gedruckt mit Genehmigung der Medizinischen Fakultät der Universität zu Köln

2025

Dekan: Universitätsprofessor Dr. med. G. R. Fink

1. Gutachter: Universitätsprofessor Dr. med. C. Pallasch
2. Gutachter: Universitätsprofessor Dr. C. Frezza
3. Gutachter: Universitätsprofessor Dr. med. S. Theurich

Erklärung

Ich erkläre hiermit, dass ich die vorliegende Dissertationsschrift ohne unzulässige Hilfe Dritter und ohne Benutzung anderer als der angegebenen Hilfsmittel angefertigt habe; die aus fremden Quellen direkt oder indirekt übernommenen Gedanken sind als solche kenntlich gemacht.

Bei der Auswahl und Auswertung des Materials sowie bei der Herstellung des Manuskriptes habe ich Unterstützungsleistungen von folgenden Personen erhalten:

Herr Prof. C. Pallasch
Frau Dr. E. Izquierdo
Herr Dr. S. Blakemore
Frau Dr. N. Nickel
Herr M. Michalik
Frau S. Chawan
Frau R. Brinker
Herr H.-H. Bartel
Frau Dr. D. Vorholt
Herr L. Albert
Frau Dr. J. Nolte
Frau R. Linke
Frau Dr. C. R. Costa Picossi
Herr Dr. J. Sáiz
Herr Dr. F. Picard
Frau A. Florin
Herr Dr. J. Meinel
Herr Dr. P. Diefenhardt
Frau Dr. A. Villaseñor
Frau Prof. C. Barbas

Weitere Personen waren an der Erstellung der vorliegenden Arbeit nicht beteiligt. Insbesondere habe ich nicht die Hilfe einer Promotionsberaterin/eines Promotionsberaters in Anspruch genommen. Dritte haben von mir weder unmittelbar noch mittelbar geldwerte Leistungen für Arbeiten erhalten, die im Zusammenhang mit dem Inhalt der vorgelegten Dissertationsschrift stehen.

Die Dissertationsschrift wurde von mir bisher weder im Inland noch im Ausland in gleicher oder ähnlicher Form einer anderen Prüfungsbehörde vorgelegt.

Wenn im weiteren Verlauf nicht anders angegeben, erfolgte die Auswertung der Daten mittels Prism Software.
Das initiale Phagozytosescreening wurde nach entsprechender Anleitung durch Frau Dr. Nickel von mir selber durchgeführt und ausgewertet. Der Entwurf aller weiteren Phagozytose-Experimente wurde durch mich erstellt. Alle weiteren Phagozytoseassays mit Zelllinien wurden von mir durchgeführt und ausgewertet. Hierzu zählen die Versuche mit alternativen Inhibitoren, alternativen Zelllinien, alternativen Antikörpern und die in Hypoxie und ohne Antikörper durchgeführten Versuche sowie die Phagozytoseassays unter Supplementierung von Stoffwechselmetaboliten und Phagozytoseassays mit Enzym-knockdown Makrophagen.
Die Enzym-knockdown Makrophagen wurden nach entsprechender Anleitung durch Frau Brinker von mir hergestellt und auf ihre knockdown-Suffizienz hin analysiert.
Die Phagozytoseassays mit Makrophagen der Irg1-knockout Mauslinie wurden nach entsprechender Anleitung durch mich von Herrn Albert durchgeführt und ausgewertet. Die Gewinnung der Makrophagen und deren Differenzierung erfolgte ebenfalls durch Herrn Albert mit Unterstützung des medizinisch-technischen Assistenten Herrn Michalik. Die Irg1-knockout Mauslinie wurde von Herrn Dr. Diefenhardt und Herrn Dr. Brähler zur Verfügung gestellt.
Die Phagozytoseassays mit primär humanen Makrophagen wurden nach entsprechender Anleitung durch mich von Frau Chawan durchgeführt und ausgewertet. Die Gewinnung der Makrophagen und deren Differenzierung erfolgte ebenfalls durch Frau Chawan.
Die Phagozytoseassays mit primären CLL Patienten-Zellen und einer Makrophagenzelllinie wurden von mir durchgeführt und analysiert.
Die Phagozytoseassays mit primären CLL Patienten-Zellen und primären humanen Makrophagen wurden nach entsprechender Anleitung durch mich von Herrn Bartel durchgeführt und analysiert. Die Gewinnung der Makrophagen und deren Differenzierung erfolgte ebenfalls durch Herrn Bartel.
Die Phagozytoseassays mit murinen Makrophagen nach S3-Behandlung wurden nach entsprechender Anleitung durch mich und Herrn Michalik von Herrn Bartel durchgeführt und analysiert. Die Gewinnung der Makrophagen erfolgte durch Herrn Bartel, Herrn Prof. Pallasch,

den medizinisch-technischen Assistenten Herrn Michalik und mich. Die Differenzierung erfolgte nach entsprechender Anleitung durch mich durch Herrn Bartel.

Die Bestimmung der Oberflächenmarker der Makrophagenzelllinie J774A.1 wurde nach entsprechender Anleitung durch Frau Dr. Vorholt von mir durchgeführt und analysiert.
Die Bestimmung der Oberflächenmarker der murinen Makrophagen nach S3-Behandlung wurden nach entsprechender Anleitung durch mich von Herrn Bartel und mir durchgeführt. Die Analyse der Daten erfolgte durch mich. Die Gewinnung der Makrophagen erfolgte durch Herrn Bartel, Herrn Prof. Pallasch, den medizinisch-technischen Assistenten Herrn Michalik und mich.

Die Färbung und Immunfluoreszenzmikroskopie der Markophagenzelllinie J774A.1 erfolgte nach Anleitung durch Frau Dr. Izquierdo durch mich.

Die metabolische Analyse mittels Seahorse FX Analyse wurde nach entsprechender Anleitung durch Frau Dr. Vorholt und Frau Dr. Izquierdo von mir durchgeführt und analysiert.

Die Herstellung der Proben für die Proteom- und Phosphoproteomanalyse erfolgte nach entsprechender Anleitung durch Frau Dr. Nolte durch Frau Chawan und mich. Die Messung der Proben sowie initiale Analyse mittels MaxQuant Software und Perseus Software erfolgte durch Frau Dr. Nolte. Die Erstellung der Abbildung der kumulativen signifikanten Veränderungen in der Proteom- und Phosphoproteomanalyse erfolgte durch Herrn Dr. Blakemore mittels Bioconductor. Die Selektion der für die Arbeit relevanten Gene in den erstellten Volcano-Plots erfolgte durch mich. Die Gene-Enrichment-Analyse und Signalwegannotationen erfolgten durch mich. Die Berechnung und Darstellung der *Normalized Upstream Kinase Scores* erfolgten durch Herrn Dr. Blakemore. Die Berechnung der *Normalized Upstream Kinase Scores* erfolgte adaptiert auf Basis der Arbeit von Beekhof et al..[1] Die Erstellung der Western Blots zur Bestimmung der Ptk2b Expression erfolgten durch Frau Linke. Die Analyse der Western Blots erfolgte durch mich.

Die Bestimmung und Analyse der Glykogenmenge in J774A.1 Makrophagen erfolgte durch mich.
Die Erstellung der Western Blots zur Bestimmung der Expression von Ugp2, P2y14, Stat1, Irf1 und Irg1 erfolgten durch die medizinisch-technische Assistentin Frau Brinker. Die Analyse der Western Blots erfolgte durch mich.

Die Erstellung der J774A.1 Makrophagen Proben für die Analyse des Metaboloms erfolgte nach entsprechender Anleitung durch Frau Dr. Izquierdo durch Frau Chawan und die medizinisch-technische Assistentin Frau Brinker. Die Messung der Proben erfolgte durch Frau

Dr. Costa Picossi, Herrn Dr. Sáiz und Frau Dr. Villaseñor. Die Analyse der Daten erfolgte durch Frau Dr. Villaseñor auf Grundlage der Vorarbeit von Frau Dr. Villaseñor und Frau Prof. Barbas.[2]

Die Bestimmung und Auswertung der Zytokinexpression in J774A.1 Makrophagen erfolgte nach Anleitung durch Frau Dr. Izquierdo durch mich. Die Bestimmung und Auswertung der Zytokinexpression in primär humanen Makrophagen erfolgte nach entsprechender Anleitung durch mich durch Frau Chawan. Die Gewinnung der Makrophagen und deren Differenzierung erfolgte ebenfalls durch Frau Chawan.

Die Bestimmung des Überlebens von primären CLL Patienten Zellen und der Chemotoxizität von Bendamustin erfolgten nach entsprechender Anleitung durch mich durch mich und Frau Linke. Die Analyse der Daten erfolgte durch mich.

Die Konzeption der *in vivo* Versuche erfolgte durch mich. Die Behandlung von C57BL/6 Mäusen mit S3 und von NOD.Cg-Prkdcscid Il2rgtm1Wjl/SzJ (NSG) Mäusen mit dem humanisierten Lymphom hMB sowie Alemtuzumab und S3 erfolgte nach entsprechender Anleitung durch den medizinisch-technischen Assistenten Herrn Michalik durch Herrn Michalik und Herrn Bartel. Die Präparierung der Mäuse erfolgte nach entsprechender Anleitung durch den medizinisch-technischen Assistenten Herrn Michalik durch Herrn Michalik, Herrn Bartel, Herrn Prof. Pallasch und mich. Die Weiterverarbeitung der gewonnenen Organe erfolgte nach entsprechender Anleitung durch mich durch Herrn Bartel und mich.
Die Analyse der Stammzellkompartimente erfolgte durch Herrn Dr. Picard unter Anleitung von Herrn Prof. Krüger. Die Bestimmung des myeloiden Progenitor-, Monozyten- und Makrophagen-Gehalts der Milzen mittels Immunphänotypisierung erfolgte durch mich.
Die Survival-Kohorte wurde durch Herrn Bartel und den medizinisch-technischen Assistenten Herrn Michalik betreut und analysiert. Dr. Blakemore war bei der Analyse beratend tätig.
Die Proben für die Immunhistochemie wurden durch Herrn Michalik, Herrn Bartel, Herrn Prof. Pallasch und mich gewonnen. Die immunhistochemische Färbung und Katalogisierung der Proben erfolgte durch Frau Florin. Die Analyse der Proben erfolgte durch mich.

Die Erstellung des Manuskripts der Publikation erfolgte durch mich. Herr Dr. Blakemore war nach Vorhandensein des initialen Manuskripts beratend hinsichtlich Sprache und Formulierung tätig. Herr Prof. Pallasch half bei der Kürzung und finalen Formulierung des Manuskripts.

Die Abbildungen der Publikation und der Dissertation wurde durch mich erstellt mit Ausnahme der Volcano-Plots und *Normalized Upstream Kinase Scores* der Proteom- und

Phosphoproteom-Analyse, welche durch Herrn Dr. Blakemore erstellt wurden. Herr Prof. Pallasch war beratend hinsichtlich Adaptation der Abbildungen tätig.
Die Erstellung des Graphical Abstracts erfolgte durch mich.

Die Betreuung der Masterarbeitstudentinnen Frau Chawan und Frau Linke sowie der Promotionsstudenten Herr Bartel und Herr Albert erfolgten durch mich sowie durch die medizinisch-technischen Assistent*innen Frau Brinker und Herr Michalik. Als Betreuer der Arbeiten war Herr Prof. Pallasch verantwortlich.

Erklärung zur guten wissenschaftlichen Praxis:

Ich erkläre hiermit, dass ich die Ordnung zur Sicherung guter wissenschaftlicher Praxis und zum Umgang mit wissenschaftlichem Fehlverhalten (Amtliche Mitteilung der Universität zu Köln AM 132/2020) der Universität zu Köln gelesen habe und verpflichte mich hiermit, die dort genannten Vorgaben bei allen wissenschaftlichen Tätigkeiten zu beachten und umzusetzen.

Köln, den 12.01.2025

Unterschrift: .....

Danksagung

Danke an meine Eltern für ihre liebevolle Förderung meines Wissensdurstes und dem Mitgeben eines großen Glaubens an mich selber und die Möglichkeiten, die mir offenstehen.
Danke an meinen Papa für die Begeisterung für die Naturwissenschaften.
Danke an meinen Doktorvater Christian für das sichere Manövrieren, die schützende Begleitung und die selbstverständliche Förderung meiner beruflichen Laufbahn.
Danke an Nadine für ihre umsichtige Einführung in das wissenschaftliche Arbeiten und danke an Elena und Stuart für all ihren wertvollen Input und Wissensaustausch.
Danke an Michael für seinen hartnäckigen Einsatz und Enthusiasmus und die fröhlichen langen Marathon-Labortage.
Danke an Reinhild für das stets am-Start-Sein, die ruhige Anleitung von mir und meinen Student*innen und das ausdauernde Überlisten kniffliger Blots.
Danke an Samruddhi, Lukas, Henrik und Rebecca für ihren großen Einsatz für unser Projekt mit viel Begeisterung.
Danke an alle Patient*innen, welche mit ihrer Bereitschaft der Probenbereitstellung solch einen wichtigen Beitrag für die Wissenschaft und die Versorgung künftiger Patient*innen leisten.

Und danke an meinen wichtigsten Halt und Begleiter über die gesamte Zeit dieser Arbeit und hoffentlich für noch so viele Jahre mehr, meinen Mann David. Du bist mein größter Motivator, freundlichster Kritiker, sanfter Ausbremser, wenn ich mich übernehme, und Aufbauer bei Rückschlägen. Du hast dich reingefuchst in diese für dich so fremde Welt der Forschung, um mich zu unterstützen, und bist so wundervoll stolz über mein Geleistetes. Danke, dass du bei mir bist, mich meine Leidenschaft leben lässt und gleichzeitig meine schönste Ablenkung bist.

Für meinen sicheren Hafen in allen Gewässern,

David

TABLE OF CONTENTS

ABBREVIATIONS

6PGD	6-phosphogluconate dehydrogenase
	6-Phosphogluconatdehydrogenase
7AAD	7-Aminoactinomycin D
ABL	Abelson kinase
Acetyl-CoA	Acetyl coenzyme A
ACLY	Adenosine triphosphate citrate lyase
ACN	Acetonitrile
ACOD1	≙ IRG1
ACTN1	Actinin alpha 1
ACTR1A	Actin related protein 1a
ADCP	Antibody-dependent cellular phagocytosis
	Antikörper-abhängige zelluläre Phagozytose
AICP	Antibody-independent cellular phagocytosis
	Antikörper-unabhängige zelluläre Phagozytose
AKT	Rho family-alpha serine/threonine-protein kinase
AMPK	AMP-activated protein kinase
	AMP-aktivierte Proteinkinase
ANOVA	Analysis of variance
APS	Ammonium persulphate solution
ARG1	Arginase 1
ATF3	Activation transcription factor 3
ATG16L1	Autophagy related 16 like 1
ATP	Adenosine triphosphate
	Adenosintriphosphat
BCA assay	Bicinchoninic acid assay
BCL2	B cell lymphoma 2
BCR	Breaking cluster region protein
BSA	Bovine serum albumin
CAR-T	Chimeric antigen receptor T cells
CARKL	Carbohydrate kinase-like protein
CAST	Calpastatin
CCR7	C-C chemokine receptor 7
CD	Cluster of differentiation
CLL	Chronic lymphocytic leukemia
	Chronische lymphatische Leukämie
CSF1	Colony stimulation factor 1

CSF1R	Colony stimulation factor 1 receptor
	Kolonie-stimulierender Faktor 1-Rezeptor
CYBB	Cytochrome b beta
DAPI	4´,6-diamin-2-phenylindole
ddH_2O	Double-distilled H_2O
DLBCL	Diffuse large B cell lymphoma
DMEM	Dulbecco´s modified eagle medium
dMRM	Dual multiple reaction monitoring
DMSO	Dimethylsulphoxide
DNA	Deoxyribonucleic acid
DPBS	Dulbecco´s phosphate-buffered saline
DTT	1,4-dithiothreit
E4P	Erythrose-4-phosphate
ECAR	Extracellular acidification rate
	Extrazelluläre Ansäuerung
EGF	Epidermal growth factor
EGFR	Epidermal growth factor receptor
EGR-2	Early growth response 2
ELISA	Enzyme-linked immunosorbent assay
ERK1/2	≙ MAPK1/2
ESI	Electrospray ionization
ETC	Electron transport chain
EZR	Ezrin
F6P	Fructose-6-phosphate
FACS	Fluorescence activated cell sorting
$FADH_2$	Flavin adenine dinucleotide
FAO	Fatty acid oxidation
FAS	Fatty acid synthesis
FBS	Fetal bovine serum
FKBP5	FKBP prolyl isomerase 5
FCCP	Carbonyl cyanide-4-(trifluoromethoxy)phenylhydrazone
FcR	Fc receptor
G3P	Glyceraldehyde-3-phosphate
G6PD	Glucose-6-phosphate dehydrogenase
Glc6P	Glucose-6-phosphate
GFP	Green fluorescent protein
GM-CSF	Granulocyte-macrophage colony-stimulating factor

GOSR1	Golgi SNAP receptor complex member 1
GTP	Guanosine-5´-triphosphate
HAGH	Hydroxyacylglutathione hydrolase
HCK	Hematopoietic cell kinase
HIF1α	Hypoxia-inducible factor-1 α
hMB	Humanized-MYC/BCL2
	Humanisiertes MYC/BCL2
HMOX-1	Heme-oxygenase-1
HPLC	High-pressure liquid chromatography
HSC	Hematopoietic stem cell
i.p.	Intraperitoneal
i.v.	Intravenous
IAA	Iodoacetic acid
IC_{50}	Half maximal inhibitory concentration
	Mittlere inhibitorische Konzentration
IDO	Indoleamine-2,3-dioxygenase
IFN-γ	Interferon-γ
IL	Interleukin
ILF2	Interleukin enhancer binding factor 2
INKA	Integrative Inferred Kinase Activity
	Integrierte abgeleitete Kinase-Aktivität
iNOS	Inducible nitric oxide synthase
INPPL1	Inositol polyphosphate phosphatase like 1
IQGAP3	IQ motif containing GTPase activating protein 3
IRF1	Interferon regulatory factor 1
	Interferon-regulierender Faktor 1
IRG1	Immune-responsive gene 1
	Immunresponsives Gen 1
ITGAV	Integrin subunit alpha V
LB-media	Lysogeny Broth media
LC	Liquid chromatography
LPS	Lipopolysaccharide
LRP1	LDL receptor related protein 1
LSK	Lin^-, $Sca\text{-}1^+$, $c\text{-}Kit^+$
M-CSF	≙ CSF1
MAPK1/2	Mitogen-activated protein kinase 1/2
	Mitogen-aktivierte Proteinkinase 1/2

MFI	Mean fluorescence intensity
MHC	Major histocompatibility complex
miRNA	Micro ribonucleic acid
mOS	Median overall survival
MPP	Multipotent progenitor
MS	Mass spectrometry
mTOR	Mammalian target of rapamycin
MYL12A	Myosin light chain 12a
NADH	Nicotinamide adenine dinucleotide
NADPH	Nicotinamide adenine dinucleotide phosphate
NECAP1	NECAP endocytosis associated 1
NO	Nitric oxide
NRF2	Nuclear factor erythroid 2-related factor 2
NSG	NOD.Cg-Prkdcscid Il2rgtm1Wjl/SzJ
NUKS	Normalized upstream kinase score
	Normalisiertes vorgeschaltete Kinase Ranking
OAS3	2´-5´-oligoadenylate synthetase 3
OCR	Oxygen consumption rate
	Sauerstoffverbrauchsrate
OXPHOS	Oxidative phosphorylation
P2Y14R	Purinergic receptor P2Y14
p53	Tumor protein 53
PAM16	Presequence translocase associated motor 16
PARP14	Poly(ADP-ribose) polymerase family member 14
PBMC	Peripheral blood mononuclear cell
PBS	Phosphate-buffered saline
PD-1	Programmed cell death 1
PD-L1	Programmed cell death ligand 1
PD-L2	Programmed cell death ligand 2
PFA	Perfluoralkoxy-polymere
PI3K	Phosphoinositide 3-kinase
PPAR	Peroxisome proliferator-activated receptor
PPP	Pentose phosphate pathway
	Pentosephosphatweg
PSP	PhosphoSitePlus
PTGS1	Prostaglandin-endoperoxide synthase 1

PTK2B	Protein tyrosine kinase 2 beta
	Protein Tyrosinkinase 2 beta
PYK2	≙ PTK2B
QC	Quality control
R5P	Ribose-5-phosphate
RIPA	Radio-immunoprecipitation assay
RM one-way ANOVA	Repeated-measures one-way ANOVA
ROS	Reactive oxygen species
RPMI 1640	Roswell park memorial institute 1640
Ru5P	Ribulose-5-phosphate
S3	1-hydroxy-8-methoxy-anthraquinone
	1-Hydroxy-8-Methoxy-Anthraquinon
S7P	Sedoheptulose-7-phosphate
SD	Standard deviation
SDH	Succinate dehydrogenase
	Succinat-Dehydrogenase
SDS	Sodiumdodecylsulfate
SEM	Standard error of the mean
SEMA4D	Semaphorin 4d
SH3BP1	SH3 domain binding protein 1
shRNA	Short-hairpin ribonucleic acid
	Short-hairpin Ribonukleinsäure
SQSTM1	Sequestosome 1
STAT1	Signal transducer and activator of transcription 1
	Signaltransduktor und Transkriptionsaktivator 1
TAM	Tumor-associated macrophages
	Tumor-assoziierte Makrophagen
TBS	Tris-buffered saline
TBS-T	Tris-buffered saline with Tween20
TCA cycle	Tricarboxylic acid cycle
TEMED	Tetramethylethylendiamin
T_H1	T helper cell 1
T_H2	T helper cell 2
TKT	Transketolase
TLR7	Toll like receptor 7
TME	Tumor microenvironment
TNFα	Tumor-necrosis factor α

TRIS	Tris(hydroxymethyl)aminomethan
UDPG	Uridine diphosphate glucose
UGP2	UDP-glucose pyrophosphorylase 2
	UDP-Glucose Pyrophosphorylase 2
YBX3	Y-box binding protein 3
X5P	Xylulose-5-phosphate

1. ZUSAMMENFASSUNG DEUTSCH

In dieser Dissertation wurde im Rahmen der Publikation von Beielstein et al.[3] der mögliche Einfluss eines veränderten Metabolismus von Makrophagen auf deren Phagozytoseaktivität und daraus folgend der Therapieeffektivität im Kontext von Chemo-Immuntherapie bei aggressiven B-Zell-Lymphomen und indolenten Lymphomen eruiert.

1.1 Makrophagen und ihr Verhalten im Tumormikromilieu

Das Tumormikromilieu ist ein entscheidender Einflussfaktor für den Verlauf von malignen Tumoren, Leukämien und Lymphomen.[4] Im Mikromilieu gibt es neben den Tumorzellen verschiedene benigne Zellen, welche den Progress und auch die Therapieantwort von Tumoren beeinflussen. Durch Veränderungen des gemeinsamen Milieus mittels Sekretion von unter anderem Zytokinen und Stoffwechselprodukten, werden vorhandene Immunzellen zu Tumor-supportiver Funktion umprogrammiert.[5] Eine im Mikromilieu vorhandene Immunzelle ist der Tumor-assoziierte Makrophage (TAM), welcher das Tumorwachstum, die -vaskularisierung und -metastasierung fördert und andere Immunzellen inhibiert.[6,7]

Entgegen dieser tumorförderlichen Eigenschaft der Makrophagen, wurde durch Pallasch et al. jedoch auch gezeigt, dass TAMs die hauptverantwortlichen Zellen für die Beseitigung von Antikörper-markierten Zellen durch Phagozytose im Rahmen von Chemo-Immuntherapien bei Lymphomen sind.[8] Gleichzeitig wurde veranschaulicht, dass diese Makrophagen im Lymphommilieu weniger phagozytieren als in anderen Kontexten.[8] So kann es zu Therapie-refraktäre Nischen und folgend zu Rezidiven kommen. Makrophagen sind also ein wichtiger Faktor im Rahmen von Chemo-Immuntherapien, jedoch dabei in ihrer phagozytierenden Funktion gehemmt.

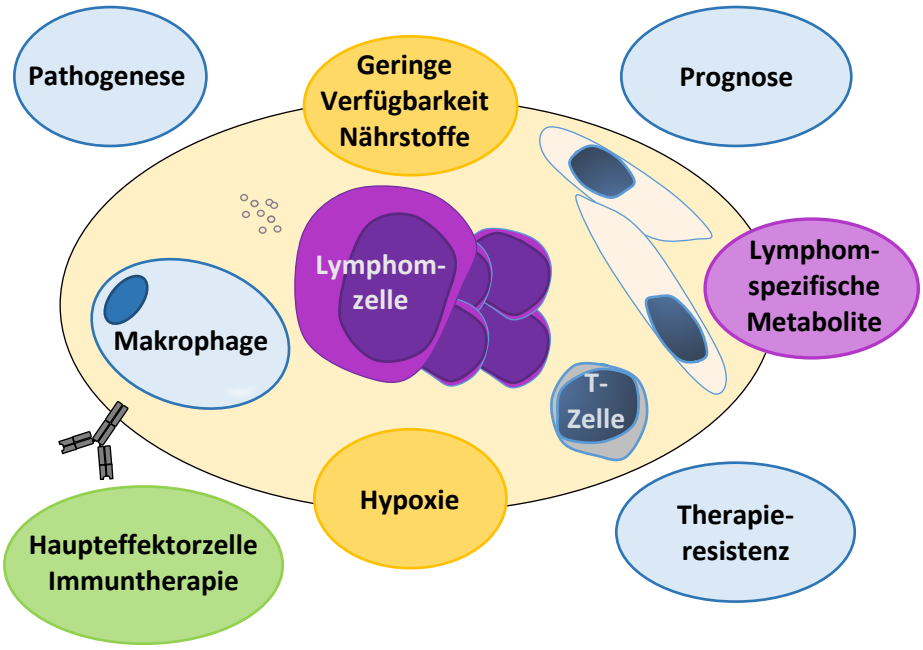

Abb. 1.1 **Tumor-assoziierte Makrophagen und das Lymphommikromilieu beeinflussen Tumorprogress und Therapieansprechen.** Im Tumormikromilieu besteht ein Wechselspiel zwischen Lymphomzellen und benignen umgebenden Zellen. Das Milieu beeinflusst durch seine Charakteristika (gelb) und Metabolite (lila) die umgebenden Zellen. Der Tumor-assoziierte Makrophage beeinflusst wiederum das Verhalten der Lymphomzellen (blau) und ist gleichzeitig die entscheidende Zelle im Kontext von Immuntherapien (grün). Abbildung modifiziert nach Pallasch et al.[9]

Die Funktion und phagozytierende Aktivität von Makrophagen hängt von ihrer Polarisation ab. Makrophagen haben ein weites Spektrum an möglichen Phänotypen, welches von pro-inflammatorischen und Phagozytose-aktiven Makrophagen (M1-artige Makrophagen) bis zu anti-inflammatorischen und Gewebe-regenerativen Makrophagen (M2-artige Makrophagen) reicht. Der TAM tendiert im Bereich dieses Spektrums Richtung M2-artig, stellt aber eine Mischung aus beiden Phänotypen dar.[10,11] Wie stark die Tendenzen ausgeprägt sind, hängt vom Tumor ab, welcher den TAM induziert.[12] TAMs wirken (je nach Polarisation in verschiedenem Ausmaß) immuninhibitorisch auf umgebende Immunzellen und sind phagozytisch wenig aktiv, sie können die Vaskularisation von Tumoren und deren Metastasierung fördern und Einfluss auf die Effizienz von Antitumor-Therapien haben.[12]
Die Polarisation in Richtung eines Phänotyps wird durch das umgebende Milieu und darin enthaltene Aktivatoren wie Zytokine, Chemokine und Stoffwechselprodukte beeinflusst. Diese Mediatoren können den Stoffwechsel von Makrophagen und daraus folgend ihre Polarisation determinieren.[13,14] Es wurde gezeigt, dass auch bereits differenzierte Makrophagen durch Veränderungen im Milieu in Richtung einer anderen Polarisation verändert werden können und hierdurch Tumor-fördernde TAMs anti-tumoröse Eigenschaften entwickeln können.[15–17]

1.2 Notwendigkeit der Therapieoptimierung in B-Zell-Leukämien und -Lymphomen

In den vergangenen Jahrzehnten wurden verschiedene neue Therapieoptionen für B-Zell-Leukämien und -Lymphome entwickelt. Hierdurch wurde eine Lebenszeitverlängerung erreicht, die Heilungsraten konnten jedoch nicht durchgreifend verbessert werden.[18–20] Die führende Therapiemodalität für B-Zell-Leukämien und -Lymphome ist eine Kombinationstherapie aus Chemotherapie und einer Immuntherapie in Form von Antikörpertherapien mit beispielsweise Rituximab oder Obinutuzumab.[18] Im Rahmen dieser Therapien sind Makrophagen wie oben beschrieben eine wichtige Zellpopulation, welche die therapeutische Wirksamkeit und damit potentiell auch die Heilungsraten beeinflussen kann.

Auf Grundlage der beschriebenen Interaktion von Makrophagen und Lymphomzellen und des metabolischen Einflusses auf die Makrophagenpolarisation und -aktivität wurde diese Studie initiiert, um eine mögliche Therapieoptimierung von Lymphomen durch Optimierung der Makrophagenfunktion durch metabolische Modulation zu eruieren.

1.3 Metabolische Modulation verändert die Phagozytoseaktivität von Makrophagen

Zur Evaluation der Phagozytoseaktivität im Kontext von Antikörpertherapien wurde eine Kokultur aus einer murinen Makrophagen- (J774A.1) und einer humanisierten aggressiven B-Zell-Lymphom Zelllinie (hMB, MYC- und BCL2-mutiert) angelegt. Die Hälfte der Proben wurde mit dem therapeutischen Antikörper Alemtuzumab, welcher gegen CD52 gerichtet ist, behandelt. Für Folgeversuche wurde die therapeutische Antikörperauswahl um aktuell angewandte Antikörper, wie Obinutuzumab und Daratumumab (gegen CD20 bzw. CD38 gerichtet), erweitert. Nach Inkubation der Zellen konnte folgend via Durchflusszytometrie die Anzahl an verbliebenen – und damit nicht phagozytierten – hMB Zellen bestimmt werden. Durch den Vergleich von Proben, welche mit Antikörper behandelt wurden, und Proben, welche nicht mit Antikörper behandelt wurden, kann die Antikörper-abhängige Phagozytoserate (antibody-dependent cellular phagocytosis; ADCP) der Makrophagen errechnet werden.

Zur Beurteilung des Einflusses der metabolischen Modulation auf das Phagozytoseverhalten von Makrophagen wurden verschiedene metabolische Inhibitoren genutzt. Die nicht-toxische Dosis gegenüber Makrophagen und hMB Zellen wurde zuvor bestimmt. Es wurde die Glykolyse mittels 2-Deoxy-D-Glucose, die mitochondrielle Aktivität mittels Oligomycin, die Energieregulation der Zelle mittels BML257 (inhibiert die AMP-aktivierte Proteinkinase; AMPK) und der Pentosephosphatweg (PPP) mittels 6-Aminonicotinamide (inhibiert das Enzym 6-Phosphogluconatdehydrogenase (6pgd) im oxidativen Teil des PPP) und Oxythiamin (inhibiert das Enzym Transketolase (Tkt) im nicht-oxidativen Teil des PPP) verwendet.

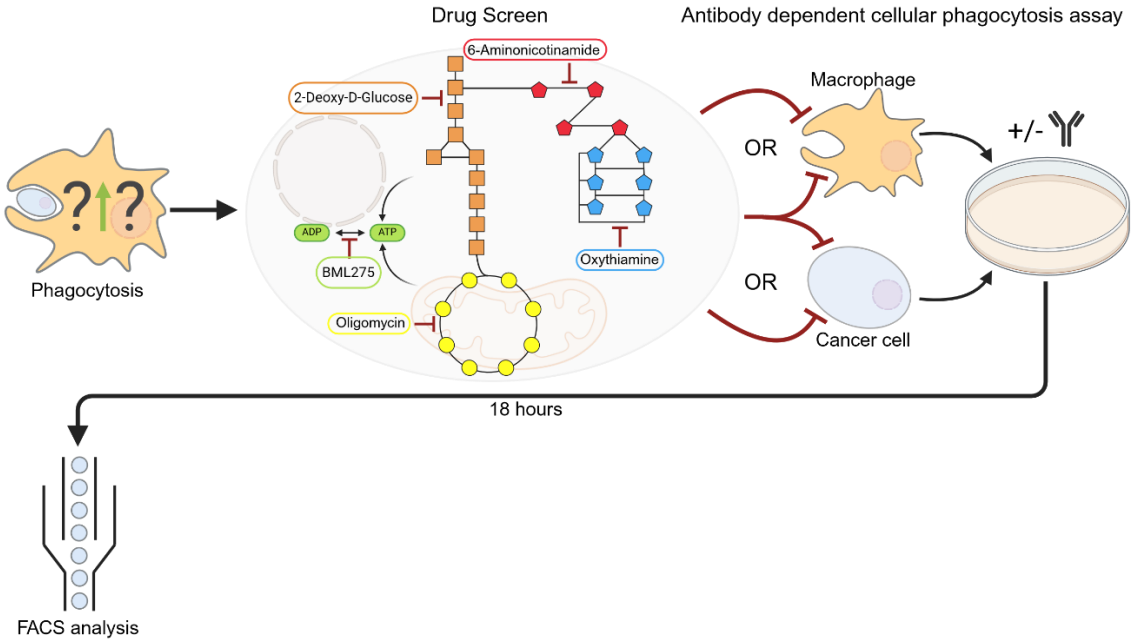

Abb. 1.2 **Schematische Darstellung des metabolischen Screenings mit Frage des Einflusses auf die Antikörper-abhängige Phagozytoseaktivität von Makrophagen in einer Makrophagen-Lymphomzell-Kokultur.** Abbildung modifiziert nach Beielstein et al.[3]

Im Screening zeigte sich, dass die meisten metabolischen Inhibitoren einen negativen Einfluss auf die Phagozytoseaktivität von Makrophagen haben. Lediglich die Hemmung des PPP führte zu einer Steigerung der Phagozytoseaktivität. Um die treibende Veränderung abhängig vom Zelltypen festzustellen, wurden die Inhibitoren entweder zur Kokultur dazu gegeben oder es erfolgte alternativ eine Vorbehandlung der Makrophagen oder der hMB Zellen vor Hinzugabe zu der Zellkultur. Hierdurch konnte gesehen werden, dass die PPP Inhibition im Gegensatz zu allen anderen Inhibitoren unter allen genannten Behandlungsarten eine Steigerung der Phagozytose erreichte, die PPP Inhibition also sowohl einen Einfluss auf die Phagozytoseaktivität der Makrophagen hat als auch die hMB Zellen empfänglicher gegenüber Phagozytose macht. Die größte Steigerung der Phagozytose wurde bei Vorbehandlung der Makrophagen erreicht.

Zur Verifizierung der Phagozytoseaktivität von Makrophagen unter PPP Inhibition wurden weitere ADCP Versuche durchgeführt. Unter Nutzung anderer Inhibitoren (Physcion für 6pgd und 6-Hydroxyphenylpyruat für Tkt), einer anderen Makrophagenzelllinie (humane THP1 Zellen) und eines alternativen Antikörpers (Obinutuzumab; gegen CD20 gerichtet) sowie Durchführung des Assays in Hypoxie (häufig vorliegend in den Therapie-refraktären Nischen von Lymphomen) konnte ebenfalls eine Steigerung der Phagozytoserate erreicht werden. Auch ohne die Hinzunahme von Antikörpern zeigte sich unter Inhibition des oxidativen Teils

des PPP eine Zunahme der Antikörper-unabhängigen Phagozytoserate (antibody-independent cellular phagocytosis; AICP). Zum Ausschluss von Ziel-ungerichteten Effekten der Inhibitoren, wurden Makrophagen erzeugt, in welchen die Expression von 6pgd oder Tkt mit Hilfe von Short-hairpin Ribonukleinsäure (shRNA) suffizient herunterreguliert wurde. Auch diese Makrophagen zeigten eine deutliche Zunahme der Phagozytoseaktivität.

Um zu eruieren, ob die Enzymaktivität selber oder die Veränderung der dazugehörigen Edukte oder Produkte Ursache für die veränderte Phagozytoseaktivität der Makrophagen ist, erfolgten ADCP Assays unter Supplementierung von PPP Edukten und Produkten. Hier zeigte sich, dass nur unter Supplementierung der Produkte von 6Pgd und Tkt eine Steigerung der Phagozytoserate erfolgte, während die Supplementierung des Tkt Edukts Erythrose-4-Phosphat zu einer Verringerung der Phagozytoseaktivität führte. Diese Beobachtung lässt vermuten, dass die Inhibition des Enzyms und nicht die Verringerung des dazugehörigen Produkts zu einer Veränderung der Phagozytoseaktivität führt. Enzyme unterliegen einem sogenannten Feedback-Mechanismus. Das heißt die Ansammlung von Edukten führt zu ihrer Aktivierung während die Ansammlung von Produkten zu ihrer Hemmung führt. Dieser Feedback-Mechanismus konnte in dieser Versuchsreihe beobachtet werden.

1.4 PPP Inhibition aktiviert Makrophagen auf vielfältige Weise

Zur weiteren Charakterisierung der Makrophagen unter PPP Inhibition wurde die Polarisation der Makrophagen via Durchflusszytometrie bestimmt. Hier zeigte sich eine Tendenz weg vom M2-ähnlichen und TAM-ähnlichen Phänotyp hin zum M1-ähnlichen Phänotyp. In der Immunfluoreszenzmikroskopie zeigten die Makrophagen unter PPP Inhibition einen aktivierten Phänotyp mit vermehrter Ausbildung von Filopodien. Filopodien werden zur Initiierung der Phagozytose genutzt. Die Stoffwechselaktivität der Makrophagen wurde mit Hilfe von Seahorse Cell Mito Stress Test und Seahorse XF Glycolytic Rate Assay charakterisiert. Hierbei können über die Sauerstoffverbrauchsrate (Oxygen consumption rate; OCR) und die extrazelluläre Ansäuerung (extracellular acidification rate; ECAR) unter schrittweiser Inhibition der mitochondriellen Aktivität und der Glykolyse Rückschlüsse auf die Aktivität dieser beiden Stoffwechselwege gezogen werden. Unter PPP Inhibition zeigte sich eine Zunahme der Aktivität beider Stoffwechselwege und eine vermehrte Adenosintriphosphat (ATP) Produktion. Dies lässt auf eine allgemeine metabolische Aktivierung der Makrophagen unter PPP Inhibition schließen. Zusammenfassend konnte so gezeigt werden, dass Makrophagen auf multiplen Wegen einen aktivierten Status unter PPP Inhibition annehmen, welche allesamt als möglicher (Mit-)Ausgangspunkt für eine gesteigerte Phagozytoseaktivität angesehen werden können.

1.5 PPP Inhibition moduliert die Immunantwort und Aktivität von Makrophagen über die UDPG-P2y14-Stat1-Irf1-Irg1-Itaconat Signalachse

Zur tiefergehenden Analyse der Veränderungen in Makrophagen unter PPP Inhibition wurde eine Proteom- und Phosphoproteom-Analyse der Zellen vorgenommen. Hier zeigte sich sowohl unter Substanz-gesteuerter als auch unter shRNA-gesteuerter PPP Inhibition eine signifikante Verringerung von anti-inflammatorischen Proteinen und eine Zunahme von pro-inflammatorischen und für die Phagozytose notwendigen Proteinen. Zur weiteren Analyse wurde ein Clustering der Proteine zu zugehörigen Signalwegen vorgenommen, in welchem sich passende Veränderungen in Signalwegen für die Immunregulation, Phagozytose und die ebenfalls zuvor beobachteten Veränderungen in Glykolyse und mitochondrieller Aktivität zeigten. Um die spezifische Veränderungen der Aktivität einzelner Kinasen zu evaluieren, wurde eine modifizierte Integrierte abgeleitete Kinase-Aktivitäts-Analyse (INKA-Analyse)[21] durchgeführt. Hier zeigte sich eine kongruente starke Verminderung der Kinaseaktivitäten des Kolonie-stimulierender-Faktor-1-Rezeptor - Protein Tyrosinkinase 2 beta - Mitogen-aktivierte Proteinkinase (Csf1r-Ptk2b-Mapk1) -Signalweges. Dieser Signalweg führt zur Expression von Interferon-regulierender Faktor 1 (Irf1), Immunresponsives Gen 1 (Irg1) und Signaltransduktor und Transkriptionsaktivator 1 (Stat1).

In 2020 beschrieben Ma et al.[22] die Regulation von Stat1 durch Beeinflussung des PPP. Hier hatte sich eine gleichgerichtete Aktivitätsänderung des Glykogen-Metabolismus und des PPP gezeigt, wodurch es zu einer Beeinflussung einer Signalkaskade über das Glykogen-Enzym UDP-Glucose Pyrophosphorylase 2 (Ugp2), den Transmembranrezeptor P2y14 und folgend von Stat1 kommt. Stat1 wiederum führt zur Expression von Irf1,[23] welches der Transkriptionsfaktor von Irg1 ist.[24] Irg1 ist ein zentrales Immun-inhibitorisches Protein in Makrophagen. Wir konnten zeigen, dass Makrophagen unter PPP Inhibition weniger Glykogen produzieren und die Proteine der Ugp2-P2y14-Stat1-Irf1-Irg1-Achse allseits signifikant reduziert sind.

Irg1 ist ein Enzym, welches seine Immun-inhibitorische Funktion über sein Produkt Itaconat ausübt. Itaconat wird durch Irg1 aus Zitrat produziert. Zur näheren Evaluation der metabolischen Veränderungen in Makrophagen führten wir eine Metabolom-Analyse durch. Hier bestätigte sich zum einen eine signifikante Verminderung des 6pgd-Produkts Ribulose-5-Phosphat und des Tkt-Produkt Sedoheptulose-7-Phosphat unter shRNA-gesteuerter PPP Inhibition. Zum anderen konnten wir eine signifikante Reduktion von Itaconat unter PPP Inhibition zeigen. In der Proteom-Analyse zeigte sich eine signifikant verminderte Expression von Irg1. Itaconat hemmt die Aktivität der Succinat-Dehydrogenase (SDH). Passend zur geringeren Itaconatmenge unter PPP Inhibition, zeigte sich eine vermehrte SDH-Aktivität mit Verminderung des zugehörigen SDH-Edukts Succinat und Vermehrung des SDH-Produkts

Malat. Da SDH ebenfalls ein Bestandteil der Atmungskette der Mitochondrien ist, ist ihre gesteigerte Aktivität eine mögliche Erklärung für die gesteigerte mitochondrielle Aktivität von Makrophagen unter PPP Inhibition. Die Immun-inhibitorische Funktion von Itaconat wird vornehmlich über die Beeinflussung von Zytokinen ausgeführt, wobei es die Expression von Interleukin-10 (IL-10) steigert und die Expression von Interleukin-6 (IL-6) hemmt.[25] Passend hierzu konnten wir eine signifikante Reduktion der IL-10-Expression und eine signifikante Zunahme der IL-6-Expression unter PPP Inhibition (und damit folgend verminderter Produktion von Itaconat) zeigen. Dies kann als zentraler Mechanismus für die beobachtete Aktivierung und pro-inflammatorische Polarisation der Makrophagen angesehen werden.

Zur Verifizierung von Irg1 als zentrales Element unserer beobachteten Veränderung der Phagozytose-Aktivität von Makrophagen, wurde ein Mausmodell genutzt, in welchem das Irg1-Gen ausgeschaltet wurde (Irg1-knockout). Makrophagen der Irg1-knockout-Mäuse zeigten eine signifikant erhöhte Phagozytoseaktivität im Vergleich zu Makrophagen aus Wildtyp-Mäusen. Dies bestätigt die Hypothese, dass eine PPP Inhibition in Makrophagen über Irg1-Inhibition zu einer Immunaktivierung und gesteigerten Phagozytoseaktivität führt.

1.6 PPP Inhibition führt auch in humanen Zellen zu einer gesteigerten Phagozytoseaktivität von Makrophagen

Um der klinische Anwendbarkeit näher zu kommen, wurde die Wirksamkeit der PPP Inhibition in humanen Zellen getestet. Monozyten gesunder Spender*innen wurden in der Anwesenheit von PPP Inhibitoren in Makrophagen differenziert. Diese Makrophagen zeigten eine signifikant erhöhte Phagozytoseaktivität und eine Zytokin-Verschiebung weg von IL-10 und hin zu IL-6 im Vergleich zu unbehandelten humanen Makrophagen. Der ADCP-Assay wurde auch mit primären Chronische lymphatische Leukämie (CLL) Patientenzellen durchgeführt. Hier führte eine Zugabe von PPP Inhibitoren und die Kokultur mit 6pgd- oder Tkt-defizienten murinen Makrophagen ebenfalls zu einer signifikant gesteigerten Phagozytose der CLL Zellen. In einer komplett humanen Kokultur bestehend aus oben genannten humanen Makrophagen und CLL Patientenzellen zeigte sich ebenfalls eine signifikant erhöhte Phagozytoserate. Diese Ergebnisse bestätigen die Wirksamkeit der PPP Inhibition auf die Phagozytoseaktivität von Makrophagen auch in humanen Zellen.

1.7 PPP Inhibition mindert den Lymphom-supportiven Effekt von Makrophagen auf primäre CLL Patienten Zellen

Neben unserem bisher betrachteten Aspekt – die Förderung von Makrophagen zur Elimination Antikörper-markierter Lymphomzellen – sind Makrophagen im Kontext der CLL vor allem als CLL-fördernde Umgebungszellen bekannt. Ohne die Anwesenheit von TAMs können CLL Zellen in Lymphknoten nicht überleben.[26] Zudem fördern TAMs die Chemotherapie-Resistenz

von CLL Zellen. Wir analysierten daher das Verhalten von humanen CLL Zellen in Kokultur mit Makrophagen unter PPP Inhibition. Es zeigte sich eine Verminderung des Überlebens von CLL Zellen in Mono-Kultur unter PPP Inhibition, was auf eine schädliche Wirkung auf CLL Zellen hinweist, sowie in Kokultur unter Inhibition des nicht-oxidativen Teils des PPP. Behandelten wir humane CLL Zellen nach Kokultur mit Makrophagen unter PPP Inhibition mit dem Chemotherapeutikum Bendamustin, war eine niedrigere Dosis von Bendamustin notwendig, um 50% der Zellen abzutöten (mittlere inhibitorische Konzentration, IC_{50}). Es zeigte sich also eine höhere Empfindlichkeit von humanen CLL Zellen gegenüber dem Chemotherapeutikum Bendamustin nach Kokultur mit Makrophagen unter PPP Inhibition oder Kokultur mit Makrophagen, welche zuvor mit PPP Inhibitoren behandelt worden waren. Dies zeigt, dass PPP Inhibition neben der Förderung der Phagozytoseaktivität auch die Tumor-supportiven Eigenschaften von Makrophagen im Kontext von Lymphomen hemmt.

1.8 PPP Inhibition steigert die Makrophagenaktivität und Myelopoese *in vivo*

Um den physiologischen Bedingungen im menschlichen Körper näher zu kommen, führten wir final *in vivo* Versuche im Mausmodell durch. Immunkompetente C57BL/6 Mäuse wurden hierfür mit dem 6pgd-Inhibitor 1-Hydroxy-8-Methoxy-Anthraquinon (S3) behandelt. Im Anschluss analysierten wir Makrophagen verschiedener Kompartimente. Wir begutachteten die Hämatopoese im Knochenmark und konnten hier eine allgemeine Steigerung der Myelopoese sowie von Vorläufer-Pools von Makrophagen und anderen Immunzellen zeigen. In der Milz zeigte sich zudem eine erhöhte Zahl von myeloiden Vorläuferzellen und Makrophagen unter S3 Behandlung. Aus dem Peritoneum gewonnene Makrophagen zeigten passend zu den vorangegangenen Experimenten einen Polarisations-Drift weg von M2- und TAM-artigen Makrophagen und hin zu M1-artigen Makrophagen mit signifikant veränderter Expression von Oberflächenmarkern. Makrophagen, differenziert aus dem Knochenmark behandelter Mäuse, zeigten eine signifikant erhöhte Phagozytoseaktivität im Vergleich zu Makrophagen unbehandelter Mäuse. Zusammengefasst konnte somit die Zunahme der Phagozytoseaktivität und Immunaktivierung auch im Immun-kompetenten *in vivo* Kontext bestätigt werden und zudem eine allgemeine Zunahme der Makrophagenanzahl gezeigt werden.

1.9 PPP Inhibition in einem aggressiven Lymphom-Mausmodell führt zu einem signifikanten Überlebensvorteil

Zur Beurteilung der Therapieeffektivität von PPP Inhibition im Kontext von Antikörper-Therapien, wurde NOD.Cg-Prkdcscid Il2rgtm1Wjl/SzJ (NSG) Mäusen das humanisierte Double-hit Lymphom (hMB) injiziert und die Mäuse anschließend mit dem klinischen Antikörper Alemtuzumab und / oder S3 behandelt. Durch Hinzunahme von S3 zur Antikörper-Therapie konnte eine signifikante Verlängerung des Überlebens der Mäuse im Vergleich zur

alleinigen Antikörper-Therapie erreicht werden.
Hierbei konnten wir histopathologisch zeigen, dass es unter der Kombinationstherapie zu einer signifikanten Reduktion der Lymphomlast und gleichzeitig zu einer gesteigerten Makrophageninvasion in Lymphomareale in der Milz kommt, hinweisend auf die erhöhte Elimination der Lymphomzellen durch die eingewanderten Makrophagen.

1.10 PPP Inhibition ist eine potente metabolische Modulation zur Steigerung der Phagozytoseaktivität von Makrophagen und folgend potentiell effektiv zur Steigerung der Effektivität von B-Zell-Lymphomtherapien

Zusammengefasst konnte in dieser Dissertation gezeigt werden, dass metabolische Modulation die Antikörper-vermittelte Phagozytoseaktivität von Makrophagen verändern kann. Hierbei führt die Inhibition des PPP zu einer Zunahme der Phagozytoseaktivität von Makrophagen. Die Makrophagen zeigen eine pro-inflammatorische Polarisation, einen aktivierten Phänotyp und eine metabolische Aktivierung. Als zugrundeliegender Mechanismus konnte der Ugp2-P2y14-Stat1-Irf1-Irg1-Signalweg identifiziert werden. Hierdurch konnte eine Verbindung zwischen metabolischer Modulation und Immunaktivität von Makrophagen gezeigt werden. Anhand von Experimenten mit humanen Makrophagen und CLL Patientenzellen konnte demonstriert werden, dass der Effekt auch in menschlichen Zellen erreicht werden und die Tumor-supportiven Eigenschaften von TAMs auf CLL Zellen vermindert werden können. In Mausmodellen konnte gezeigt werden, dass der Phagozytose-fördernde und aktivierende Effekt auf Makrophagen auch *in vivo* erhalten bleibt und ein signifikanter Überlebensvorteil durch die Hinzunahme von einem PPP Inhibitor zur Antikörper-Therapie in einem aggressiven Lymphommodell erreicht werden kann. Somit zeigt die Inhibition des PPP ein neues therapeutisches Prinzip, um die Effizienz von Immuntherapien wie Antikörper-basierten Lymphomtherapien in der Klinik weiter zu verbessern. Zur Evaluation der Wirksamkeit im klinischen Kontext sind Folgestudien notwendig, welche in Folgeprojekten realisiert werden sollen.

2. ABSTRACT

Progression and therapeutic response in B cell lymphoma depend on the interaction with macrophages in the tumor microenvironment (TME). A central aspect of the TME is its limited supply of nutrients which implicates metabolic reprograming of immune cells such as changed phagocytic effector capacity of macrophages.

In this project, we particularly aimed to elucidate the role of metabolic modulation of macrophages on their phagocytic activity and to improve macrophage effector cell function in the context of immunotherapies. We have shown that metabolic modulation is able to influence the phagocytic activity of macrophages. Inhibition of the pentose phosphate pathway (PPP) induced an increased chronic lymphocytic leukemia (CLL) cell and lymphoma cell phagocytosis by macrophages. Supplementation of the PPP-intermediates ribulose-5-phosphate and sedoheptulose-7-phosphate increased the phagocytosis while erythrose-4-phosphate inhibited the macrophage-mediated target cell depletion, pointing toward inhibition of the producing enzymes as origin of the observed increased phagocytosis rate. Under PPP inhibition, the phenotype of macrophages was changed. The oxygen consumption and the glycolysis of macrophages was increased and the cells developed a more activated morphology with formation of filopodia, which are involved in the phagocytosis initiation by engulfing target cells. Moreover, cytokine secretion was shifted away from anti-inflammatory IL-10 and toward pro-inflammatory IL-6 secretion. PPP inhibition of macrophages significantly reduced CLL cell support *in vitro* abrogating the “nurse-like” effect of macrophages. PPP inhibition in CLL cells also diminished their viability, pointing toward a possible therapeutic effect also on the site of lymphoma cells. The increased lymphoma cell clearance and phenotypic alterations of macrophages were also observed under PPP enzyme knockdown of transketolase (TKT) and 6-phosphogluconatedehydrogenase (6PGD) in macrophages and by inhibiting the PPP in primary murine and human macrophages. In a multi-omics assessment of PPP inhibition on proteome, phosphoproteome and metabolome level, we found protein expression alterations regulating metabolism and immunity. A connection between PPP inhibition and changed immune profile by influencing the glycogen metabolism and the subsequent modulation of the UGPD-Stat1-Irg1-itaconate axis was identified. The importance of this signaling axis was demonstrated with an Irg1-knockout mouse model. Macrophages of Irg1-knockout mice also showed an increased phagocytic capacity in comparison to wild-type mice macrophages. Macrophages of immune-competent wild-type mice treated with the PPP inhibitor S3 also showed an activated phenotype, a pro-inflammatory polarization and an increased phagocytic activity. The addition of the PPP inhibitor S3 to antibody therapy in an aggressive lymphoma mouse model reached a significant prolongation of overall survival in comparison to antibody treatment only and led to increased macrophage infiltration into lymphoma bearing sides with concomitant reduction of lymphoma cell amount.

In total, an increased activation and repolarization of macrophages toward a pro-inflammatory and phagocytic active phenotype was observed by inhibiting the PPP. We were able to point out the underlying signaling axis, which connects metabolic regulation and immune activity in macrophages.

We hypothesize the PPP as a key regulator of macrophage activity determining support of malignant B cell growth, their capacity of tumor-cell clearance and thereby therapy outcome in immunotherapy of B cell lymphoma and CLL. With these new insights we have identified the PPP as a targetable modulator of macrophage polarization and promising target to improve the efficacy of immunotherapies in B cell lymphoma and CLL.

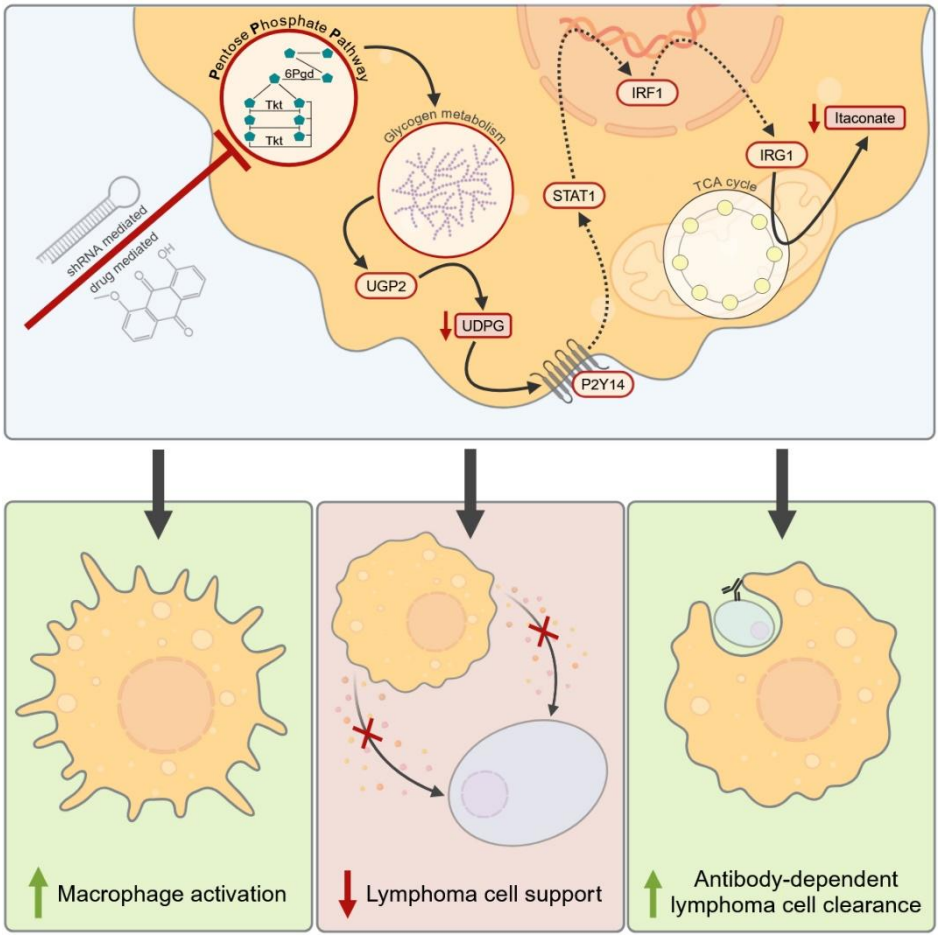

Fig. 2.1 **Graphical abstract of the results of the thesis and the publication of Beielstein et al.**[3] shRNA- and drug-mediated PPP inhibition causes glycogen metabolism changes, which lead to diminished activity of the STAT1-IRG1-itaconate axis. This leads to macrophage activation, less lymphoma cell support and increased antibody-dependent lymphoma cell clearance.

3. INTRODUCTION

3.1 The tumor microenvironment

A malignant tumor is not only composed of transformed malignant cells, but also consists of the tumor microenvironment (TME). The TME includes benign cells like stromal cells, the vasculature, and also different immune cells. Depending on the type of tumor, the immune cell infiltration differs. For example, in Hodgkin lymphoma the tumor consists only of one percent of malignant cells, the great majority consists of surrounding immune cells.[27] It has been demonstrated that there is a close interplay and a strong dependence of several types of leukemia and lymphoma on the TME.[28,29] The tumor cells build up a special milieu by cytokine secretion, nutrient uptake, metabolic product secretion, and oxygen consumption. By that they also differ the milieu occurrence for the bystanding cells and thereby the action of the infiltrating immune cells can be changed from anti- to pro-tumoral activity.[5] Due to that significant influence, the TME has been defined as one hallmark of cancer, whose transformed- and non-transformed cell interactions determine cancer progression and therapeutic response.[4]

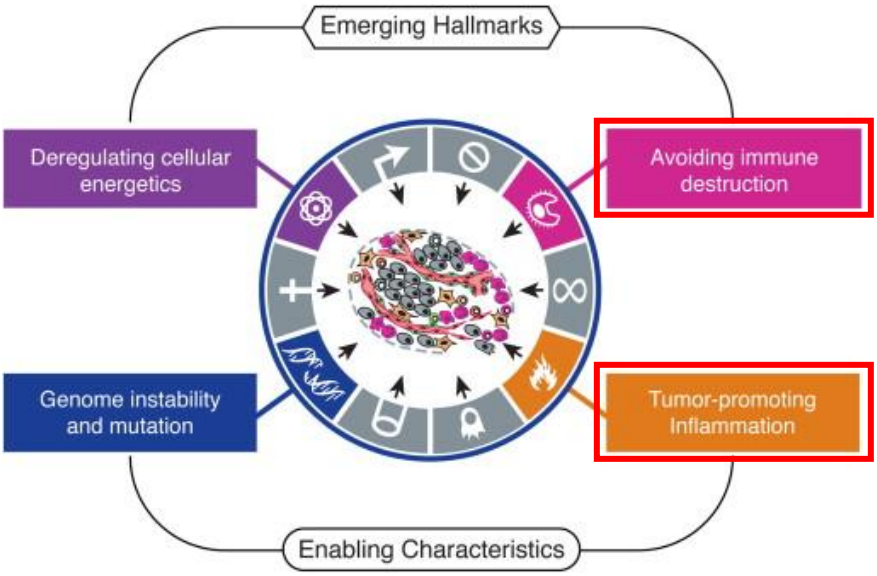

Fig. 3.1 **Newly defined hallmarks of cancer.** Due to the great influence on tumor progression, the capability of tumor cells to modify immune cells to avoid immune destruction and to change the inflammatory response toward tumor-supportive function has been implemented as two central hallmarks of cancer. Figure modified from Hanahan et al.[4]

3.1.1. Tumor-associated macrophages

One type of immune cell in the TME, which has been identified as tumor-supportive, is the tumor-associated macrophage (TAM).[6] TAMs are immuno-suppressive toward other tumor-infiltrating immune cells, e.g. by high expression of inhibitory immune checkpoint receptors like programmed cell death 1 (PD-1), programmed cell death ligand 1 (PD-L1), programmed cell death ligand 2 (PD-L2) and by cytokine secretion. And they are tumor-supportive by promoting vascularization and metastasis.[7,30] The high expression of PD-1 also reduces the anti-tumor function of TAMs by suppression of their phagocytic activity.[31] Moreover, TAMs act as supportive bystander cells for several tumor types by cell contact and cytokine secretion. An impressive example is the CLL. CLL cells undergo spontaneous apoptosis if they do not have contact with TAMs.[26] In the context of anti-tumor therapy, TAMs are also tumor-supportive by facilitating tumor cell recovery through angiogenesis and stem cell maintenance.[32]

In contrast to these tumor-supportive functions, Pallasch et al. have shown that macrophages are central for tumor cell clearance in the context of immunotherapy in aggressive B cell lymphoma.[8] Macrophages are able to detect antibody-labeled tumor cells and phagocyte those labeled cells causing therapy efficacy. A relevant type of aggressive B cell lymphoma is the diffuse large B cell lymphoma (DLBCL), which accounts for 22% of all B cell non-Hodgkin lymphoma.

3.2 Actual therapy of diffuse large B cell lymphoma and its limitations

Actually, the front-line strategy in therapy of DLBCL is chemo-immunotherapy. By adding antibodies like rituximab or obinutuzumab to conventional chemotherapy, a highly increased treatment response, event-free survival and overall survival was achieved.[18] Unfortunately, by using this treatment strategy, 30-40% of patients still do not response or relapse. If relapse occurs, the treatment response to second line therapies remains poor.[18] In the last years several efforts were made to increase first-line therapy response and to improve second-line therapy efficacy.[19] For relapse therapy, the use of chimeric antigen receptor T cells (CAR-T) in third-line therapy greatly improved response rates and the use of CAR-Ts in second-line therapy is currently under investigation. Nevertheless, still 50% of patients do not response to CAR-T therapy and 35% occur relapse.[20] The use of bispecific antibodies, which bind to the lymphoma cells and T cells and thereby should connect effector and target cell directly to improve T cell anti-lymphoma activity, is actually under clinical investigation showing promising therapeutic effects. However, the optimal application combination with other therapies to achieve maximal efficacy with minimal side effects has to be found up to now.[33] For frail patients, the use of antibody-drug conjugates (ADCs) has been approved in 2022 in first and second/further line therapies. This conjugates enable the cell-specific application of chemotherapy or immunomodulatory drugs to tumor cells carrying the appropriate epitope for

the conjugated antibody. The treatment with ADCs is able to improve the cure rates and the median progression free survival time in first line therapy[34] and the response rate and the median progression free survival in further therapy lines.[35–37] But there are difficulties with severe side effects and following discontinuation of therapy, the overall response rates are still beneath 60% and cure rates are not improved.

As the treatment of relapsed/refractory DLBCL remains challenging, an improvement of first-line therapy is eligible, but up to now, no advancement was achieved.[19] Pallasch et al. have shown that DLBCL cells impair the ability for phagocytosis in TAMs and thereby diminish chemo-immunotherapy efficacy and causing relapse.[8] Therefore, the improvement of macrophage function in the context of chemo-immunotherapy could be a promising aim to enhance therapy response in first-line therapy of DLBCL.

As antibodies are also used in other types of lymphoma – like obinutuzumab in CLL or blinatumomab in acute lymphocytic leukemia –, the potential of increased macrophage function may be expanded for improvement of therapy in other types of lymphoma too.

3.2.1. DLBCL cell model for experimental investigation

To investigate DLBCL and possible therapeutic options for clinical treatment, Leskov et al. generated the hMB cell line.[38] hMB cells represent a humanized mouse model of aggressive "double-hit" lymphoma by overexpression of the genes c-MYC and b-cell lymphoma-2 (BCL2) in human hematopoietic stem cell (HSC)-derived B-lineage cells. The cells express green fluorescent protein (GFP) and can be targeted by antibodies used in clinics. Like most double-hit lymphoma patient cells, hMB cells have a low expression of CD20. hMB cells show a high chemotherapeutic resistance. By this humanized model, hMB cells can be used in cell culture and in murine *in vivo* models with simultaneous investigation of human therapeutics.

3.3 Macrophage function and polarization

Macrophages are part of the innate immunity and found in all organs and tissues of the human body.[39,40] They fulfil a broad spectrum of different functions from endo- and phagocytosis over cytokine, metabolite and enzyme secretion[41] to antigen presentation to the adaptive immune system.[42] Thereby they play an important role in tissue repair and remodeling, wound healing, immune defense, and inflammation.[43,44]

The actual function of macrophages is determined by their differentiation and polarization. As monocytes they leave the bone marrow[45] and by microenvironmental stimuli they differentiate into a certain macrophage subtype or dendritic cells.[13]

There is a continuum of macrophages subtypes with the two maximal states of polarization – M1 and M2.[46–50] M1 displays the status of classically activated, pro-inflammatory and phagocytic active macrophages, which are able to induce T helper 1 cell activation, while M2 displays the status of alternative activated macrophages, which are acting anti-inflammatory

and tissue regenerative causing T helper 2 cell activation. Due to the broad mixture of possible stimuli leading to macrophage polarization, a status on the whole range in between these two extremes is feasible.

TAMs carry characteristics of M1 and M2 macrophages with a gradient toward the anti-inflammatory and phagocytic inactive M2 phenotype.[11,51] How distinct this gradient is, depends on the tumor, which induces the TAM phenotype.[12]

The resulting polarization and phenotype of macrophages is determined by the microenvironment in which they are differentiated. Polarization factors are occurring cytokines, chemokines, and metabolites. For example – beside others – interferon-γ (IFN-γ) or the granulocyte-macrophage colony-stimulating factor (GM-CSF) are cytokines that lead to M1 induction and lipopolysaccharide (LPS) is a metabolite that does so. In contrast, M2 macrophages are induced beside others by the cytokines colony stimulation factor (CSF1, also known as M-CSF) or interleukin-4 (IL-4) and -10 (IL-10), whereupon IL-4 is inducing a more tissue repair-active subtype while IL-10 induces a more anti-inflammatory active one.[48] The occurrence of TAMs is – among others – driven by the acidification of the TME caused by lactate and pyruvate secretion of cancer cells,[52–54] an example for metabolites as polarization factors and moreover for the above mentioned immune cell modification by tumor cells. These polarization factors bind to macrophage receptors by which signaling cascades are activated, which lead to changes in macrophage metabolism. These changes in metabolism are crucial for the opportunity of polarization and the resulting macrophage function.[13,14]

Whereas for several years, the polarization of macrophages was seen as a one-way road by which the definitive phenotype of a macrophage is determined for its lifetime, the last years have brought up the insight that macrophage polarization is recomposed by changing microenvironment.[16,55–57] This phenomenon is also taking place when macrophages enter tumor sides.[15,58] Interestingly, it was shown that this repolarization can also be used to repolarize TAMs so that they act less tumor-supportive and show more anti-tumor activity.[17,59]

3.4 Immunometabolism of macrophages

The polarization and activation of macrophages require changes in their metabolic activity.[13,14] Distinct metabolic patterns are typical for different macrophage subtypes. To highlight the changes in metabolism, the two extremes of the macrophage polarization spectrum by elucidating the metabolic activity of M1 macrophages in contrast to M2 macrophages as well as the TAM subtype will be displayed in the upcoming chapters.

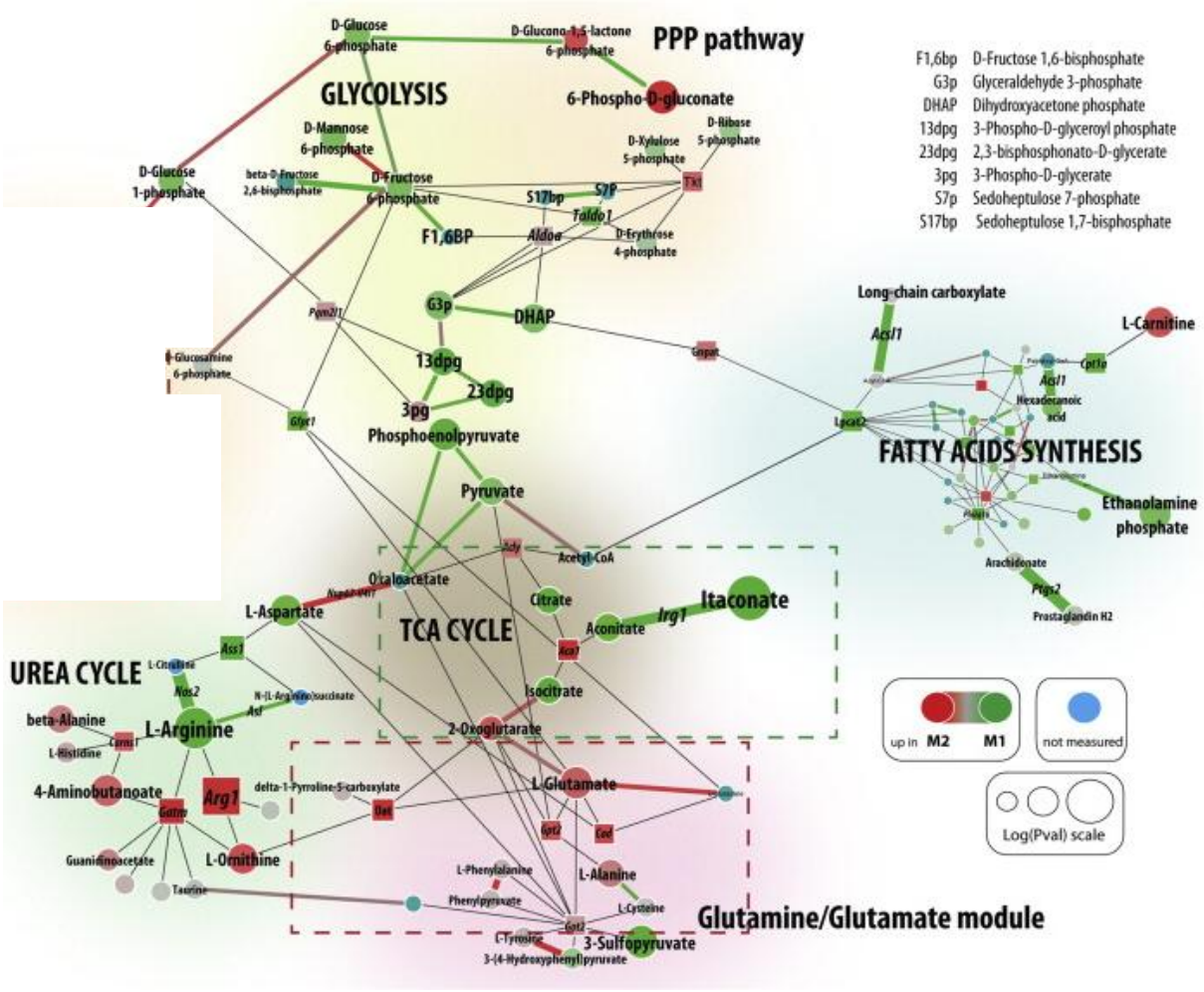

Fig. 3.2 **Changes in metabolism needed for M1 or M2 polarization in macrophages.** Macrophages undergo fundamental and distinct changes for polarization into different macrophage subtypes. Changes in metabolite amount (round nodes) and enzyme activity (square nodes) are displayed. Node size display the change in expression and node color the point in the macrophage polarization spectrum (M2 red, M1 green) where this expression change takes place. Figure modified from Jha et al.[13]

3.4.1. Glycolysis

Glycolysis is an adenosine triphosphate (ATP) and metabolite producing pathway, whose intermediates are used to fuel the pentose phosphate pathway and to provide precursors for the glycogen and fatty acid synthesis and the amino acid metabolism. Enzymes of the glycolysis moreover act as activators or inhibitors for several cytokines (e.g. tumor-necrosis factor α; TNFα), transcription factors (e.g. hypoxia-inducible factor-1 α; HIF1α), or immune modulatory ligands (e.g. PD-L1).

The general induction of glycolysis is crucial for macrophage activation and initiation of phagocytic function despite their subtype.[60–62] It was shown, that M1 macrophages are more dependent on glycolysis and show higher increase of glycolytic activity, whereas M2

macrophages display just slightly increases.[60,63] The increased glycolytic activity leads to increased production of pro-inflammatory cytokines[64] and the energy carriers ATP and nicotinamide adenine dinucleotide (NADH) needed for increased phagocytic activity, a typical characteristic of M1 macrophages.

In TAMs the glycolysis is upregulated.[54] In contrast to the regulation of glycolysis in M2 macrophages, the degree of polarization toward the anti-inflammatory and tumor-promoting M2 phenotype in TAMs as well as their anti-inflammatory cytokine secretion is increased with increasing glycolytic activity.[52,65] The secreted lactate and pyruvate of tumor cells is fueled into the glycolysis of TAMs and thereby favors their tumor-supportive and immunosuppressive function.[65,66]

3.4.2. Pentose phosphate pathway

The pentose phosphate pathway (PPP) has several interchanging points with the glycolysis and offers an opportunity to degrade glucose without the need of ATP. It is the major source of nicotinamide adenine dinucleotide phosphate (NADPH), which is needed for synthetic reactions, the glutathione synthesis and thereby reactive oxygen species (ROS) clearance but also for respiratory burst initiation. Moreover, NADPH is needed in fatty acid synthesis (FAS) used for among others endoplasmic reticulum and Golgi complex expansion, whereby an increased cytokine secretion can be achieved. Intermediates of the PPP are used to fuel other metabolic pathway. Glyceraldehyde-3-phosphate and fructose-6-phosphate can be used either for gluconeogenesis or glycolysis and ribose-5-phosphate is used for nucleotide production including micro ribonucleic acid (miRNA) production. miRNA is able to regulate gene expression.

As regulatory point of macrophage polarization in the context of PPP regulation, the sedoheptulose kinase (*car*bohydrate *k*inase-*l*ike protein, CARKL) is mentioned.[67] In M1 macrophages CARKL is downregulated. Thereby the PPP is activated causing increased NADPH production with subsequent increased ROS, cytokine, and miRNA production. Moreover, the glycolysis is supported with observed tendency away from aerobic and toward anaerobic glycolysis. By these changes, especially the changed cytokine production with increase of interleukin-6 (IL-6), interleukin-1β (IL-1β), and TNFα, the M1 phenotype in macrophages is induced.[67]

In contrast, in M2 macrophages CARKL is slightly upregulated, leading to sedoheptulose-7-phosphate accumulation and PPP inhibition. This causes a decrease of pro-inflammatory cytokines while IL-10 is increased. By less NADPH production, the ROS production and FAS is diminished.[67]

It has been shown that the PPP is also upregulated in TAMs[54] but how this is regulated and which implications this has is not investigated up to now.

3.4.3. Tricarboxylic acid cycle

The Tricarboxylic acid cycle (TCA cycle) is fueled from several metabolic pathways like glycolysis, amino acid degradation, fatty acid oxidation, and the glutamate metabolism. It produces different energy carriers like NADH, flavin adenine dinucleotide ($FADH_2$), guanosine-5'-triphosphate (GTP), and ATP and provides substances for the electron transport chain (ETC), which is the most efficient energy producing pathway in the cell. Intermediates of the TCA cycle are used to fuel the fatty acid synthesis, prostaglandin and porphyrin synthesis, the amino acid metabolism, and the gluconeogenesis.

In the context of macrophage polarization, the TCA cycle shows very distinct regulation.

In M1 macrophages the TCA cycle is interrupted at two sides.[13] The first interruption point is the isocitrate-dehydrogenase, whereby citrate is accumulated. Citrate is used as educt for the ATP citrate lyase (ACLY), which leads to educt production for pro-inflammatory cytokines, for the fatty acid and phospholipid synthesis, and for prostaglandin synthesis. Moreover, ACLY produces NADPH causing increased nitric oxide (NO) and ROS amounts,[68] used for respiratory burst in the context of phagocytosis and inflammatory response.[69] Furthermore, citrate is metabolized into itaconate, the most highly induced metabolite in M1 macrophages.[13,70] Itaconate has antibacterial effects, but also inhibits the pro-inflammatory cytokine production to prevent macrophages from over-activation.[25] Itaconate leads to succinate-dehydrogenase (SDH) inhibition, the second breakpoint observed in M1 macrophages[13,71] with following decreased ETC activity. The increase of the SDH educt succinate leads to stabilization of the transcription factor HIF1α, which causes increased glycolytic activity and pro-inflammatory IL-1β production and secretion, promoting the M1 phenotype polarization.[72]

In M2 macrophages instead, the TCA cycle stays intact.[13] By increased glutamine metabolism the TCA cycle is fueled with increased amounts of α-ketoglutarate, which is causing epigenetic changes crucial for M2 polarization.[13] M2 macrophages use the energy carriers of the TCA cycle to fuel the ETC to fulfil their energetic needs as the glycolysis is not used to do so.

The regulation of the TCA cycle in TAMs is – up to now – not fully understood. As there is also an increase of citrate and succinate observed in TAMs,[73] an interruption of the TCA cycle like in M1 macrophages is probable [74]. Moreover, it was shown that the resulting metabolite itaconate acts tumor-supportive by potentiating tumor growth.[75] On the other hand, it was also mentioned that glutamate is fueled into the TCA cycle to maintain ETC activity,[65] an attribute of M2 macrophages. As TAMs show a mixed phenotype of M1 and M2 macrophages they seem to also use a mix of metabolic adaption in the context of the TCA cycle.

3.4.4. Electron transport chain and oxidative phosphorylation

The ETC is fueled by NADH and $FADH_2$ produced by glycolysis and the TCA cycle. These energy carriers and O_2 are used to implement electron transfer whereby an electron gradient

is generated. The energy of this gradient is then used to produce ATP by the ATP-synthase, this reaction is called the oxidative phosphorylation (OXPHOS).

In M1 macrophages a reversed electron transport was observed. By that, the macrophages use the ETC to produce ROS and not to produce ATP.[76]

For M2 macrophages, in contrast, the intact ETC and OXPHOS is indispensable. Without its activity no M2 polarization can take place.[77,78]

As discussed before, in TAMs the ETC and OXPHOS also seem to stay intact to fuel the cells with ATP.[65]

3.4.5. Fatty acid metabolism

Fatty acids are energy carrier and building blocks for cell compartments, the cell membrane, steroids, and prostaglandins. Thereby fatty acids are used for a broad range of physiological functions in the body. Fatty acids can be ingested by endocytosis or produced by FAS. As precursors for FAS, metabolites of glycolysis, the TCA cycle, and the PPP can be used. To generate branched-chain fatty acids, amino acids are needed. Fatty acids can be stored as triacylglycerol in the cells as lipid droplets and can be degraded by demand for energy by fatty acid oxidation (FAO) even though the FAO is the slowest pathway for energy supply. By FAO, high amounts of ATP and NADH, $FADH_2$ and acetyl coenzyme A (acetyl-CoA) can be produced.[79]

In M1 macrophages the FAS is upregulated and necessary for the inflammatory function of them.[74,80–83] Fatty acids can act as signaling molecules inducing cytokine production and gene transcription causing immune regulation.[84–87] Moreover, induction of FAS is important for phagocytosis.[83]

In contrast, M2 macrophages rely on FAO to fuel their energy need.[78,88] This is achieved by upregulated uptake of triglycerides. The induction of the M2 phenotype rely on the binding of fatty acids to the peroxisome proliferator-activated receptor β/δ (PPAR β/δ), whereby gene regulation needed for M2 polarization is induced.[89–91]

There is just little evidence about fatty acid metabolism regulation in the context of TAM polarization. There are striking studies showing a fatty acid regulation like it is seen in M1 and in M2 macrophages.[65,92–94] If both sides are true and if there is an interplay between these two ways of activation, the underlying regulation has not been unveiled so far.

3.4.6. Amino acid metabolism

Amino acids are building blocks for proteins and branched-chain fatty acids. The amino acids glutamine and aspartate are required for purine and pyrimidine synthesis and thereby for cell proliferation, and glutamine can be fueled into the TCA cycle. In macrophages, these two amino acids are important for NO and cytokine production.[74,79]

M1 macrophages do not rely on glutamine metabolism.[13] In M1 macrophages arginine is used as source for NO synthesis and L-citrulline synthesis via inducible nitric oxide synthase (iNOS).[95,96] NO suppresses the OXPHOS und upregulates the glycolysis,[97,98] wherefore it is seen as a key regulator of M1 polarization.

M2 macrophages instead increase their glutamine utilization to perform N-glycosylation of M2-associated receptors. Glutamine is fluxed into the TCA cycle, which causes the increased TCA cycle activity needed for M2 polarization.[13] M2 macrophages degrade arginine via arginase 1 (ARG1) to ornithine and urea.[95,96] Ornithine is used as metabolite for wound healing and tissue repair[95,99] and its degrading enzyme, the ornithine decarboxylase, functions as a macrophage polarization enzyme suppressing M1 polarization.[100] Moreover, the activity of ARG1 causes immunosuppression by suppressed T cell response.[101] Via the missing production of NO in M2 macrophages, the OXPHOS is able to act unhindered.[102]

In TAMs there are hints for increased glutamine metabolism but no clear evidence.[103] In the context of arginine metabolism, TAMs show low NO production[104,105] and increased ARG1 expression.[51,52,54,106,107] The amount of ARG1 expression was shown to have a direct effect on tumor progression[108–110] by immunosuppression of macrophages due to M2 polarization and tumor cell support by providing polyamines and protecting them from cytotoxic NO influence. Via the metabolism of another amino acid, tryptophan, TAMs show a further immunosuppressive characteristic. The increased expression of the tryptophan degrading enzyme indoleamine-2,3-dioxygenase (IDO) causes T cell inhibition.[111]

3.5 Purpose of thesis

To improve the survival and clinical benefit of lymphoma patients, further investigation is needed. Up to now, lot of trials failed to achieve substantial improvement. With the increasing evidence of the importance of the TME on lymphoma cell survival, progression and especially on therapy response, the modulation of the TME has become a new field of interest for improving lymphoma therapy.

A central cell of the TME is the macrophage, the TAM. Its tumor-supportive functions have been widely described, but it was also shown that TAMs are central for the therapeutic effect of antibody-based therapy.[8] There is a wide range how macrophages are polarized and subsequently fulfil different functions. A central aspect for the polarization of macrophages is the metabolic status and metabolic modification of the cell. The activation or deactivation of several metabolic pathways have the opportunity to greatly influence and change the action of macrophages. It has been shown that these modulations also can be used to redirect tumor-supporting TAMs toward anti-tumor function.[17,59]

The lymphoma cells themselves have the ability for influencing macrophage metabolism and function to improve their pro-tumoral actions for their support.

Regarding the interplay of lymphoma cells and macrophages and the great influence of TAMs on therapy efficacy on the one hand and the metabolic sensitivity and plasticity of macrophages with great impact on their pro- or anti-tumoral function on the other hand, the metabolic modulation of macrophages opens up a new field of investigation to improve lymphoma therapy for increasing therapy efficacy and patients' survival.

In this study we aimed to investigate the influence of metabolic pathway modulation on the anti-lymphoma function and especially phagocytic capacity of macrophages in the context of antibody-based immunotherapy in DLBCL and other lymphoma entities.

Detected pathways, which have a positive effect on macrophages´ anti-lymphoma function, were explored in detail, the macrophage phenotype was determined and the treatment was transferred into primary human cells and *in vivo* settings to investigate the potential for clinical implementation.

4. PUBLICATION

Cell Reports
Medicine

Article

Macrophages are activated toward phagocytic lymphoma cell clearance by pentose phosphate pathway inhibition

Graphical abstract

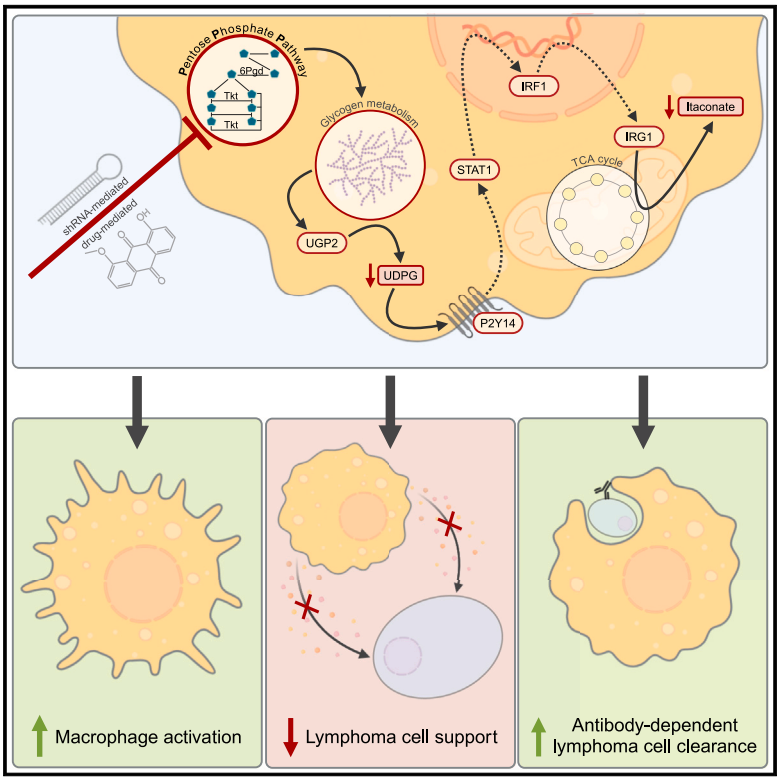

Authors

Anna C. Beielstein, Elena Izquierdo, Stuart Blakemore, ..., Marcus Krüger, Coral Barbas, Christian P. Pallasch

Correspondence

christian.pallasch@uk-koeln.de

In brief

Beielstein et al. have shown that the metabolic inhibition of the pentose phosphate pathway in macrophages leads to increased macrophage activation, less lymphoma cell support, and increased antibody-dependent lymphoma cell clearance by macrophages. A significantly improved overall survival in a therapeutic lymphoma mouse model is achieved.

Highlights

- Macrophage-mediated lymphoma cell phagocytosis is increased by PPP inhibition
- PPP inhibition is an immune-regulatory switch for macrophage function
- PPP inhibition is linked to the modulation of the UDPG-Stat1-Irg1-itaconate axis
- PPP inhibition is tolerable *in vivo* and boosts therapeutic B cell lymphoma targeting

Beielstein et al., 2024, Cell Reports Medicine *5*, 101830
December 17, 2024
https://doi.org/10.1016/j.xcrm.2024.101830

Cell Reports Medicine

CellPress
OPEN ACCESS

Article

Macrophages are activated toward phagocytic lymphoma cell clearance by pentose phosphate pathway inhibition

Anna C. Beielstein,[1,2] Elena Izquierdo,[1,2,3] Stuart Blakemore,[1,2] Nadine Nickel,[1,2] Michael Michalik,[2] Samruddhi Chawan,[1,2] Reinhild Brinker,[2] Hans-Henrik Bartel,[1,2] Daniela Vorholt,[1,2] Lukas Albert,[1,2] Janica L. Nolte,[2] Rebecca Linke,[1,2] Carolina Raíssa Costa Picossi,[4] Jorge Sáiz,[4] Felix Picard,[5,6] Alexandra Florin,[7] Jörn Meinel,[7] Reinhard Büttner,[7] Paul Diefenhardt,[6,8] Sebastian Brähler,[6,8] Alma Villaseñor,[4] Holger Winkels,[5,6] Michael Hallek,[1,2,6] Marcus Krüger,[1,2,6] Coral Barbas,[4] and Christian P. Pallasch[1,2,6,9,*]

[1]Department I of Internal Medicine, Centre for Integrated Oncology (CIO) Aachen-Bonn-Cologne-Duesseldorf, University Hospital Cologne, 50937 Cologne, Germany

[2]Cologne Excellence Cluster for Cellular Stress Responses in Ageing-Associated Diseases (CECAD), University of Cologne, 50931 Cologne, Germany

[3]Departamento de Ciencias Médicas Básicas, Facultad de Medicina, Instituto de Medicina Molecular Aplicada – Nemesio Díez (IMMA-ND), Universidad San Pablo-CEU, CEU Universities, Urbanización Montepríncipe, 28668 Boadilla del Monte, Spain

[4]Centro de Metabolómica y Bioanálisis (CEMBIO), Facultad de Farmacia, Universidad San Pablo-CEU, CEU Universities, Urbanización Montepríncipe, 28668 Boadilla del Monte, Spain

[5]Department III of Internal Medicine, Faculty of Medicine and University Hospital Cologne, University of Cologne, 50937 Cologne, Germany

[6]Centre for Molecular Medicine Cologne (CMMC), University of Cologne, 50937 Cologne, Germany

[7]Institute of Pathology, Faculty of Medicine and University Hospital Cologne, University of Cologne, 50937 Cologne, Germany

[8]Department II of Internal Medicine, Faculty of Medicine and University Hospital Cologne, University of Cologne, 50937 Cologne, Germany

[9]Lead contact

*Correspondence: christian.pallasch@uk-koeln.de

https://doi.org/10.1016/j.xcrm.2024.101830

SUMMARY

Macrophages in the B cell lymphoma microenvironment represent a functional node in progression and therapeutic response. We assessed metabolic regulation of macrophages in the context of therapeutic antibody-mediated phagocytosis. Pentose phosphate pathway (PPP) inhibition induces increased phagocytic lymphoma cell clearance by macrophages *in vitro*, in primary human chronic lymphocytic leukemia (CLL) patient co-cultures, and in mouse models. Addition of the PPP inhibitor S3 to antibody therapy achieves significantly prolonged overall survival in an aggressive B cell lymphoma mouse model. PPP inhibition induces metabolic activation and pro-inflammatory polarization of macrophages while it decreases macrophages' support for survival of lymphoma cells empowering anti-lymphoma function. As a mechanism of macrophage repolarization, the link between PPP and immune regulation was identified. PPP inhibition causes decreased glycogen level and subsequent modulation of the immune modulatory uridine diphosphate glucose (UDPG)-Stat1-Irg1-itaconate axis. Thus, we hypothesize the PPP as a key regulator and targetable modulator of macrophage activity in lymphoma to improve efficacy of immunotherapies and prolong survival.

INTRODUCTION

The tumor microenvironment (TME) represents a hallmark of cancer, and interactions between its transformed and non-transformed immune bystander cells determine disease progression and therapeutic response.[1] Tumor cells generate a tumor-supportive environment by cytokine and metabolite secretion. These mediators alter occurrence of bystander cells and shift the activity of the infiltrating immune cells from an anti- to a pro-tumoral response.[2] Tumor-associated macrophages (TAMs) play a critical role in promoting tumor growth, facilitating vascularization and metastasis and suppressing other immune cells.[3,4]

However, we have shown that macrophages are central for tumor cell clearance in aggressive B cell lymphoma during immunotherapy, although their phagocytic capacity becomes impaired by lymphoma cells.[5]

Recent decades have seen the development of numerous new treatment strategies for B cell malignancies, which have extended patient survival but struggled to substantially increase cure rates. The front-line strategy is chemo-immunotherapy, combining therapeutic antibodies like rituximab or obinutuzumab with chemotherapy. We demonstrated that leukemia cells in therapy-refractory niches reduce the engulfment of antibody-targeted tumor cells by macrophages, diminishing therapy efficacy and leading to relapse.[5]

Please cite this article in press as: Beielstein et al., Macrophages are activated toward phagocytic lymphoma cell clearance by pentose phosphate pathway inhibition, Cell Reports Medicine (2024), https://doi.org/10.1016/j.xcrm.2024.101830

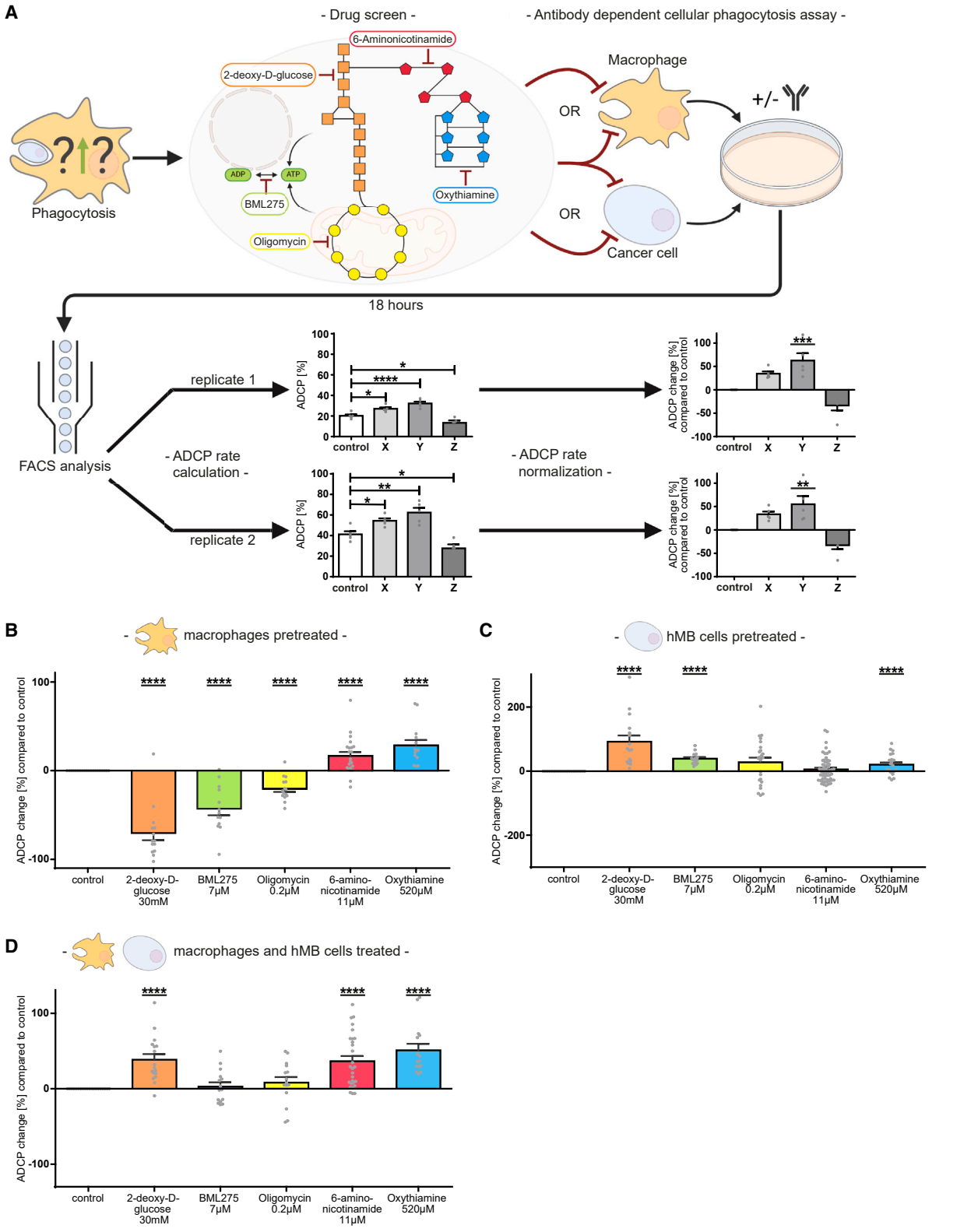

(legend on next page)

Macrophage function depends on their local environment, which impacts their differentiation and polarization. Macrophages are a heterogeneous population with different subtypes exerting pro-inflammatory and phagocytic (M1-like macrophages) and anti-inflammatory and tissue-regenerative (M2-like macrophages) activities. TAMs represent a blend of these characteristics tending toward the anti-inflammatory and phagocytic inactive phenotype.[6,7] The TME includes activation mediators such as cytokines, chemokines, and metabolites, which control the polarization of contained macrophages. Changes in the microenvironment can alter macrophage metabolism, which is crucial for polarization and the closely linked macrophage function.[8,9] Changes in the cellular metabolism have the ability to repolarize the macrophage phenotype by which pro-tumoral TAMs could acquire anti-tumoral activity.[10–12]

The interaction between macrophages and lymphoma cells, as well as macrophages metabolic sensitivity, opens up a promising strategy to optimize anti-cancer therapy. Modulating macrophage metabolism may improve their anti-tumor efficacy and diminish their tumor-supportive function.

In the present study, we demonstrate that pentose phosphate pathway (PPP) inhibition in macrophages increases their activity and phagocytic capacity whereby pro-tumoral bystander function is diminished. As a driving mechanism, we discovered a connection between metabolism and immune regulation by modulation of the UDPG-Stat1-Irg1-itaconate axis. The effects of PPP inhibition were transmitted into human patient samples and also reproduced *in vivo*, where significantly increased survival in an aggressive lymphoma mouse model was achieved. These results open up a promising field of treatment strategy against B cell malignancies in clinical use.

RESULTS

Metabolic inhibition of the PPP leads to increased phagocytic capacity of macrophages

To investigate how metabolic modulation of TAMs in the context of immunotherapy affects phagocytic capacity, we performed a metabolism-focused screening approach for antibody-dependent cellular phagocytosis (ADCP). Key metabolic pathways were blocked using representative inhibitors in a macrophage and humanized aggressive B cell lymphoma (hMB; cell line information see STAR Methods) co-culture-assay system, and phagocytosis was assessed through specific antibody targeting (alemtuzumab; anti-CD52) (Figure 1A). The antibody alemtuzumab was used as a tool compound for the first screening approach as several types of lymphoma downregulate CD20 expression but not CD52 expression, also seen in hMB cells. Several other antibodies, currently in clinical use, were investigated in further analysis.

Inhibition of glycolysis (via 2-deoxy-D-glucose), AMP-activated protein kinase (AMPK)-mediated cell energy regulation (via BML-275), mitochondrial ATP production (via oligomycin), and the PPP (via 6-aminonicotinamide and oxythiamine) was screened using non-toxic inhibitor concentrations (Figure S1). The inhibition was conducted in co-culture and by pre-treatment of each cell type (macrophage or hMB cell), to infer specific macrophage vs. lymphoma cell phagocytic interactions. As the basal phagocytosis rate of macrophages is variable, the change in phagocytosis under treatment was calculated in comparison to the basal phagocytosis rate (=ADCP change, Figures 1A and S2).

Glycolysis inhibition significantly increased ADCP rates in co-culture (+40%, $p < 0.01$) and by pre-treatment of lymphoma cells (+95%, $p < 0.0001$), while macrophage pre-treatment significantly diminished ADCP rate (−71%, $p < 0.001$) (Figures 1B–1D). Similarly, AMPK inhibition increased ADCP rate significantly by lymphoma cell pre-treatment (+39%, $p < 0.0001$) and significantly diminished ADCP rate by pre-treatment of macrophages (−42%, $p < 0.001$) (Figures 1C and 1D). Inhibition of mitochondrial ATP production also diminished ADCP rate significantly by macrophage pre-treatment (−21%, $p < 0.0001$) (Figure 1D).

Sole inhibition of the PPP induced significantly increased ADCP rates by co-culture treatment and macrophage pre-treatment. The increase was induced by both inhibition of the oxidative part of the PPP via 6-phosphogluconate dehydrogenase inhibition (6Pgd; inhibitor 6-aminonicotinamide) (co-culture +40% $p < 0.01$; macrophage pre-treatment +15%, $p < 0.05$) and inhibition of the non-oxidative part via transketolase inhibition (Tkt; inhibitor oxythiamine) (co-culture +51% $p < 0.001$; macrophage pre-treatment +28%, $p < 0.01$) (Figures 1B and 1D). Moreover, lymphoma cell pre-treatment with oxythiamine increased phagocytic rate significantly (+19%, $p < 0.0001$) (Figure 1C).

Of note, Tkt inhibition induced the highest increase in phagocytic capacity in the co-culture and by pre-treatment of macrophages in the screening approach.

Thus, inhibition of glycolysis, AMPK, and mitochondrial ATP production negatively affected macrophages' phagocytic capacity, while blocking PPP favored lymphoma cell clearance by macrophages.

Cross validation of PPP inhibition in macrophages confirms increased ADCP rates

To further investigate the PPP in the context of macrophages' function and as a target for improving immunotherapy, we applied alternative inhibitors (6Pgd: physcion, Tkt: *p*-hydroxyphenylpyruvate)[13,14] and confirmed significant increases in ADCP rates (physcion +26%, $p < 0.0001$; *p*-hydroxyphenylpyruvate +25%, $p < 0.001$) (Figure 2A). Additionally, we recapitulated the phagocytosis assays with the human monocyte cell line THP1 using an alternative antibody (obinutuzumab; anti-CD20

Figure 1. Metabolic inhibition of the pentose phosphate pathway leads to increased phagocytic rate of macrophages

(A) Scheme of ADCP-based metabolic screening approach.

(B–D) Summary of ADCP change compared to basal phagocytosis rate of J774A.1 macrophages under inhibition of respective metabolic pathways. (B) Inhibition of only macrophages. (C) Inhibition of only hMB cells. (D) Inhibition of all co-culture components. Technical replicates (B) $n = 15–22$, (C) $n = 15–58$, (D) $n = 15–28$; biological replicates (B) $n = 3–5$, (C) $n = 3–12$, (D) $n = 3–6$. Data are shown as mean ± SEM. *p* values were calculated using unpaired t test. $^{*}p < 0.05$; $^{**}p < 0.01$; $^{***}p < 0.001$; $^{****}p < 0.0001$. See also Figures S1 and S2.

Please cite this article in press as: Beielstein et al., Macrophages are activated toward phagocytic lymphoma cell clearance by pentose phosphate pathway inhibition, Cell Reports Medicine (2024), https://doi.org/10.1016/j.xcrm.2024.101830

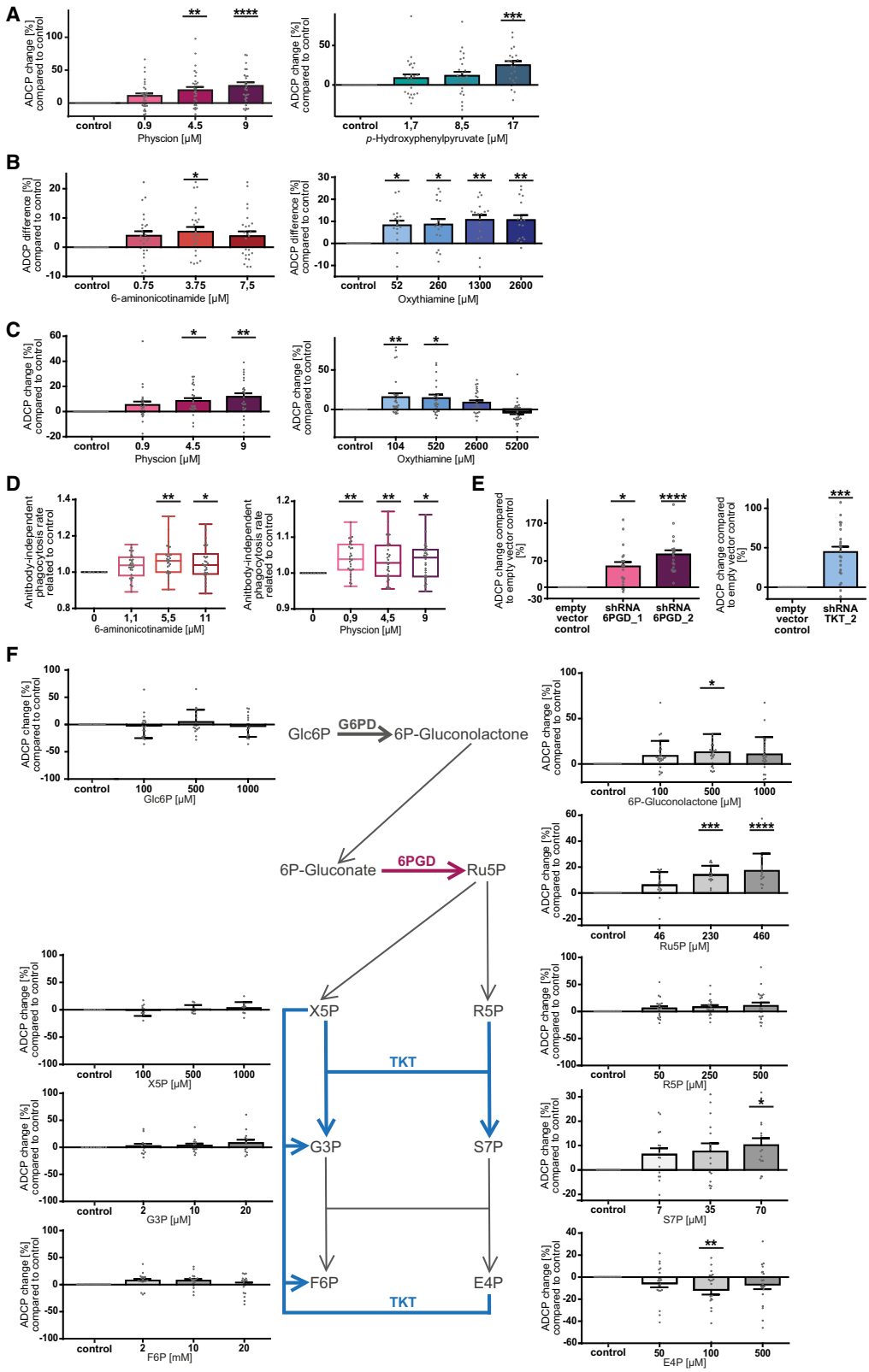

(legend on next page)

type II), also identifying significant induction of ADCP (6-aminonicotinamide $p < 0.05$; oxythiamine $p < 0.01$) (Figure 2B).

Since hypoxia is a functional aspect of the TME *in vivo*, we also conducted ADCP assays under hypoxic conditions (O_2 1.5%) and observed significantly increased ADCP rates (physcion +12%, $p < 0.01$; oxythiamine +20%, $p < 0.01$) (Figure 2C).

To evaluate if PPP inhibition also increases phagocytic capacity of macrophages without the targeting function of antibodies, we assessed antibody-independent cellular phagocytosis (AICP) (Figure 2D) and observed significantly increased AICP rates only by inhibition of the oxidative part of the PPP (6-aminonicotinamide $p < 0.01$, physcion $p < 0.01$) (Figure S3D).

To abrogate off-target effects of the PPP inhibitors, we generated short hairpin RNA (shRNA) knockdown for the respective enzymes in macrophages (Figures S3P–S3S). Silencing of 6Pgd and Tkt significantly increased macrophages' ADCP rates (6Pgd +87%, $p < 0.0001$; Tkt +45%, $p < 0.001$) (Figure 2E).

Altogether, we demonstrate that PPP enzyme inhibition by metabolic inhibitors as well as 6Pgd and Tkt knockdown in macrophages promotes phagocytosis of lymphoma cells and warrants further investigation of the molecular function.

Increased phagocytosis is driven by PPP enzyme inhibition and not by PPP metabolite shifting

To identify which specific components and metabolites of the PPP directly affect phagocytic function, we performed ADCP assays with supplementation of single educts and products of the PPP (Figure 2F). We observed unaltered ADCP rates using the non-exclusive PPP metabolites glucose-6-phosphate (Glc6P), ribose-5-phosphate (R5P), xylulose-5-phosphate (X5P), glyceraldehyde-3-phosphate (G3P), and fructose-6-phosphate (F6P). In contrast, supplementation of the PPP-exclusive glucose-6-phosphate dehydrogenase (G6pd) product 6-phosphogluconolactone significantly increased ADCP rate (+13%, $p < 0.05$), as well as the products of 6pgd (ribulose-5-phosphate [Ru5P]; +17%, $p < 0.0001$) and of Tkt (sedoheptulose-7-phosphate [S7P]; +20%, $p < 0.05$) (Figure 2F; right panel). In contrast, supplementing the Tkt educt erythrose-4-phosphate (E4P) significantly reduced ADCP rate (−12%, $p < 0.01$) (Figure 2F; right panel).

In conclusion, products of Tkt and 6Pgd promote macrophages' phagocytic activity while enzyme educts diminish it, indicating that inhibition of the enzymes itself and not a decrease in their products causes increased phagocytic capacity.

PPP inhibition induces pro-inflammatory polarization and activation in macrophages

To test whether PPP inhibition alters macrophage differentiation and activation, we assessed expression of markers delineating polarization by flow cytometry (Figures 3A and 3B; Table S1). We observed a trend of increased M1-like marker expression and decreased M2-like and TAM marker expression under PPP inhibition and knockdown.

To evaluate macrophage morphology, we performed fluorescent microscopy (Figure 3C). Under PPP inhibition the macrophages underwent a profound change in morphology from a round, centered appearance to a spread and outlaying phenotype with filopodia surrounding the cell body.

As macrophages' metabolic status greatly influences their activity and polarization, we assessed glycolytic and mitochondrial activity with the Seahorse XF Mito Stress test (Figures 3D–3G, Figure S4). We observed a significant increase of the oxygen consumption rate (OCR) ($p < 0.0001$) and extracellular acidification rate (ECAR) ($p < 0.0001$) (Figure 3D) indicating an increased mitochondrial respiration and glycolytic activity and thus an increased metabolic activity of macrophages. Further analysis identified significant increase of mitochondrial basal activity (physcion $p < 0.01$; oxythiamine $p < 0.001$), mitochondrial maximal capacity (physcion $p < 0.05$; oxythiamine $p < 0.01$), glycolytic maximal capacity (physcion $p < 0.05$; oxythiamine $p < 0.001$), and ATP production (physcion $p < 0.05$; oxythiamine $p < 0.0001$) of macrophages (Figures 3E–3G).

Taken together, these data show an activation of macrophages by shifted polarization, cytoskeletal reorganization, and increased metabolic activity under PPP inhibition as possible functional basis of increased phagocytosis.

PPP inhibition changes the proteomic profile of macrophages toward pro-inflammatory activity

To investigate the mediators of increased phagocytic capacity in macrophages, we performed a multi-omics (proteomics, phosphoproteomics, and metabolomics) screening under chemical or shRNA-mediated PPP inhibition.

A uniform regulation pattern of proteins involved in macrophage polarization and activation was observed by the use of independent inhibitors and PPP enzyme knockdowns (Figures 4A and 4B, Table S2). Under compound-mediated PPP inhibition, the anti-inflammatory proteins Ptgs1, Sqstm1, and Ybx3[15–17]

Figure 2. Cross validation of PPP inhibition in macrophages confirms increased ADCP rates

(A–C) ADCP change compared to basal phagocytosis rate of J774A.1 macrophages under inhibition of PPP. (A) Alternative inhibitor physcion of 6-phosphogluconate dehydrogenase (6Pgd) in oxidative part of PPP (red) and *p*-hydroxyphenylpyruvate for inhibition of transketolase (Tkt) in non-oxidative part of PPP (blue). (B) Using human monocyte cell line THP1 and CD20 antibody obinutuzumab under inhibition of 6Pgd by 6-aminonicotinamide (red) and inhibition of Tkt by oxythiamine (blue). (C) ADCP assay performed under hypoxic conditions and inhibition of 6Pgd by physcion (red) or inhibition of Tkt by oxythiamine (blue). (D) Antibody-independent cellular phagocytosis of hMB cells by J774A.1 macrophages compared to control under inhibition of 6Pgd by 6-aminonicotinamide (left) and physcion (right).

(E) ADCP change compared to basal phagocytosis rate of empty vector control J774A.1 macrophages under shRNA-mediated knockdown of 6Pgd (red) and Tkt (blue).

(F) ADCP change compared to basal phagocytosis rate of J774A.1 macrophages under supplementation of metabolites of the PPP. Enzyme reactions in focus colored in violet (6Pgd) and blue (Tkt). *E4P*, erythrose-4-phosphate; *F6P*, fructose-6-phosphate; *G3P*, glyceraldehyde-3-phosphate; *Glc6P*, glucose-6-phosphate; *R5P*, ribose-5-phosphate; *Ru5P*, ribulose-5-phosphate; *S7P*, sedoheptulose-7-phosphate; *X5P*, xylulose-5-phosphate. Data are shown as mean ± SEM. Technical replicates (A) $n = 30$, (B) $n = 17–25$, (C) $n = 25–28$, (D) $n = 30$, (E) $n = 20–23$, (F) $n = 13–20$; biological replicates (A) $n = 6$, (B) $n = 4–5$, (C) $n = 5–6$, (D) $n = 6$, (E) $n = 4–5$, (F) $n = 3–4$. *p* values were calculated using one-way ANOVA. $^*p < 0.05$; $^{**}p < 0.01$; $^{***}p < 0.001$; $^{****}p < 0.0001$. See also Figures S1 and S3.

Please cite this article in press as: Beielstein et al., Macrophages are activated toward phagocytic lymphoma cell clearance by pentose phosphate pathway inhibition, Cell Reports Medicine (2024), https://doi.org/10.1016/j.xcrm.2024.101830

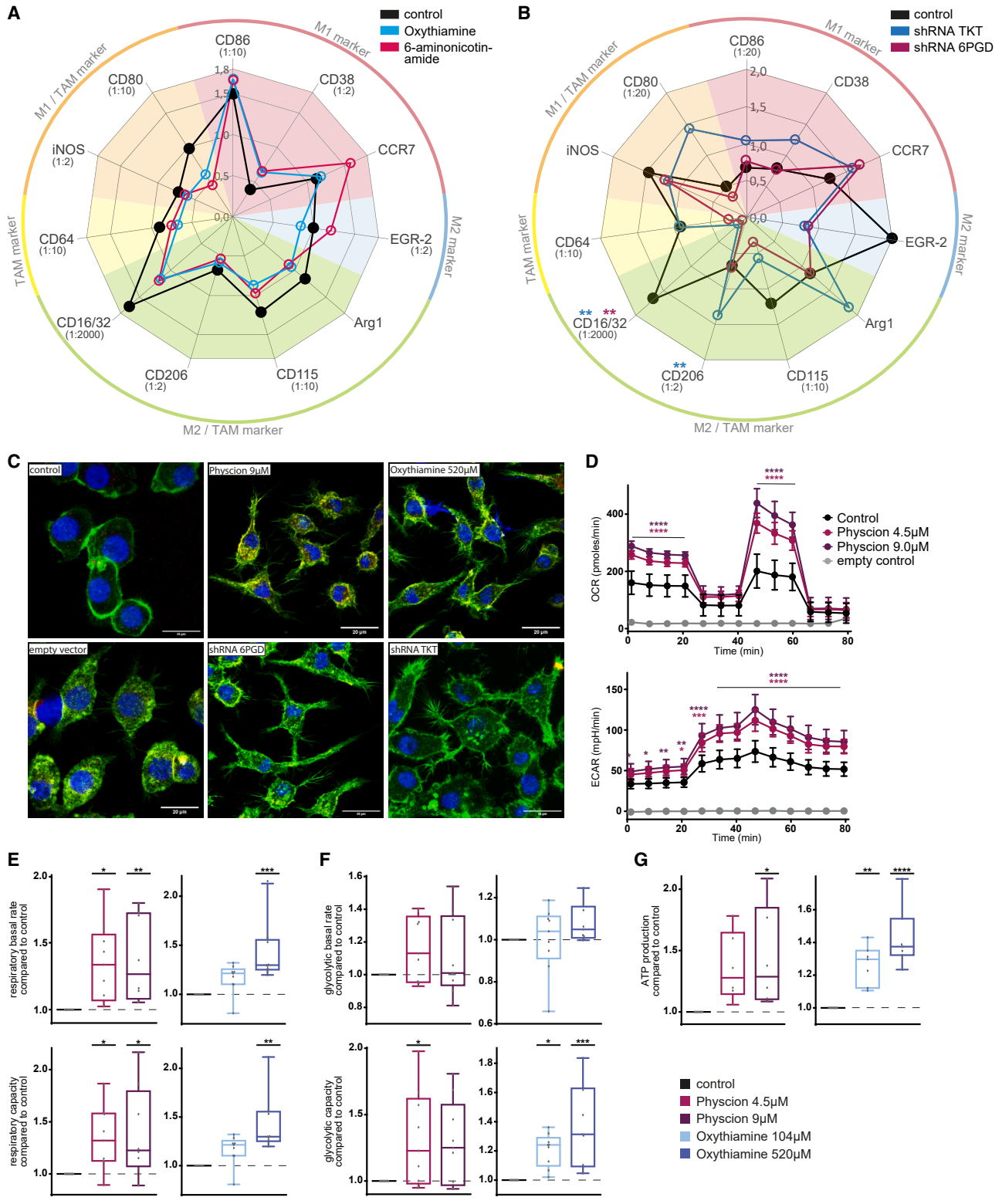

Figure 3. PPP inhibition induces pro-inflammatory polarization and activation in macrophages

(A and B) Radar plot of surface marker expression of J774A.1 macrophages. Expression of characteristic surface marker for different macrophage subtypes measured by immunofluorescent staining. Mean fluorescence intensity (MFI) is depicted. To improve readability, high MFI has been downscaled (factor named in brackets next to marker). (A) Compound mediated PPP inhibition. (B) shRNA-mediated PPP knockdown.

(legend continued on next page)

and the TAM- and M2-typical proteins Hagh and Ezr[18,19] were significantly downregulated, while the pro-inflammatory proteins Pam16 and Gosr1 were significantly upregulated (Figure 4A). By using shRNA, an even more pronounced regulation was seen. Negative regulators of cytokine expression and pro-inflammatory signaling were significantly downregulated while promoters of pro-inflammatory activation were significantly upregulated (Atg16l1, Cast, Csf1r, Cybb, Inppl1, Oas3, Parp14, Fkbp5, Ilf2, Tlr7).[20,21] Moreover, there was a significant increase in protein expression needed for phagocytosis (Actn1, Actr1a, Iqgap3, Itgav, Lrp1, Myl12a, Necap1, Sh3bp1) (Figure 4B; for phosphoproteomic analysis see Table S3).

We performed pathway enrichment analysis for functional annotation (Figures 4C and 4D), showing similar enrichment clusters for both compound-mediated and shRNA-mediated inhibition of the oxidative and the non-oxidative part of the PPP. A strong enrichment was seen for immune activity (Figure 4C) including cytokine signaling, antigen processing, and antigen presentation with up to 124 involved proteins and significantly changed phosphorylation patterns (Figure 4D). Moreover, enrichment in proteins relevant to phagocytosis and cytoskeletal organization was observed. In line with our metabolic flux analysis (Figures 3D–3G), we observed great enrichment for proteins influencing mitochondrial and glycolytic activity (Figure 4C). Particularly analysis of phosphoproteomics uncovered a significant enrichment in signaling pathways important for immune signaling (mitogen-activated protein kinase [Mapk]-Erk, Egf/Egfr, p53, Pi3k-Akt) and metabolic regulation (Pi3k-Akt, Hif1a) (Figure 4D).

To further analyze the impact of altered protein phosphorylation, we performed an adapted upstream kinase analysis on the basis of integrative inferred kinase activity (INKA) analysis (Table S4).[22] The five most inactivated kinases are displayed (Figure 4E), highlighting the decrease of Hck in the normalized upstream kinase score (NUKS). Hck supports M2-like macrophage polarization, TAM activity, tumor growth, and tumor cell evasion[23] and activates the Csf1 receptor (Csf1r).[24] Csf1r signaling likewise induces M2-like macrophage polarization.[25] Csf1r and its downstream kinase Mapk1 were also one of the five most inactivated kinases (Figure 4E). In combined analysis of PPP inhibitors, the Csf1r downstream kinase Ptk2b (Pyk2) was the most negatively regulated kinase (Figure 4F). Accordingly, a significant downregulation of Ptk2b in PPP knockdown macrophages was observed (Figures 4G and S5A). Furthermore, the most downregulated protein in both knockdown macrophages was Sema4d (Figure 4B), which is an activator of the Ptk2b pathway.[26]

Following the Csf1r pathway further downstream (Figure 4H), decreased immune-regulatory gene 1 (Irg1 = Acod1) expression, a major node in immunosuppressive regulation of macrophages, was seen in proteomic analysis (Table S2). Changed Irg1 expression is one possible mechanism leading to altered macrophage activity and phagocytosis.[27] With the exception of Hmox-1, all included signal molecules of the regarded Csf1r pathway were significantly downregulated in proteomic analysis (Figure 4H) (Table S2).

PPP inhibition modulates glycogen metabolism and the immune response signaling axis UDPG-Stat1-Irg1-itaconate of macrophages

Regarding the critical role of Irg1 on macrophage polarization, we aimed to explore the connection between metabolic modulation, Irg1 regulation, and the resulting macrophage phenotype.

PPP and glycogenolysis activity are coupled causing suppression of both pathways if one is inhibited.[28] We quantified glycogen levels identifying significant decreased glycogen amount under all conditions ($p < 0.0001$, Figure 5A). Glycogen metabolism influences signaling regulating Stat1 activity.[28] Thus, we hypothesized that inhibition of PPP would lead to suppression of glycogenolysis with subsequent decreased uridine diphosphate glucose (UDPG) production and thereby to an inhibition of P2y14 expression with following decreased Stat1 activity. Decreased Stat1 activity leads to less Irf1 and thereby to a decreased Irg1 expression, which possibly leads to functional increasing macrophage activity and phagocytosis.[29,30]

To validate this hypothesis, we performed western blot analysis of the hypothesized pathway-associated proteins and identified significant reductions in expression ($p < 0.0001$, Figure 5B) with the highest decline of Irg1 amount (>80%, $p < 0.0001$, Figure S5). The hypothesized pathway linking PPP activity and Irg1 expression is displayed in Figure 5C.

As Irg1 acts as a metabolic enzyme and changes in immune activity are driven by its product itaconate, we investigated the connection between metabolism and enzyme expression by metabolomic assessment (Tables S5 and S6) and compared it to changes in enzyme expression of interest detected in proteomics (Table S2) (Figures 5D and S4C).

The metabolomic screening[31] confirmed a significantly decreased amount of exclusive 6Pgd and Tkt products ribulose-5-phosphate and sedoheptulose-7-phosphate ($p < 0.0001$, Figure 5D) in 6pgd and Tkt knockdown macrophages, while drug-mediated inhibition did not show a significantly decreased amount (Figure S4C).

In line with the hypothesized pathway, a significant downregulation of Irg1 was observed under PPP inhibition ($p < 0.01$) with subsequent significantly decreased amount of itaconate ($p < 0.0001$) (Figure 5E). Itaconate is an inhibitor of succinate dehydrogenase (Sdh). Accordingly, there was a significant

(C) Immunofluorescent microscopy of J774A.1 macrophages under compound-mediated PPP inhibition and shRNA-mediated PPP knockdown. Blue, phalloidin staining of nucleus; green, actin staining of cytoskeleton.

(D–G) Measurement of metabolic activity of J774A.1 macrophages under compound-mediated PPP inhibition by Seahorse analysis. Inhibition of non-oxidative part of PPP by oxythiamine, inhibition of oxidative part of PPP by physcion. (D) One representative example of XF Mito Stress test measurement of ECAR und OCR. (E) Respiratory basal rate and capacity. (F) Glycolytic basal rate and capacity. (G) ATP production. Data are shown in (A and B) as mean of four replicates, in (D) as mean of six replicates in one experiment ±SD, and in (E–G) as mean ± 5–95 percentile. Technical replicates (A and B) $n = 4$, (D) $n = 6$, (E–G) $n = 18–27$; biological replicates (A and B) $n = 4$, (D) $n = 1$, (E–G) $n = 6–9$. p values were calculated using one-way ANOVA, (D) using two-way ANOVA. $^{*}p < 0.05$; $^{**}p < 0.01$; $^{***}p < 0.001$; $^{****}p < 0.0001$. See also Figure S4 and Table S1.

Please cite this article in press as: Beielstein et al., Macrophages are activated toward phagocytic lymphoma cell clearance by pentose phosphate pathway inhibition, Cell Reports Medicine (2024), https://doi.org/10.1016/j.xcrm.2024.101830

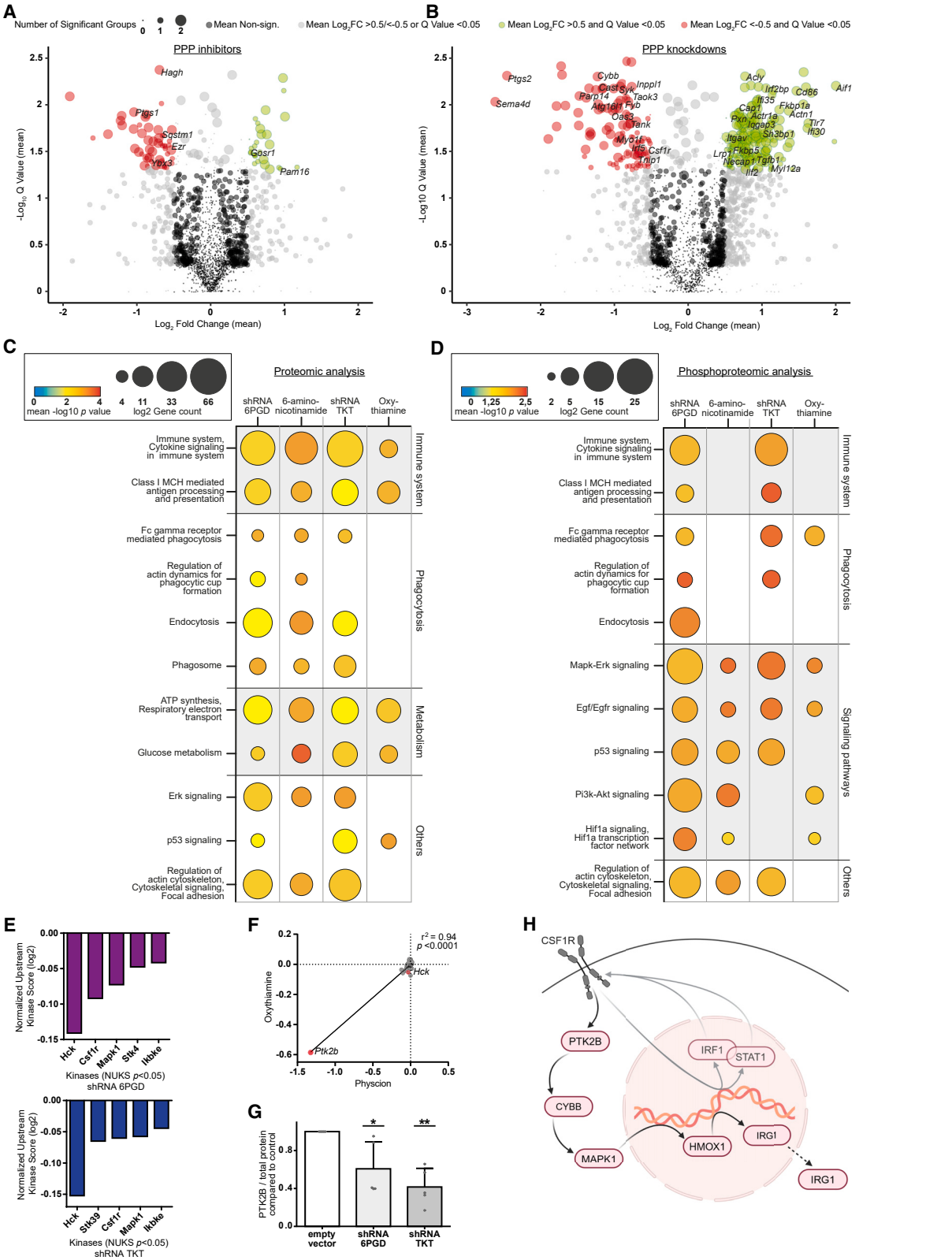

(legend on next page)

decrease of the Sdh educt succinate ($p < 0.001$) and a significant increase of the Sdh product malate ($p < 0.0001$) (Figure 5E). This indicates less suppression of Sdh due to decreased itaconate production by which mitochondrial oxidative activity is increased as observed in the metabolic flux analysis (Figures 3F and 3G). Besides the use of citrate for itaconate production, citrate is also an educt of the ATP citrate lyase (Acly) for acetyl-coenzyme A production. It has been shown that Acly activity is an inducer of macrophage activation and supports pro-inflammatory cytokine production—for example interleukin (IL)-6—in macrophages.[32] In proteomic analysis a significant increase of Acly expression under PPP inhibition was observed ($p < 0.01$, Figure 5E).

Itaconate is widely known as a regulatory immunosuppressive metabolite in macrophages, which promotes anti-inflammatory IL-10 secretion and inhibits pro-inflammatory IL-6 secretion.[27] Moreover, we observed significantly increased nuclear factor κB1 expression under PPP inhibition and knockdown (Table S2), an activator of IL-6 and inhibitor of IL-10 production. In line with these findings, we observed significantly increased IL-6 secretion ($p < 0.05$, Figure 5F) and significantly decreased IL-10 secretion ($p < 0.0001$, Figure 5G) by PPP inhibition.

To further prove the functional role of the Irg1-itaconate pathway, we evaluated the phagocytic activity of macrophages of $Irg1^{-/-}$ knockout mice. A significantly increased phagocytic activity of bone marrow-derived macrophages in ADCP assay *ex vivo* was observed in comparison to $Irg1^{+/+}$ wild-type mice (+34%, $p < 0.05$, Figure 5H).

In conclusion, we connected metabolic activity and immune regulation in macrophages via the UDPG-Stat1-Irg1-itaconate signaling axis provoked by PPP activity. Irg1 downregulation increases macrophage activation via itaconate reduction with subsequent metabolic activation and a pro-inflammatory shift in cytokine secretion. This also leads *in vivo* to an increased phagocytic capacity of macrophages.

PPP inhibition in primary human cells increases phagocytic capacity of macrophages and decreases their bystander function

To translate our findings into human context, we isolated primary human monocytes from healthy donors and differentiated them into macrophages by macrophage colony stimulating factor (M-CSF) under PPP inhibition. After testing cytotoxicity of the PPP inhibitors to primary human macrophages, ADCP assays with non-toxic concentrations of inhibitors were performed. Inhibition of both parts of the PPP significantly increased ADCP rates (physcion +64%; oxythiamine +92%, $p < 0.0001$, Figures 6A and 6B). The human macrophages showed a similar switch toward pro-inflammatory cytokine secretion with significantly increased IL-6 ($p < 0.05$) and significantly decreased IL-10 secretion ($p < 0.0001$) (Figures 6C and 6D).

To address effector function of macrophages in the context of primary human leukemia cells, primary chronic lymphocytic leukemia (CLL) cells of five individual patients were used for ADCP assays. A significant increase of phagocytosis was observed under PPP inhibition (+22%, $p < 0.001$, Figure 6E) and by using knockdown macrophages (Tkt +60%; 6Pgd +92%, $p < 0.0001$, Figure 6F) (Figures S6C and S6D).

To evaluate phagocytosis in a fully human setting, we performed ADCP assay with primary human monocyte-derived macrophages differentiated in the presence of PPP inhibitors and primary CLL patient cells (12 individual patients). A significantly increased phagocytic capacity was observed (+24%, $p < 0.0001$, Figures 6G and S6E). Thereby, we have demonstrated that primary indolent lymphoma and primary human macrophages are also affected by PPP modulation.

Beyond the inefficient phagocytic function, TAMs exert direct supportive effects on tumor cells. CLL cells depend on macrophages as "nurse-like" bystander cells to survive.[33] Macrophages in the microenvironment of CLL are polarized toward tumor-promoting TAMs and support CLL cells by chemokine secretion and immunosuppressive signaling. We therefore evaluated the effect of PPP-inhibited macrophages on primary CLL cells. Interestingly, PPP inhibition in mono-cultured primary CLL cells decreased their viability significantly ($p < 0.0001$, Figure 6H, left), as well as inhibition of the non-oxidative part of the PPP in co-culture ($p < 0.01$, Figure 6H, right).

As TAMs are also important mediators in chemotherapy resistance, we evaluated if the co-cultivation under PPP inhibition affects the susceptibility of primary CLL cells toward apoptosis by chemotherapy. We observed significantly increased bendamustine-induced apoptosis among primary CLL cells under inhibition of both parts of the PPP ($p < 0.001$, Figures 6I–6L) (for individual patient data see Figures S6F–S6J). This boost in apoptosis was achieved by

Figure 4. PPP inhibition changes the proteomic profile of macrophages towards pro-inflammatory activity

(A and B) Volcano plots showing mean change of proteomic transcription under (A) compound-mediated PPP inhibition by 6-aminonicotinamide and oxythiamine compared to untreated J774A.1 macrophages and (B) shRNA-mediated PPP knockdown of 6Pgd and Tkt compared to empty vector control J774A.1 macrophages. Circle size represents number of significantly changed conditions. Red circles: significantly downregulated abundance; green circles: significantly upregulated abundance. Proteins known to participate in immune system are annotated in significant groups.

(C and D) Pathway enrichment analysis of (C) proteomics and (D) phosphoproteomics of J774A.1 macrophages under compound-mediated PPP inhibition and shRNA-mediated PPP knockdown. Protein count in listed pathways represented in circle size, mean −log10 *p* value represented in heatmap analysis.

(E and F) Analysis of significantly negative changed protein activity in *normalized upstream kinase score* (*NUKS*). (E) Top five most downregulated enzymes in *NUKS* analysis under shRNA-mediated PPP knockdown of 6Pgd and Tkt and (F) integrative analysis of compound-mediated PPP inhibition by physcion and oxythiamine.

(G) Western blot analysis of Ptk2b expression in J774A.1 macrophages under shRNA-mediated PPP knockdown of 6Pgd and Tkt compared to empty vector control.

(H) Scheme of hypothesized mechanism leading to pro-inflammatory phenotype of macrophages. In (G) data are shown as mean ± SEM. Technical replicates (A–F) $n = 1$, (G) $n = 5$; biological replicates (A–F) $n = 3$, (G) $n = 5$. *p* values in (G) were calculated using one-way ANOVA. $^{*}p < 0.05$; $^{**}p < 0.01$; $^{***}p < 0.001$; $^{****}p < 0.0001$. See also Tables S2–S5.

Please cite this article in press as: Beielstein et al., Macrophages are activated toward phagocytic lymphoma cell clearance by pentose phosphate pathway inhibition, Cell Reports Medicine (2024), https://doi.org/10.1016/j.xcrm.2024.101830

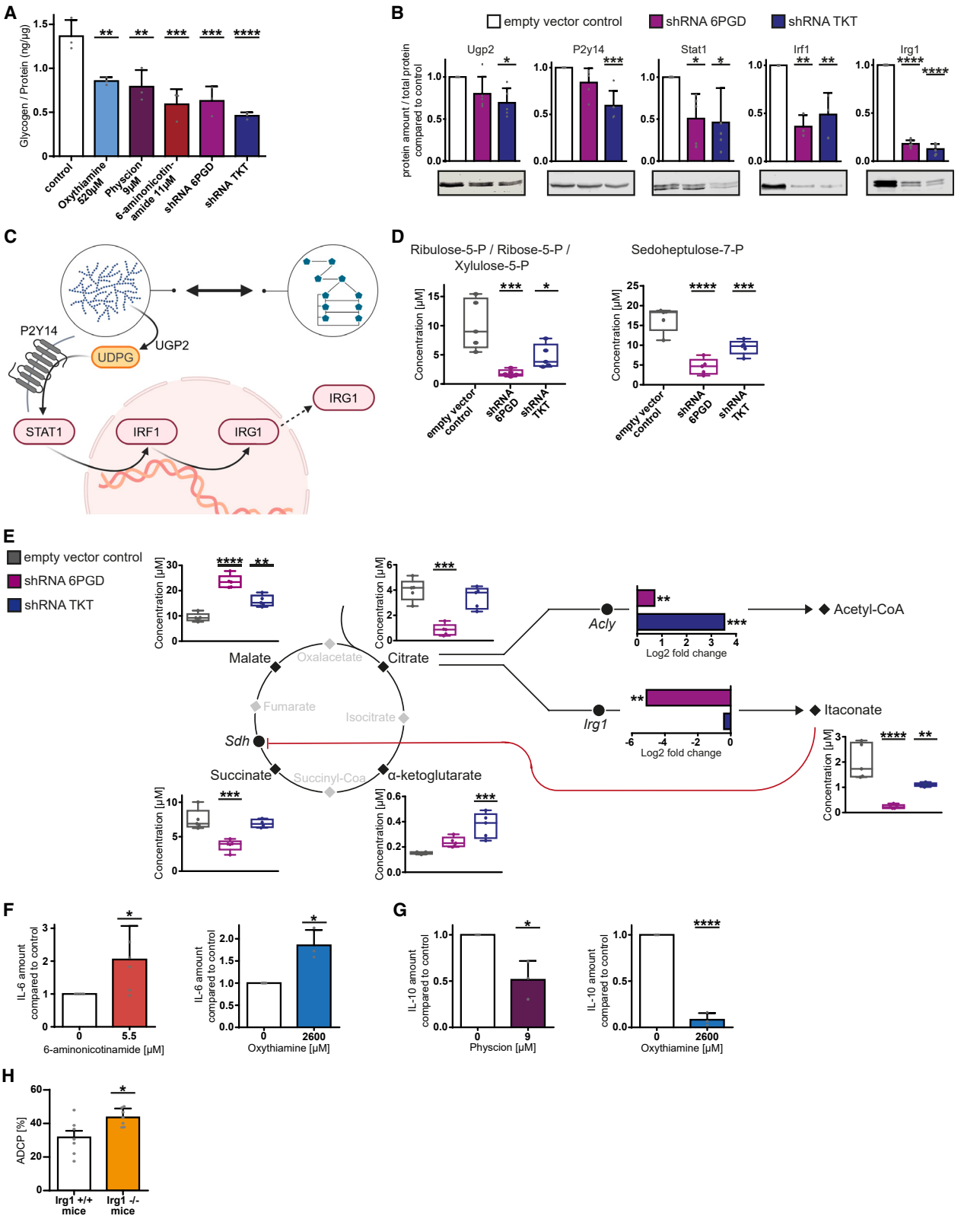

(legend on next page)

PPP inhibition in co-culture ($p < 0.001$, Figures 6I and 6K) and by macrophages pre-treatment before exposing them to primary CLL cells ($p < 0.01$, Figures 6J and 6L).

These observations underline the role of altered macrophage support under PPP inhibition in the TME such as direct leukemia cell support or resistance to chemotherapy.

PPP inhibition increases macrophages' maturation and pro-inflammatory polarization *in vivo*

To evaluate if PPP inhibition preserves its effect on macrophages *in vivo*, we treated C57BL/6J mice with the PPP inhibitor S3 (1-hydroxy-8-methoxy-anthraquinone). S3 is a more stable derivate of the 6Pgd inhibitor physcion.[13]

Investigating the myelopoiesis under PPP inhibition, a significant increase of cells in the LSK compartment (Lin^-, $Sca\text{-}1^+$, $c\text{-}Kit^+$) was seen ($p < 0.0001$, Figure 7A). PPP inhibition significantly increased the amount of hematopoietic stem cells (HSCs; $p < 0.05$, Figure 7B) and multipotent progenitor (MPP) cells (Figure 7B), including MPP pools known to fuel the myeloid compartment (MPP2 $p < 0.001$; MPP3 $p < 0.01$; MPP5 $p < 0.01$, Figure 7B).[34,35] This coincided with a significantly increased frequency of myeloid progenitor cells ($p < 0.01$, Figure 7C) and macrophages ($p < 0.001$, Figure 7C) in the bone marrow, indicating propelled myelopoiesis.

We further investigated the polarization of *in vivo* macrophages (Table S8) and detected a shift away from M2-like subtype with significantly decreased Arg1 expression ($p < 0.05$) and toward pro-phagocytic M1-like subtype with significantly increased CD38 expression ($p < 0.05$) in unstimulated peritoneal macrophages (Figure 7D) (for other compartments see Figure S7A). These findings are in line with our *in vitro* observations.

Moreover, *in vivo* PPP inhibition significantly increased phagocytic activity of bone marrow-derived macrophages in ADCP assay *ex vivo* (+74%, $p < 0.001$, Figure 7E).

Altogether, we have shown that PPP inhibition *in vivo* activates macrophages' inflammatory polarization and maturation as well as their phagocytic capacity, which increases their anti-tumor function *in vivo*.

PPP inhibition boosts anti-leukemic treatment and thereby prolongs survival in an aggressive lymphoma mouse model

To focus on the therapeutic effect of PPP inhibition *in vivo*, we evaluated treatment effects in an aggressive lymphoma mouse model.

We used the humanized double-hit lymphoma mouse model (hMB),[36] which is amenable for modeling human-specific antibody therapy. We treated the mice with the therapeutic antibody alemtuzumab and the PPP inhibitor S3. As the lymphoma reflects aggressive disease, untreated mice died rapidly after tumor cell injection (median overall survival [mOS] 22 days, Figure 7F). By treatment with S3 only, this rapid tumor progression persisted. As shown in our previous work, treatment with alemtuzumab increases survival significantly in this aggressive lymphoma mouse model[5] (mOS 25 days, $p = 1.4e{-}05$, Figures 7F and S7B). By adding the PPP inhibitor S3 to alemtuzumab, an additional significant prolongation of mouse survival was achieved in comparison to antibody treatment only (mOS 27 days, $p = 0.0059$, Figures 7F and S7B) with a stable increased number at risk up to day 25 (survival of 88%, Figure 7F). Immunohistochemical analysis of spleens showed a marked reduction of $CD19^+$ lymphoma cell infiltration with concomitant increase of $CD68^+$ macrophage infiltration after treatment with alemtuzumab and S3 in comparison to vehicle control (Figures 7G and S7C).

We finally demonstrated *in vivo* that PPP inhibition in the context of a highly aggressive lymphoma model increases the efficacy of antibody therapy to prolong overall survival significantly.

DISCUSSION

TAMs are key drivers in various cancers associated with poor outcome and diminished efficacy of immunotherapies.[1,3,5] The influence of glucose and mitochondrial metabolism on macrophages' polarization and activity has been established.[8,9,37] Activation of the PPP in macrophages has been implicated in immune tolerance and granuloma formation.[38,39] However, no

Figure 5. PPP inhibition modulates glycogen metabolism and the immune response signaling axis UDPG-Stat1-Irg1-itaconate of macrophages

(A) Total glycogen amount in J774A.1 macrophages under compound-mediated PPP inhibition and shRNA-mediated knockdown of 6Pgd and Tkt.

(B) Western blot analysis of protein expression of hypothesized connecting pathway in J774A.1 macrophages under shRNA-mediated knockdown of 6Pgd and Tkt compared to empty vector control. Mean expression displayed in bar graph analysis and one representative western blot example.

(C) Scheme of working hypothesis of PPP metabolism modulating immune response.

(D) Amount of 6pgd product ribulose-5-phosphate and Tkt product sedoheptulose-7-phosphate under shRNA-mediated inhibition of 6pgd and Tkt in J774A1 macrophages.

(E) Metabolomic analysis of tricarboxylic acid cycle and citrate metabolism with display of enzyme expression of key enzymes under shRNA-mediated PPP knockdown of 6Pgd and Tkt compared to empty vector control J774A.1 macrophages. Amount of metabolites displayed in box and whiskers. Change in enzyme expression displayed in bar graphs. Genes: succinate dehydrogenase (Sdh), ATP citrate lyase (Acly), immunoregulatory gene 1 (Irg1 = Acod1).

(F and G) Cytokine expression under 6Pgd inhibition by 6-aminonicotinamide or physcion and Tkt inhibition by oxythiamine in J774A.1 macrophages. (F) IL-6 expression compared to untreated control. (G) IL-10 expression compared to untreated control.

(H) ADCP assay of bone marrow-derived macrophages of $Irg1^{+/+}$ wild-type mice and $Irg1^{-/-}$ knockout mice. Macrophages differentiated out of femoral bone marrow with M-CSF. In (A), (B), and (F–H), bar plots are shown as mean ± SEM; in (D and E) metabolite amount is shown as minimum to maximum and protein expression is shown as calculated −Log2 fold change of control and knockdown macrophages. Technical replicates (A) $n = 15$, (B) $n = 3$–6, (D) $n = 3$, (E) $n = 3$, (F and G) $n = 9$–18, (H) $n = 35$; biological replicates (A) $n = 3$, (B) $n = 3$–6, (D) $n = 3$, (E) $n = 3$, (F and G) $n = 3$–6, (H) $n = 7$. p values were calculated in (A, B, D, and E) using one-way ANOVA, protein expression in (E) using student's t test, and in (F–H) using unpaired t test. $^*p < 0.05$; $^{**}p < 0.01$; $^{***}p < 0.001$; $^{****}p < 0.0001$. See also Figures S4 and S5 and Tables S6 and S7.

Please cite this article in press as: Beielstein et al., Macrophages are activated toward phagocytic lymphoma cell clearance by pentose phosphate pathway inhibition, Cell Reports Medicine (2024), https://doi.org/10.1016/j.xcrm.2024.101830

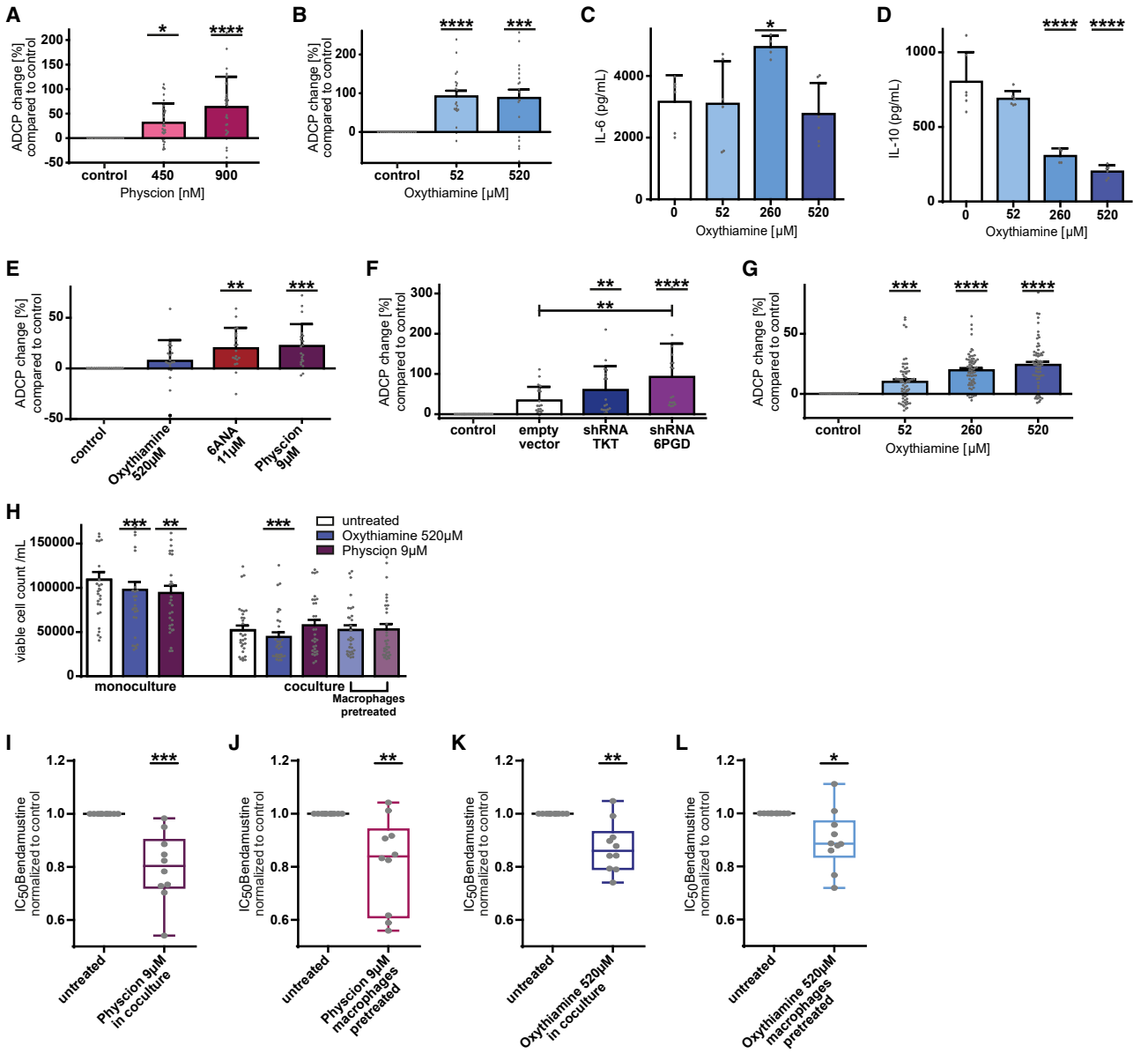

Figure 6. PPP inhibition in primary human cells increases phagocytic capacity of macrophages and decreases their tumor-supportive bystander function

(A and B) ADCP change compared to basal phagocytosis rate of human monocyte-derived macrophages. (A) ADCP change of monocyte-derived macrophages differentiated in the presence of physcion and M-CSF, (B) ADCP change of monocyte-derived macrophages differentiated in the presence of oxythiamine and M-CSF.

(C and D) Cytokine expression of monocyte-derived macrophages differentiated in the presence of oxythiamine and M-CSF. (C) IL-6 expression, (D) IL-10 expression.

(E and F) ADCP change of J774A.1 macrophages phagocyting primary CLL patient cells compared to basal phagocytosis rate. (E) ADCP change under compound-mediated PPP inhibition. (F) ADCP change under shRNA-mediated PPP knockdown.

(G) ADCP change of monocyte-derived macrophages differentiated in the presence of oxythiamine and M-CSF phagocyting primary CLL patient cells compared to basal phagocytosis rate.

(H) Viability of primary CLL patient cells after incubation with PPP inhibitors physcion or oxythiamine in mono-culture and in co-culture with J774A.1 macrophages. In co-culture setting, cells were treated in parallel or macrophages were pre-treated before onset of co-culture.

(I–L) Half maximal inhibitory concentration (IC_{50}) for individual primary CLL patient cell samples to bendamustine treatment compared to control. Cells were incubated with bendamustine after protective macrophage co-culture with untreated J774A.1 macrophages vs. PPP inhibition. (I and J) Inhibition of 6Pgd in oxidative part of PPP by physcion, (I) co-culture treatment, (J) macrophage pre-treatment. (K and L) Inhibition of Tkt in non-oxidative part of PPP by oxythiamine,

(legend continued on next page)

functional implications of the PPP in TAM regulation have been established nor the effects of PPP inhibition on immune regulation have been identified. Here, we show that modulation of the PPP in TAMs serves as a robust regulator of phagocytic function and macrophage activity and prolongs survival in aggressive B cell lymphoma therapy.

Metabolic inhibition screening in lymphoma-macrophage co-cultures emphasized detrimental effects on macrophage function for the majority of investigated pathways. Only inhibition of the PPP showed a significant increase of phagocytosis with a synergistic effect on effector and target cells. This was true across various *in vitro* and *in vivo* macrophage model systems of both murine and human descent by compound and genetic targeting. Even though the time-dependent effects of PPP inhibition differ between chemical compounds and genetic targeting, we observed similar phenotype under compound-mediated as well as shRNA-mediated PPP inhibition. The increased phagocytosis rate appeared also under hypoxic conditions as an approximation of physiological status of therapy-refractory niches of lymphoma—the lymph nodes and bone marrow[40,41]—indicating therapeutic efficacy by metabolic inhibition in contrast to other therapy modalities in these niches.

Previous reports demonstrated reduced cancer and leukemia cell growth in mice upon PPP inhibition.[13,42] Especially in CLL, macrophages play a pivotal role as supportive bystander cells in the TME, without which CLL cells would undergo spontaneous apoptosis.[33] We have shown that PPP inhibition diminishes this pro-survival bystander function of macrophages and acts as a sensitizer to genotoxic regimens.

Alterations of the PPP enzymes 6PGD and TKT have been previously described in many cancer types.[43–47] Overexpression of TKT was closely associated with aggressive hepatocellular carcinoma features,[48] and 6PGD was shown to promote metastasis,[49] while suppression of 6Pgd attenuates cell proliferation and tumor growth[42] and overcomes cisplatin resistance[50] and Tkt inhibition sensitizes cancer cells to targeted therapy and reduces growth of metastatic lesions.[48] PPP inhibition by physcion, S3, or 6-aminonicotinamide has demonstrated anti-tumorigenic effects in several solid tumor types and chemotherapeutic-resistant acute myeloid leukemia cells,[47,51,52] without affecting non-malignant cells.[42] Moreover, 6Pgd inhibition in $CD8^+$ T cells led to an increased effector function with higher tumoricidal activity.[53]

We have previously shown that macrophage effector polarization is crucial in therapeutic antibody-based regimens of B cell lymphoma and can be modulated.[54–56] We now identified macrophage metabolism as an essential switch of macrophage effector function in lymphoma.

We demonstrated that increase of phagocytosis is driven by PPP enzyme inhibition, rather than metabolite accumulation. Non-exclusive PPP metabolites did not influence phagocytosis, possibly due to degradation via glycolysis (G3P, F6P) or nucleotide synthesis (R5P) before entering PPP flux. In contrast, exclusive PPP metabolites altered phagocytosis activity: supplementation of the G6pd product 6-phosphogluconate, the 6Pgd product ribulose-5-phosphate, and the Tkt product sedoheptulose-7-phosphate increased phagocytosis, while supplementation of the Tkt educt erythrose-4-phosphate decreased phagocytic activity in macrophages. This points to a feedback inhibition of the respective PPP enzymes and emphasizes the enzyme inhibition as driving force for increased phagocytosis.

PPP is a central linker between glucose metabolism, amino acid biosynthesis, fatty acid metabolism, and redox homeostasis.[43] A gain in metabolic activity was observed under PPP inhibition with increased glycolytic and mitochondrial capacity causing enhanced ATP production, fueling macrophages' activation. An increase of glycolysis is well described within the phenotypical switch to pro-inflammatory macrophages.[57] We observed profound alteration of morphology and macrophage polarity, demonstrated by a decrease of markers associated with M2-like macrophages and TAMs, which represent immunosuppressive and tumor-promoting macrophage subtypes,[3,58,59] while exclusive M1 marker, expressed on pro-inflammatory macrophages, was increased.[60–63]

In total, the restriction of one metabolic pathway—the PPP—gives rise to numerous paths of activation, which renders a profound alteration of phenotype and particular phagocytic activity in macrophages. Thereby the anti-tumor function could be improved from independent directions.

Our detailed multi-omics and functional analysis provides evidence that these effects are directly related to 6Pgd and Tkt enzyme activity loss, which polarizes macrophages to a pro-inflammatory phenotype through downregulation of Stat1 and Irg1. The functional switch between PPP enzyme activity and subsequent polarization program is Csf1r expression and activity of glycogen metabolism.

Csf1r activation induces Hmox-1 expression,[64,65] which induces Irg1 expression,[66] a central inhibitory regulator of macrophage activation.[27] We demonstrated significant downregulation of Csf1r pathway proteins. Via Csf1r signaling, macrophages are polarized toward an M2-like or TAM phenotype by directly activating Erk1/2 (Mapk1/2) and Hck signaling.[24,25,67–69] Both, Mapk1 and Hck activity was shown to be decreased under PPP inhibition in upstream kinase analysis.

Considering the relevant role of Csf1r in macrophage ontogeny, activation, and polarization, reduced Csf1r expression might be responsible for macrophage activation under PPP inhibition. Therefore, Csf1r blockade might be a promising strategy to increase macrophage activity in the context of tumor therapy. Several CSF1R inhibitors are currently under clinical investigation.[70] Nevertheless, as CSF1R is a macrophage-exclusive receptor, only a macrophage-exclusive effect could be achieved by using CSF1R inhibition, in contrast to the previously described multi-cellular effects of 6PGD and TKT inhibition.

PPP inhibition has been functionally linked to inhibition of glycogenolysis causing decreased UDPG production.[28] UDPG

(K) co-culture treatment, (L) macrophage pre-treatment. In (A–H) data are shown as mean ± SEM, in (I–L) as minimum to maximum. Technical replicates (A) $n = 28$, (B) $n = 20$, (C and D) $n = 18$, (E and F) $n = 20$, (G) $n = 65$, (H) $n = 30$, (I–L) $n = 30$; biological replicates (A) $n = 6$, (B) $n = 4$, (C and D) $n = 6$, (E and F) $n = 5$, (G) $n = 12$, (H) $n = 10$, (I–L) $n = 10$. p values were calculated in (A–G) using one-way ANOVA, in (H) using repeated measures (RM) one-way ANOVA, and in (I–L) using paired t test. $^*p < 0.05$; $^{**}p < 0.01$; $^{***}p < 0.001$; $^{****}p < 0.0001$. See also Figure S6.

Please cite this article in press as: Beielstein et al., Macrophages are activated toward phagocytic lymphoma cell clearance by pentose phosphate pathway inhibition, Cell Reports Medicine (2024), https://doi.org/10.1016/j.xcrm.2024.101830

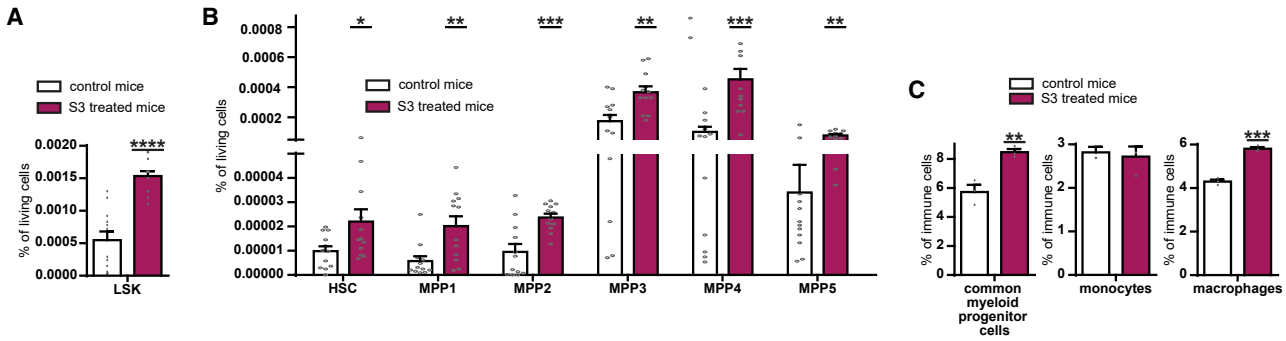

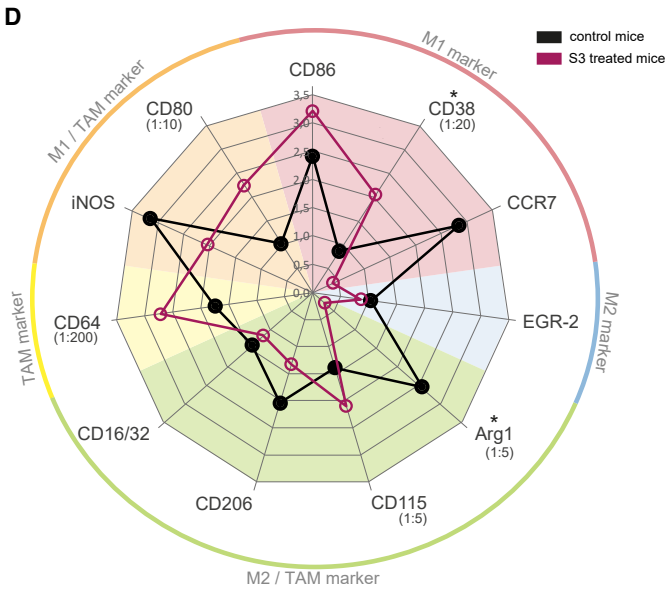

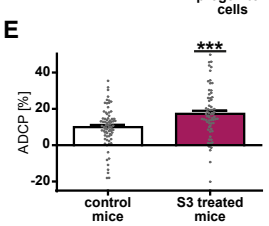

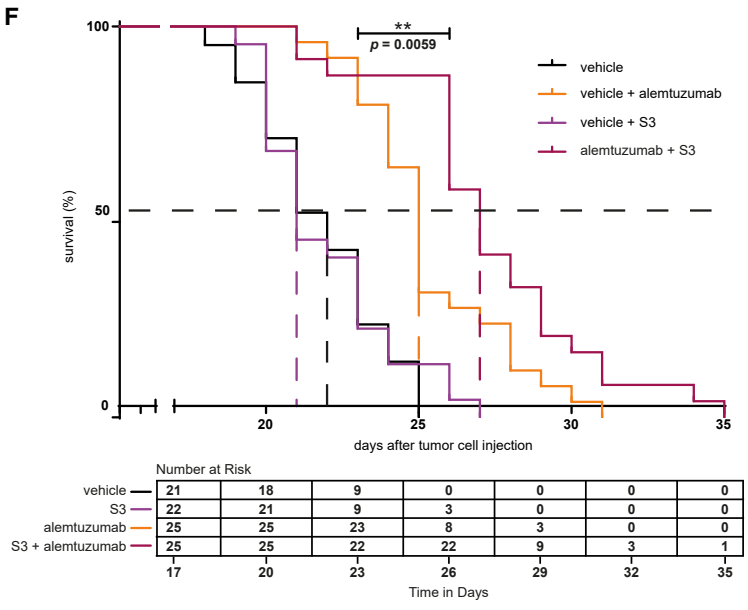

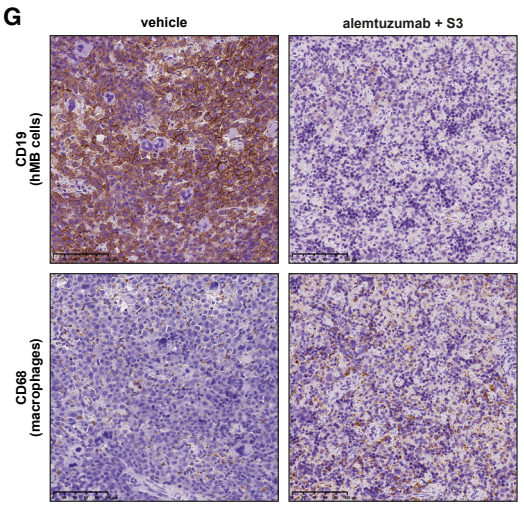

(legend on next page)

as a signaling molecule activates the P2y14 receptor (P2y14r). P2y14r activation in turn increases Stat1 expression and Mapk1 phosphorylation.[71] Considering that Stat1 is a major regulator of Irf1 expression,[29] which is the transcription factor of Irg1,[72] the signaling cascade induced by PPP inhibition in macrophages is causing an altered Irg1 expression. Irg1 is almost exclusively expressed in activated immune cells and a key driver of immune inhibition via itaconate production.[27] Itaconate inhibits glycolysis and mitochondrial activity by Sdh inhibition[73] and promotes anti-inflammatory macrophage phenotype[74] and tumor growth by increased reactive oxygen species secretion by TAMs.[75] In contrast to the publication of Ma et al.,[28] we observed a decreased amount of glycogen under PPP inhibition, but simultaneously increased glycolysis as a possible indicator for a shift of glucose processing causing decreased glycogen synthesis and glycogenolysis. Subsequently, we observed decreased expression of all UDPG-Stat1-Irg1-itaconate pathway proteins under PPP inhibition, particularly lower amounts of itaconate and an increased Sdh and Acly activity. Acly activity is known to induce macrophage activation and pro-inflammatory cytokine production.[32] These changes subsequently resulted in a pro-inflammatory cytokine switch, phenotypic shift toward M1-like macrophages, and diminished primary leukemia cell support. The metabolic alterations observed here support the hypothesis of the connection between PPP inhibition, itaconate abundance, and immune regulation.

Furthermore, the transcription factor Irf1 induces inducible nitric oxide synthase (iNos) expression,[72] consistent with the observed decreased iNos expression under PPP inhibition. High iNos expression and activity have been correlated with malignancy and poor survival in several solid tumors and leukemia.[76]

Despite the pro-inflammatory transcriptional function of Stat1 in LPS-stimulated macrophages, we show an alternative mechanism of macrophage activation by metabolic depression of the anti-inflammatory properties of Stat1 via itaconate regulation leading to a pro-phagocytic phenotype of macrophages. In TAMs, Stat1 has been shown to be the generator of the blended M1/M2 phenotype and supporter of the anti-inflammatory and pro-tumorigenic properties.[77,78]

As reduced expression of Irf1 also influences Stat1 and Csf1r expression,[79] Irf1 appears as the junction between all recapitulated pathways, which are leading to the changed macrophage activity and polarization.

Taken together, these signaling connections show a narrow network, which links PPP inhibition and immune regulation in macrophages and cancer cells.

We demonstrated a highly significant increase of phagocytosis in primary human cells, indicating efficacy for potential clinical use.

To model lymphoma in patients, we performed *in vivo* experiments with the PPP inhibitor S3, whose low toxicity and high effectiveness in treatment of other tumor entities were demonstrated before.[13,42] In the aggressive lymphoma mouse model,[36] PPP inhibition has an amplification effect on antibody therapy leading to significant prolonged overall survival in comparison to antibody treatment only with associated increased macrophage lymphoma infiltration. PPP inhibition *in vivo* increased myelopoiesis and gave rise to progenitor cell expansion, indicating increased provision of a variety of immune cells. Macrophages displayed pro-inflammatory polarization and significantly increased phagocytic capacity after PPP inhibition *in vivo*.

We have proven *in vivo* the efficacy of PPP inhibition leading to macrophage activation and improving therapy response by antibody-mediated phagocytic clearance of lymphoma with prolongation of overall survival.

In conclusion, PPP inhibition may serve as immune-modulatory therapy repolarizing macrophages. We demonstrated metabolic modulation as a key mechanism of macrophage regulation. PPP inhibition causes diminished Irg1 expression leading to reduced anti-inflammatory itaconate production. Our work indicates PPP inhibition as a dual-principle therapy targeting cancer cells and their immune-microenvironment simultaneously, with implications for cancer treatment, especially in the context of antibody-based regimens.

Limitations of the study

This study has several important limitations to consider. The screening process was conducted primarily from the perspective of ADCP and emphasized a therapeutic angle, which may

Figure 7. PPP inhibition increases myelopoiesis, macrophages' maturation, and pro-inflammatory polarization *in vivo* and boosts anti-leukemic treatment response in an aggressive humanized lymphoma mouse model

(A) Progenitor cell compartment LSK (Lin$^-$, Sca-1$^+$, c-Kit$^+$) in bone marrow of C57BL/6J mice treated with vehicle (control) or PPP inhibitor S3 i.p. for 7 days.

(B) Multipotent progenitor (MPP) subsets in bone marrow of C57BL/6J mice treated with vehicle (control) or PPP inhibitor S3 intraperitoneally (i.p.) for 7 days. HSC (CD34$^-$, CD48$^-$, CD150$^+$, CD135$^-$), MPP1 (CD34$^+$, CD48$^-$, CD150$^+$, CD135$^-$), MPP2 (CD34$^+$, CD48$^+$, CD150$^+$, CD135$^-$), MPP3 (CD34$^+$, CD48$^+$, CD150$^-$, CD135$^-$), MPP4 (CD34$^+$, CD48$^+$, CD150$^-$, CD135$^+$), MPP5 (CD34$^+$, CD48$^-$, CD150$^-$, CD135$^-$).

(C) Percentage of myeloid lineage cells of whole cell amount in bone marrow of NSG mice transfected with hMB cells, treated with vehicle or PPP inhibitor S3 i.p. for 12 days, and euthanized on day 15. Common myeloid progenitor cells (CD41$^+$, CD34$^+$), monocytes (Ly6c$^+$, CX3CR1$^+$), macrophages (F4/80$^+$, CD64$^+$).

(D) Expression of characteristic surface marker for different macrophage subtypes on peritoneal macrophages measured by immunofluorescent staining. Mean fluorescence intensity (MFI) is depicted. To improve readability, high MFI has been downscaled (factor named in brackets next to marker). C57BL/6J mice treated with vehicle (control) or PPP inhibitor S3 i.p. for 7 days.

(E) ADCP assay of bone marrow-derived macrophages. C57BL/6J mice treated with vehicle (control) or PPP inhibitor S3 i.p. for 7 days, macrophages differentiated out of femoral bone marrow with M-CSF.

(F) Survival curve of aggressive lymphoma (hMB) bearing mice treated with PPP inhibitor S3 +/− therapeutic antibody alemtuzumab.

(G) One representative example of immunohistochemical staining of hMB cells (CD19$^+$) and macrophages (CD68$^+$) in spleen of aggressive lymphoma (hMB) bearing mice treated with vehicle or alemtuzumab + S3. In (A–C and E) data are shown as mean ± SEM, in (D) data are shown as mean of ten replicates. Technical replicates (A and B) $n = 12$, (C) $n = 3$, (D) n = 9–10, (E) $n = 70$–75, (F) $n = 21$–25, (G) $n = 4$; biological replicates (A and B) $n = 12$, (C) $n = 3$, (D) n = 9–10, (E) $n = 14$–15, (F) $n = 21$–25, (G) $n = 4$. p values were calculated in (A–E) using unpaired t test and in (F) using Benjamini-Hochberg test. *$p < 0.05$; **$p < 0.01$; ***$p < 0.001$; ****$p < 0.0001$. See also Figure S7 and Table S8.

have limited the scope of the findings. While the PPP was a focus, its role in modulating lymphoma progression requires further investigation to fully understand its impact on the TME. The study concentrated on macrophages as targets for PPP inhibition. The effects of this inhibition on other immunotherapeutic approaches, such as bispecific antibodies and CAR-T cells, remain to be demonstrated. Crucially, the role of PPP inhibition in human patients has yet to be established through clinical trials. These limitations highlight areas for future research to build upon this study's results and provide a more comprehensive understanding of PPP inhibition in lymphoma treatment.

RESOURCE AVAILABILITY

Lead contact

Further requests for information should be directed to and will be fulfilled by the lead contact, Christian P. Pallasch (christian.pallasch@uk-koeln.de).

Materials availability

This study did not generate new unique reagents.

Data and code availability

- Proteomic and phosphoproteomic data have been deposited at PRIDE:PXD042428. Metabolomic data have been deposited at UCSD Metabolomics Workbench: ST003516.
- The data are publicly available as of the date of publication. Accession numbers are listed in the key resources table.
- This paper does not report original code.
- Any additional information required to reanalyze the data reported in this paper is available from the lead contact upon request.

ACKNOWLEDGMENTS

We are indebted to our patients who contributed tissue and blood samples to this study. This work was funded by the Deutsche Forschungsgemeinschaft (DFG, German Research Foundation) KFO286 and SFB1530 (SFB-Geschaeftszeichen – 455784452, Project B02). C.P.P. was supported by the "Foerderprogramm Nachwuchsforschungsgruppen NRW 2015–2021," CAP Program of the Center for Molecular Medicine Cologne, the "Deutsche Jose-Carreras Leukaemiestiftung e.V." (DJCLS 07R/2021), and a research grant by Gilead Sciences. A.C.B. was supported by Studentische Forschungsfoerderung/Begabtenfoerderung" of Koeln Fortune program of the medical faculty of University of Cologne. We would like to thank Thomas Wunderlich for advice and critical reading. We are grateful for technical assistance from the CECAD imaging and animal facilities. Graphics have been created in BioRender: graphical abstract BioRender.com/y35w412, Figure 1A BioRender.com/n22i592, Figure 4H BioRender.com/c70j052, and Figure 5C BioRender.com/b93t764.

AUTHOR CONTRIBUTIONS

Study design, A.C.B., N.N., and C.P.P.; data analysis and acquisition, A.C.B., S.B., M.K., M.M., S.C., R. Brinker, H.-H.B., D.V., L.A., J.L.N., R.L., C.R.C.P., J.S., F.P., A.F., and A.V.; bioinformatic analysis, A.C.B., E.I., S.B., J.L.N., A.V., and M.K.; analytical tools, R. Büttner, H.W., M.K., A.V., and C.B.; clinical samples and annotation, C.P.P. and M.H.; study supervision and funding, C.P.P.; manuscript preparation, A.C.B., S.B., and C.P.P.

DECLARATION OF INTERESTS

The authors declare no competing interests.

STAR★METHODS

Detailed methods are provided in the online version of this paper and include the following:

- KEY RESOURCES TABLE
- EXPERIMENTAL MODEL AND STUDY PARTICIPATION DETAILS
  - Mouse strains
  - Cell lines
  - Primary cells
  - Microbe strains
- METHOD DETAILS
  - Antibody-dependent cellular phagocytosis assay (ADCP)
  - Antibody-independent cellular phagocytosis assay (AICP)
  - Bone marrow derived macrophage generation
  - CLL patient cell co-culture
  - CLL patient cell chemotoxicity stain
  - ELISA
  - Immunofluorescent microscopy
  - Immune phenotyping
  - Immunohistochemical staining of murine spleen
  - *In vivo* experiments
  - Knockdown cell production
  - Metabolomics
  - Maturation staining of primary murine macrophages
  - Phosphoproteomics
  - Primary human macrophages
  - Proteomics
  - SeaHorse analysis
  - Viability stain
  - Western Blot analysis
- QUANTIFICATION AND STATISTICAL ANALYSIS
  - Statistical analysis
  - Proteomic and phosphoproteomic analysis

SUPPLEMENTAL INFORMATION

Supplemental information can be found online at https://doi.org/10.1016/j.xcrm.2024.101830.

Received: February 29, 2024
Revised: August 27, 2024
Accepted: October 25, 2024
Published: November 26, 2024

REFERENCES

1. Hanahan, D., and Weinberg, R.A. (2011). Hallmarks of cancer: the next generation. Cell *144*, 646–674. https://doi.org/10.1016/j.cell.2011.02.013.
2. Beielstein, A.C., and Pallasch, C.P. (2019). Tumor Metabolism as a Regulator of Tumor-Host Interactions in the B-Cell Lymphoma Microenvironment-Fueling Progression and Novel Brakes for Therapy. Int. J. Mol. Sci. *20*, 4158.
3. Cassetta, L., and Pollard, J.W. (2018). Targeting macrophages: Therapeutic approaches in cancer. Nat. Rev. Drug Discov. *17*, 887–904.
4. Yang, L., and Zhang, Y. (2017). Tumor-associated macrophages: from basic research to clinical application. J. Hematol. Oncol. *10*, 58.
5. Pallasch, C.P., Leskov, I., Braun, C.J., Vorholt, D., Drake, A., Soto-Feliciano, Y.M., Bent, E.H., Schwamb, J., Iliopoulou, B., Kutsch, N., et al. (2014). Sensitizing protective tumor microenvironments to antibody-mediated therapy. Cell *156*, 590–602. https://doi.org/10.1016/j.cell.2013.12.041.
6. Biswas, S.K., Gangi, L., Paul, S., Schioppa, T., Saccani, A., Sironi, M., Bottazzi, B., Doni, A., Vincenzo, B., Pasqualini, F., et al. (2006). A distinct and unique transcriptional program expressed by tumor-associated

macrophages (defective NF-κB and enhanced IRF-3/STAT1 activation). Blood *107*, 2112–2122.

7. Gallina, G., Dolcetti, L., Serafini, P., De Santo, C., Marigo, I., Colombo, M.P., Basso, G., Brombacher, F., Borrello, I., Zanovello, P., et al. (2006). Tumors induce a subset of inflammatory monocytes with immunosuppressive activity on CD8+ T cells. J. Clin. Invest. *116*, 2777–2790.
8. Jha, A.K., Huang, S.C.C., Sergushichev, A., Lampropoulou, V., Ivanova, Y., Loginicheva, E., Chmielewski, K., Stewart, K.M., Ashall, J., Everts, B., et al. (2015). Network integration of parallel metabolic and transcriptional data reveals metabolic modules that regulate macrophage polarization. Immunity *42*, 419–430.
9. Diskin, C., and Pålsson-McDermott, E.M. (2018). Metabolic modulation in macrophage effector function. Front. Immunol. *9*, 270. https://doi.org/10.3389/fimmu.2018.00270.
10. de-Brito N, M., Duncan-Moretti, J., da-Costa H, C., Saldanha-Gama, R., Paula-Neto, H.A., Dorighello, G.G., Simões, R.L., and Barja-Fidalgo, C. (2020). Aerobic glycolysis is a metabolic requirement to maintain the M2-like polarization of tumor-associated macrophages. Biochim. Biophys. Acta. Mol. Cell Res. *1867*, 118604.
11. Hörhold, F., Eisel, D., Oswald, M., Kolte, A., Röll, D., Osen, W., Eichmüller, S.B., and König, R. (2020). Reprogramming of macrophages employing gene regulatory and metabolic network models. PLoS Comput. Biol. *16*, 683–696.
12. Simões, R.L., De-Brito, N.M., Cunha-Costa, H., Morandi, V., Fierro, I.M., Roitt, I.M., and Barja-Fidalgo, C. (2017). Lipoxin A4 selectively programs the profile of M2 tumor-associated macrophages which favour control of tumor progression. Int. J. Cancer *140*, 346–357.
13. Elf, S., Lin, R., Xia, S., Pan, Y., Shan, C., Wu, S., Lonial, S., Gaddh, M., Arellano, M.L., Khoury, H.J., et al. (2017). Targeting 6-phosphogluconate dehydrogenase in the oxidative PPP sensitizes leukemia cells to antimalarial agent dihydroartemisinin. Oncogene *36*, 254–262.
14. Solovjeva, O.N., and Kochetov, G.A. (1999). Inhibition of transketolase by p-hydroxyphenylpyruvate. FEBS Lett. *462*, 246–248.
15. Weigert, A., Strack, E., Snodgrass, R.G., and Brüne, B. (2018). mPGES-1 and ALOX5/-15 in tumor-associated macrophages. Cancer Metastasis Rev. *37*, 317–334.
16. Mylka, V., Deckers, J., Ratman, D., De Cauwer, L., Thommis, J., De Rycke, R., Impens, F., Libert, C., Tavernier, J., Vanden Berghe, W., et al. (2018). The autophagy receptor SQSTM1/p62 mediates anti-inflammatory actions of the selective NR3C1/glucocorticoid receptor modulator compound A (CpdA) in macrophages. Autophagy *14*, 2049–2064.
17. Coles, L.S., Diamond, P., Occhiodoro, F., Vadas, M.A., and Shannon, M.F. (1996). Cold shock domain proteins repress transcription from the GM-CSF promoter. Nucleic Acids Res. *24*, 2311–2317.
18. Bartish, M., Tong, D., Pan, Y., Wallerius, M., Liu, H., Ristau, J., de Souza Ferreira, S., Wallmann, T., van Hoef, V., Masvidal, L., et al. (2020). MNK2 governs the macrophage antiinflammatory phenotype. Proc. Natl. Acad. Sci. USA *117*, 27556–27565.
19. Chang, Y.-T., Peng, H.-Y., Hu, C.-M., Huang, S.-C., Tien, S.-C., and Jeng, Y.-M. (2020). Pancreatic cancer-derived small extracellular vesical Ezrin regulates macrophage polarization and promotes metastasis. Am. J. Cancer Res. *10*, 12–37.
20. Iwata, H., Goettsch, C., Sharma, A., Ricchiuto, P., Goh, W.W.B., Halu, A., Yamada, I., Yoshida, H., Hara, T., Wei, M., et al. (2016). PARP9 and PARP14 cross-regulate macrophage activation via STAT1 ADP-ribosylation. Nat. Commun. *7*, 12849.
21. Zhang, Y., Li, X., Wang, C., Zhang, M., Yang, H., and Lv, K. (2020). lncRNA AK085865 Promotes Macrophage M2 Polarization in CVB3-Induced VM by Regulating ILF2-ILF3 Complex-Mediated miRNA-192 Biogenesis. Mol. Ther. Nucleic Acids *21*, 441–451.
22. Beekhof, R., Alphen, C., Henneman, A.A., Knol, J.C., Pham, T.V., Rolfs, F., Labots, M., Henneberry, E., Ys Le Large, T., de Haas, R.R., et al. (2019). INKA , an integrative data analysis pipeline for phosphoproteomic inference of active kinases. Mol. Syst. Biol. *15*, e8250. https://doi.org/10.15252/msb.20188250.
23. Poh, A.R., O'Donoghue, R.J.J., and Ernst, M. (2015). Hematopoietic cell kinase (HCK) as a therapeutic target in immune and cancer cells. Oncotarget *6*, 15752–15771.
24. Dwyer, A.R., Mouchemore, K.A., Steer, J.H., Sunderland, A.J., Sampaio, N.G., Greenland, E.L., Joyce, D.A., and Pixley, F.J. (2016). Src family kinase expression and subcellular localization in macrophages: implications for their role in CSF-1-induced macrophage migration. J. Leukoc. Biol. *100*, 163–175.
25. Foucher, E.D., Blanchard, S., Preisser, L., Garo, E., Ifrah, N., Guardiola, P., Delneste, Y., and Jeannin, P. (2013). IL-34 Induces the Differentiation of Human Monocytes into Immunosuppressive Macrophages. Antagonistic Effects of GM-CSF and IFNγ. PLoS One *8*, e56045. https://doi.org/10.1371/journal.pone.0056045.
26. Basile, J.R., Afkhami, T., and Gutkind, J.S. (2005). Semaphorin 4D/Plexin-B1 Induces Endothelial Cell Migration through the Activation of PYK2, Src, and the Phosphatidylinositol 3-Kinase-Akt Pathway. Mol. Cell Biol. *25*, 6889–6898.
27. O'Neill, L.A.J., and Artyomov, M.N. (2019). Itaconate: the poster child of metabolic reprogramming in macrophage function. Nat. Rev. Immunol. *19*, 273–281.
28. Ma, J., Wei, K., Liu, J., Tang, K., Zhang, H., Zhu, L., Chen, J., Li, F., Xu, P., Chen, J., et al. (2020). Glycogen metabolism regulates macrophage-mediated acute inflammatory responses. Nat. Commun. *11*, 1769. https://doi.org/10.1038/s41467-020-15636-8.
29. Taniguchi, T., Ogasawara, K., Takaoka, A., and Tanaka, N. (2001). IRF family of transcription factors as regulators of host defense. Annu. Rev. Immunol. *19*, 623–655.
30. Tallam, A., Perumal, T.M., Antony, P.M., Jäger, C., Fritz, J.V., Vallar, L., Balling, R., Del Sol, A., and Michelucci, A. (2016). Gene Regulatory Network Inference of Immunoresponsive Gene 1 (IRG1) Identifies Interferon Regulatory Factor 1 (IRF1) as Its Transcriptional Regulator in Mammalian Macrophages. PLoS One *11*, e0149050. https://doi.org/10.1371/journal.pone.0149050.
31. Fernández-García, M., Mesquita, I., Ferreira, C., Araújo, M., Saha, B., Rey-Stolle, M.F., García, A., Silvestre, R., and Barbas, C. (2023). Leishmania donovani Induces Multiple Dynamic Responses in the Metabolome Associated with Amastigote Differentiation and Maturation Inside the Human Macrophage. J. Proteome Res. *22*, 2256–2270.
32. Lauterbach, M.A., Hanke, J.E., Serefidou, M., Mangan, M.S.J., Kolbe, C.C., Hess, T., Rothe, M., Kaiser, R., Hoss, F., Gehlen, J., et al. (2019). Toll-like Receptor Signaling Rewires Macrophage Metabolism and Promotes Histone Acetylation via ATP-Citrate Lyase. Immunity *51*, 997–1011.e7.
33. Burger, J.A., Tsukada, N., Burger, M., Zvaifler, N.J., Dell'Aquila, M., and Kipps, T.J. (2000). Blood-derived nurse-like cells protect chronic lymphocytic leukemia B cells from spontaneous apoptosis through stromal cell-derived factor-1. Blood *96*, 2655–2663.
34. Pietras, E.M., Reynaud, D., Kang, Y.A., Carlin, D., Calero-Nieto, F.J., Leavitt, A.D., Stuart, J.M., Göttgens, B., and Passegué, E. (2015). Functionally Distinct Subsets of Lineage-Biased Multipotent Progenitors Control Blood Production in Normal and Regenerative Conditions. Cell Stem Cell *17*, 35–46.
35. Sommerkamp, P., Romero-Mulero, M.C., Narr, A., Ladel, L., Hustin, L., Schönberger, K., Renders, S., Altamura, S., Zeisberger, P., Jäcklein, K., et al. (2021). Mouse multipotent progenitor 5 cells are located at the interphase between hematopoietic stem and progenitor cells. Blood *137*, 3218–3224.
36. Leskov, I., Pallasch, C.P., Drake, A., Iliopoulou, B.P., Souza, A., Shen, C.H., Schweighofer, C.D., Abruzzo, L., Frenzel, L.P., Wendtner, C.M., et al. (2013). Rapid generation of human B-cell lymphomas via combined expression of Myc and Bcl2 and their use as a preclinical model for biological therapies. Oncogene *32*, 1066–1072.

37. Izquierdo, E., Cuevas, V.D., Fernández-Arroyo, S., Riera-Borrull, M., Orta-Zavalza, E., Joven, J., Rial, E., Corbi, A.L., and Escribese, M.M. (2015). Reshaping of Human Macrophage Polarization through Modulation of Glucose Catabolic Pathways. J. Immunol. *195*, 2442–2451.

38. He, D., Mao, Q., Jia, J., Wang, Z., Liu, Y., Liu, T., Luo, B., and Zhang, Z. (2021). Pentose Phosphate Pathway Regulates Tolerogenic Apoptotic Cell Clearance and Immune Tolerance. Front. Immunol. *12*, 797091. https://doi.org/10.3389/FIMMU.2021.797091.

39. Nakamizo, S., Sugiura, Y., Ishida, Y., Ueki, Y., Yonekura, S., Tanizaki, H., Date, H., Yoshizawa, A., Murata, T., Minatoya, K., et al. (2023). Activation of the pentose phosphate pathway in macrophages is crucial for granuloma formation in sarcoidosis. J. Clin. Invest. *133*, e171088. https://doi.org/10.1172/JCI171088.

40. Caldwell, C.C., Kojima, H., Lukashev, D., Armstrong, J., Farber, M., Apasov, S.G., and Sitkovsky, M.V. (2001). Differential Effects of Physiologically Relevant Hypoxic Conditions on T Lymphocyte Development and Effector Functions. J. Immunol. *167*, 6140–6149.

41. Spencer, J.A., Ferraro, F., Roussakis, E., Klein, A., Wu, J., Runnels, J.M., Zaher, W., Mortensen, L.J., Alt, C., Turcotte, R., et al. (2014). Direct measurement of local oxygen concentration in the bone marrow of live animals. Nature *508*, 269–273.

42. Lin, R., Elf, S., Shan, C., Kang, H.B., Ji, Q., Zhou, L., Hitosugi, T., Zhang, L., Zhang, S., Seo, J.H., et al. (2015). 6-Phosphogluconate dehydrogenase links oxidative PPP, lipogenesis and tumour growth by inhibiting LKB1–AMPK signalling. Nat. Cell Biol. *17*, 1484–1496.

43. Stincone, A., Prigione, A., Cramer, T., Wamelink, M.M.C., Campbell, K., Cheung, E., Olin-Sandoval, V., Grüning, N.M., Krüger, A., Tauqeer Alam, M., et al. (2015). The return of metabolism: Biochemistry and physiology of the pentose phosphate pathway. Biol. Rev. *90*, 927–963.

44. Chen, H., Wu, D., Bao, L., Yin, T., Lei, D., Yu, J., and Tong, X. (2019). 6PGD inhibition sensitizes hepatocellular carcinoma to chemotherapy via AMPK activation and metabolic reprogramming. Biomed. Pharmacother. *111*, 1353–1358.

45. Liu, H., Huang, D., McArthur, D.L., Boros, L.G., Nissen, N., and Heaney, A.P. (2010). Fructose induces transketolase flux to promote pancreatic cancer growth. Cancer Res. *70*, 6368–6376.

46. Zheng, W., Feng, Q., Liu, J., Guo, Y., Gao, L., Li, R., Xu, M., Yan, G., Yin, Z., Zhang, S., et al. (2017). Inhibition of 6-phosphogluconate dehydrogenase reverses cisplatin resistance in ovarian and lung cancer. Front. Pharmacol. *8*, 421. https://doi.org/10.3389/fphar.2017.00421.

47. Bhanot, H., Weisberg, E.L., Reddy, M.M., Nonami, A., Neuberg, D., Stone, R.M., Podar, K., Salgia, R., Griffin, J.D., and Sattler, M. (2017). Acute myeloid leukemia cells require 6-phosphogluconate dehydrogenase for cell growth and NADPH-dependent metabolic reprogramming. Oncotarget *8*, 67639–67650.

48. Xu, I.M.J., Lai, R.K.H., Lin, S.H., Tse, A.P.W., Chiu, D.K.C., Koh, H.Y., Law, C.T., Wong, C.M., Cai, Z., Wong, C.C.L., and Ng, I.O.L. (2016). Transketolase counteracts oxidative stress to drive cancer development. Proc. Natl. Acad. Sci. USA *113*, E725–E734.

49. Chan, B., VanderLaan, P.A., and Sukhatme, V.P. (2013). 6-Phosphogluconate dehydrogenase regulates tumor cell migration in vitro by regulating receptor tyrosine kinase c-Met. Biochem. Biophys. Res. Commun. *439*, 247–251.

50. Zhang, H., Zhang, H., Wang, S., Ni, Z., and Wang, T. (2019). 1-Hydroxy-8-methoxy-anthraquinon reverses cisplatin resistance by inhibiting 6PGD in cancer cells. Open Life Sci. *14*, 454–461.

51. Gao, F., Liu, W., Guo, Q., Bai, Y., Yang, H., and Chen, H. (2017). Physcion blocks cell cycle and induces apoptosis in human B cell precursor acute lymphoblastic leukemia cells by downregulating HOXA5. Biomed. Pharmacother. *94*, 850–857.

52. Budihardjo, I.I., Walker, D.L., Svingen, P.A., Buckwalter, C.A., Desnoyers, S., Eckdahl, S., Shah, G.M., Poirier, G.G., Reid, J.M., Ames, M.M., and Kaufmann, S.H. (1998). 6-Aminonicotinamide sensitizes human tumor cell lines to cisplatin. Clin. Cancer Res. *4*, 117–130.

53. Daneshmandi, S., Cassel, T., Lin, P., Higashi, R.M., Wulf, G.M., Boussiotis, V.A., Fan, T.W.M., and Seth, P. (2021). Blockade of 6-phosphogluconate dehydrogenase generates CD8+ effector T cells with enhanced anti-tumor function. Cell Rep. *34*, 108831. https://doi.org/10.1016/j.celrep.2021.108831.

54. Lossos, C., Liu, Y., Kolb, K.E., Christie, A.L., Van Scoyk, A., Prakadan, S.M., Shigemori, K., Stevenson, K.E., Morrow, S., Plana, O.D., et al. (2019). Mechanisms of lymphoma clearance induced by high-dose alkylating agents. Cancer Discov. *9*, 944–961. https://doi.org/10.1158/2159-8290.CD-18-1393.

55. Barbarino, V., Henschke, S., Blakemore, S.J., Izquierdo, E., Michalik, M., Nickel, N., Möllenkotte, I., Vorholt, D., Müller, L., Brinker, R., et al. (2020). Macrophage-Mediated Antibody Dependent Effector Function in Aggressive B-Cell Lymphoma Treatment is Enhanced by Ibrutinib via Inhibition of JAK2. Cancers *12*, 2303.

56. Izquierdo, E., Vorholt, D., Blakemore, S., Sackey, B., Nolte, J.L., Barbarino, V., Schmitz, J., Nickel, N., Bachurski, D., Lobastova, L., et al. (2022). Extracellular vesicles and PD-L1 suppress macrophages, inducing therapy resistance in TP53-deficient B-cell malignancies. Blood *139*, 3617–3629.

57. Rodríguez-Prados, J.-C., Través, P.G., Cuenca, J., Rico, D., Aragonés, J., Martín-Sanz, P., Cascante, M., and Boscá, L. (2010). Substrate Fate in Activated Macrophages: A Comparison between Innate, Classic, and Alternative Activation. J. Immunol. *185*, 605–614.

58. Bronte, V., Brandau, S., Chen, S.H., Colombo, M.P., Frey, A.B., Greten, T.F., Mandruzzato, S., Murray, P.J., Ochoa, A., Ostrand-Rosenberg, S., et al. (2016). Recommendations for myeloid-derived suppressor cell nomenclature and characterization standards. Nat. Commun. *7*, 12150.

59. Solinas, G., Schiarea, S., Liguori, M., Fabbri, M., Pesce, S., Zammataro, L., Pasqualini, F., Nebuloni, M., Chiabrando, C., Mantovani, A., and Allavena, P. (2010). Tumor-Conditioned Macrophages Secrete Migration-Stimulating Factor: A New Marker for M2-Polarization, Influencing Tumor Cell Motility. J. Immunol. *185*, 642–652.

60. Hesketh, M., Sahin, K.B., West, Z.E., and Murray, R.Z. (2017). Macrophage Phenotypes Regulate Scar Formation and Chronic Wound Healing. Int. J. Mol. Sci. *18*, 1545.

61. Woo, M.-S., Yang, J., Beltran, C., and Cho, S. (2016). Cell Surface CD36 Protein in Monocyte/Macrophage Contributes to Phagocytosis during the Resolution Phase of Ischemic Stroke in Mice. J. Biol. Chem. *291*, 23654–23661.

62. Kwiecień, I., Polubiec-Kownacka, M., Dziedzic, D., Wołosz, D., Rzepecki, P., and Domagała-Kulawik, J. (2019). CD163 and CCR7 as markers for macrophage polarization in lung cancer microenvironment. Cent. Eur. J. Immunol. *44*, 395–402.

63. Jablonski, K.A., Amici, S.A., Webb, L.M., Ruiz-Rosado, J.d.D., Popovich, P.G., Partida-Sanchez, S., and Guerau-de-Arellano, M. (2015). Novel markers to delineate murine M1 and M2 macrophages. PLoS One *10*, e0145342. https://doi.org/10.1371/journal.pone.0145342.

64. Otero, K., Turnbull, I.R., Poliani, P.L., Vermi, W., Cerutti, E., Aoshi, T., Tassi, I., Takai, T., Stanley, S.L., Miller, M., et al. (2009). Macrophage colony-stimulating factor induces the proliferation and survival of macrophages via a pathway involving DAP12 and β-catenin. Nat. Immunol. *10*, 734–743.

65. Lin, C.C., Hsiao, L.D., Cho, R.L., and Yang, C.M. (2019). Carbon monoxide releasing molecule-2-upregulated ROS-dependent heme oxygenase-1 axis suppresses lipopolysaccharide-induced airway inflammation. Int. J. Mol. Sci. *20*, 3157. https://doi.org/10.3390/ijms20133157.

66. Jamal Uddin, M., Joe, Y., Kim, S.K., Oh Jeong, S., Ryter, S.W., Pae, H.O., and Chung, H.T. (2016). IRG1 induced by heme oxygenase-1/carbon monoxide inhibits LPS-mediated sepsis and pro-inflammatory cytokine production. Cell. Mol. Immunol. *13*, 170–179.

67. Poh, A.R., Love, C.G., Masson, F., Preaudet, A., Tsui, C., Whitehead, L., Monard, S., Khakham, Y., Burstroem, L., Lessene, G., et al. (2017). Inhibition of Hematopoietic Cell Kinase Activity Suppresses Myeloid Cell-Mediated Colon Cancer Progression. Cancer Cell *31*, 563–575.e5.

68. Fleetwood, A.J., Lawrence, T., Hamilton, J.A., and Cook, A.D. (2007). Granulocyte-Macrophage Colony-Stimulating Factor (CSF) and Macrophage CSF-Dependent Macrophage Phenotypes Display Differences in Cytokine Profiles and Transcription Factor Activities: Implications for CSF Blockade in Inflammation. J. Immunol. *178*, 5245–5252.

69. Stanley, E.R., and Chitu, V. (2014). CSF-1 receptor signaling in myeloid cells. Cold Spring Harb. Perspect. Biol. *6*, a021857. https://doi.org/10.1101/cshperspect.a021857.

70. Cannarile, M.A., Weisser, M., Jacob, W., Jegg, A.M., Ries, C.H., and Rüttinger, D. (2017). Colony-stimulating factor 1 receptor (CSF1R) inhibitors in cancer therapy. J. Immunother. Cancer *5*, 53. https://doi.org/10.1186/s40425-017-0257-y.

71. Lazarowski, E.R., and Harden, T.K. (2015). UDP-sugars as extracellular signaling molecules: Cellular and physiologic consequences of P2Y14 receptor activation. Mol. Pharmacol. *88*, 151–160.

72. Tallam, A., Perumal, T.M., Antony, P.M., Jäger, C., Fritz, J.V., Vallar, L., Balling, R., Del Sol, A., and Michelucci, A. (2016). Gene Regulatory Network Inference of Immunoresponsive Gene 1 (IRG1) Identifies Interferon Regulatory Factor 1 (IRF1) as Its Transcriptional Regulator in Mammalian Macrophages. PLoS One *11*, e0149050. https://doi.org/10.1371/journal.pone.0149050.

73. Lampropoulou, V., Sergushichev, A., Bambouskova, M., Nair, S., Vincent, E.E., Loginicheva, E., Cervantes-Barragan, L., Ma, X., Huang, S.C.C., Griss, T., et al. (2016). Itaconate Links Inhibition of Succinate Dehydrogenase with Macrophage Metabolic Remodeling and Regulation of Inflammation. Cell Metab. *24*, 158–166.

74. Mills, E.L., Ryan, D.G., Prag, H.A., Dikovskaya, D., Menon, D., Zaslona, Z., Jedrychowski, M.P., Costa, A.S.H., Higgins, M., Hams, E., et al. (2018). Itaconate is an anti-inflammatory metabolite that activates Nrf2 via alkylation of KEAP1. Nature *556*, 113–117.

75. Weiss, J.M., Davies, L.C., Karwan, M., Ileva, L., Ozaki, M.K., Cheng, R.Y., Ridnour, L.A., Annunziata, C.M., Wink, D.A., and McVicar, D.W. (2018). Itaconic acid mediates crosstalk between macrophage metabolism and peritoneal tumors. J. Clin. Invest. *128*, 3794–3805.

76. Nath, N., and Kashfi, K. (2020). Tumor associated macrophages and 'NO. Biochem. Pharmacol. *176*, 113899. https://doi.org/10.1016/j.bcp.2020.113899.

77. Biswas, S.K., Gangi, L., Paul, S., Schioppa, T., Saccani, A., Sironi, M., Bottazzi, B., Doni, A., Vincenzo, B., Pasqualini, F., et al. (2006). A distinct and unique transcriptional program expressed by tumor-associated macrophages (defective NF-κB and enhanced IRF-3/STAT1 activation). Blood *107*, 2112–2122.

78. Van Ginderachter, J.A., Movahedi, K., Hassanzadeh Ghassabeh, G., Meerschaut, S., Beschin, A., Raes, G., and De Baetselier, P. (2006). Classical and alternative activation of mononuclear phagocytes: Picking the best of both worlds for tumor promotion. Immunobiology *211*, 487–501.

79. Zenke, K., Muroi, M., and Tanamoto, K.I. (2018). IRF1 supports DNA binding of STAT1 by promoting its phosphorylation. Immunol. Cell Biol. *96*, 1095–1103.

Please cite this article in press as: Beielstein et al., Macrophages are activated toward phagocytic lymphoma cell clearance by pentose phosphate pathway inhibition, Cell Reports Medicine (2024), https://doi.org/10.1016/j.xcrm.2024.101830

STAR★METHODS

KEY RESOURCES TABLE

REAGENT or RESOURCE	SOURCE	IDENTIFIER
Antibodies		
Rabbit polyclonal anti-β-actin	BioLegend	Cat#622101; RRID:AB_315945
Sheep polyclonal anti-Arg1	RnD Systems	Cat#IC5868P
Mouse monoclonal anti-CCR7 (CD197)	BioLegend	Cat#353213; RRID:AB_10915474
Rat monoclonal anti-CD11b	BioLegend	Cat#101226; RRID:AB_830642
Rat monoclonal anti-CD115 (CSF-1R)	BioLegend	Cat#135523; RRID:AB_2566459
Rat monoclonal anti-CD16/32	BioLegend	Cat#156607; RRID:AB_2800705
Rat monoclonal anti-CD19	Thermo Fisher Scientific	Cat#14-0194-80; RRID:AB_2637170
Mouse monoclonal anti-CD200R	BioLegend	Cat#329305; RRID:AB_2074201
Mouse monoclonal anti-CD206	BD Biosciences	Cat#551135; RRID:AB_394065
Rat monoclonal anti-CD38	BioLegend	Cat#102717; RRID:AB_2072892
Mouse monoclonal anti- CD64	BioLegend	Cat#305025; RRID:AB_2561587
Rabbit polyclonal anti-CD68	Abcam	Cat#ab125212; RRID:AB_10975465
Rat monoclonal anti-CD68	BioLegend	Cat#137017; RRID:AB_2562949
Mouse monoclonal anti-CD80	BD Biosciences	Cat#557227; RRID:AB_396606
Rat monoclonal anti-CD86	Miltenyi Biotec	Cat#130-123-724,;RRID:AB_2889634
Mouse monoclonal anti-CX3CR1	BioLegend	Cat#149007; RRID:AB_2564491
Rat monoclonal anti-EGR-2	Thermo Fisher Scientific	Cat#17-6691-82; RRID:AB_11151502
Rat monoclonal anti-F4/80	BioLegend	Cat#123110; RRID:AB_893486
Rat monoclonal anti-F4/80	BioLegend	Cat#123124; RRID:AB_893475
Human cell line monoclonal anti-F4/80	Miltenyi Biotec	Cat #130-102-327; RRID:AB_2651701
Mouse monoclonal anti-human HLA-DR (MHC II)	BioLegend	Cat#307604; RRID:AB_314682
Mouse Histofine Simple Stain Mouse MAX-PO	Nichirei Biosciences	Cat#414341F; RRID:AB_2819094
Rat monoclonal anti-IL-10	BioLegend	Cat#505025; RRID:AB_11149682
Mouse monoclonal anti-iNOS	Novus Biologicals	Cat#NBP2-22119; RRID:AB_2905500
Rabbit monoclonal anti-IRF1 (D5E4)	Cell Signaling Technology	Cat#8478; RRID:AB_10949108
Rabbit polyclonal anti-IRG1	Cell Signaling Technology	Cat#17805; RRID:AB_3064865
Rat monoclonal anti-Ly6c	BioLegend	Cat#128011; RRID:AB_1659242
Rabbit polyclonal anti-P2RY14	LSBio	Cat#LS-C409714
Rabbit monoclonal anti-PD-1 (D7D5W)	Cell Signaling Technology	Cat#84651; RRID:AB_2800041
Rabbit polyclonal anti-PD-L1	Thermo Fisher Scientific	Cat#PA5-20343; RRID:AB_11153819
Mouse monoclonal anti-phosphogluconate dehydrogenase (G-2) (6PGD)	Santa Cruz Biotechnology, INC.	Cat#sc-398977; RRID:AB_2827766
Rabbit monoclonal anti- Protein-tyrosine kinase 2-beta (PYK2)	Abcam	Cat#ab32571; RRID:AB_777566
Rabbit polyclonal anti-SIRP1a	SIGMA-ALDRICH	Cat#SAB2102154; RRID:AB_10605073
Rabbit monoclonal anti-STAT1	Cell Signaling Technology	Cat#80916; RRID:AB_2799965
Mouse monoclonal anti-TGF-beta1	BioLegend	Cat#349706; RRID:AB_10680787
Rabbit polyclonal anti-transketolase (TKT)	Biorbyt Ltd.	Cat#orb247362
Rabbit polyclonal anti-UGP2	Thermo Fisher Scientific	Cat#PA5-27760; RRID:AB_2545236
Bacterial and virus strains		
5-alpha Competent E. coli	New England Biolabs Inc.	Cat#C2987H

(*Continued on next page*)

Continued

REAGENT or RESOURCE	SOURCE	IDENTIFIER
Chemicals, peptides, and recombinant proteins		
1-hydroxy-8-methoxy-anthraquinone (S3)	SIGMA-ALDRICH	Cat#R164046
1-hydroxy-8-methoxy-anthraquinone (S3)	SAGECHEM LIMITED	Cat#S474625
1,4-Dithiothreit	CARL ROTH	Cat#6908.2
2-deoxy-D-glucose	SIGMA-ALDRICH	Cat#D8357
6-aminonicotinamide	SIGMA-ALDRICH	Cat#A0630; CAS: 329-89-5
6-phosphogluconolactone	SIGMA-ALDRICH	Cat#P7877
Acetonitril	SIGMA-ALDRICH	Cat#34851
Alemtuzumab	MabCampath	NDC code 58468-0357-3
Alpha-ketoglutaric acid	SIGMA-ALDRICH	Cat#61234
Adenosine-5′-diphosphate	SIGMA-ALDRICH	Cat#01905
Adenosine-5′-triphosphate	SIGMA-ALDRICH	Cat#A2383
β-nicotinamide adenine dinucleotide (NAD)	SIGMA-ALDRICH	Cat#N1511
Bendamustine hydrochloride hydrate	SIGMA-ALDRICH	Cat#B5437
BML-275 hydrochloride	SIGMA-ALDRICH	Cat#ADVH7F38323F
Citric acid	SIGMA-ALDRICH	Cat#94676
DAPI (4′,6-Diamidino-2-phenylindoldihydrochlorid)	SIGMA-ALDRICH	Cat#D9542
Daratumumab	Janssen-Cilag International N.V.	EMEA/H/C/004077
D-erythrose-4-phosphate sodium	SIGMA-ALDRICH	Cat#E0377; CAS: 103302-15-4
D-fructose 1,6-biphosphate	SIGMA-ALDRICH	Cat#F6803
D-fructose-6-phosphate disodium salt hydrate	SIGMA-ALDRICH	Cat#F3627; CAS: 26177-86-6
D-glucose-6-phosphate sodium salt	SIGMA-ALDRICH	Cat#G7879
DL-glyceraldehyde-3-phosphate	SIGMA-ALDRICH	Cat#G5251
dNTP mix	Thermo Fisher Scientific	Cat#R0192
D-ribose-5-phosphate disodium salt hydrate	SIGMA-ALDRICH	Cat#R7750; CAS: 18265-46-8
D-ribulose-5-phosphate sodium salt	SIGMA-ALDRICH	Cat#R9875
D-sedoheptulose-7-phosphate lithium salt	SIGMA-ALDRICH	Cat#78832
D-xylulose-5-phosphate lithium salt	SIGMA-ALDRICH	Cat#78963
Dihydronicotinamide adenine dinucleotide (NADH)	SIGMA-ALDRICH	Cat#47861
DL-glyceraldehyde-3-phosphate	SIGMA-ALDRICH	Cat#G5251; CAS: 591-59-3
Glacial acetic acid	VWR International	Cat#1005706
Glutathione (reduced)	SIGMA-ALDRICH	Cat#PHR1359
Glutathione–glycine-$^{13}C_2$,^{15}N trifluor	SIGMA	Cat#683620
Itaconic acid	SIGMA-ALDRICH	Cat#93598
L-malic acid	SIGMA-ALDRICH	Cat#09172
L-succinic acid	SIGMA-ALDRICH	Cat#46937
Lactic acid	SIGMA-ALDRICH	Cat#46937
LentiX GoStix Plus	Takara Bio Inc.	Cat#631280
Lymphoprep	STEMCELL Technologies	Cat#07801
M-CSF, recombinant human	Thermo Fisher Scientific	Cat#PHC9501
M-CSF, recombinant mouse	Thermo Fisher Scientific	Cat#PMC2044
Microbeads CD14 human	Miltenyi Biotec	Cat#130-050-201; RRID:AB_2665482
Nicotinamid-adenin-dinucleotid-phosphate (NADP)	SIGMA-ALDRICH	Cat#481972

(*Continued on next page*)

Continued

REAGENT or RESOURCE	SOURCE	IDENTIFIER
Obinutuzumab	Roche Registration Limited	EMEA/H/C/002799
Oligomycin	SIGMA-ALDRICH	Cat#O4876
Oxythiamine chloride hydrochloride	SIGMA-ALDRICH	Cat#O4000
PageRuler prestained NIR Protein ladder	Thermo Fisher Scientific	Cat#26635
P-hydroxyphenylpyruvate 98%	SIGMA-ALDRICH	Cat#114286; CAS: 156-39-8
Physcion	SIGMA-ALDRICH	Cat#17797; CAS: 521-61-9
Pyruvic acid	SIGMA-ALDRICH	Cat#19215
Restriction Endonuclease EcoR1	New England Biolabs Inc.	Cat#R0101L
Restriction Endonuclease Xho1	New England Biolabs Inc.	Cat#R0146L
Succinic acid D6	SIGMA-ALDRICH	Cat#488356
Vent polymerase	New England Biolabs Inc.	Cat#M0245S
Critical commercial assays		
7AAD viability staining eBioscience	Thermo Fisher Scientific	Cat#A1310
BCA Protein Assay Kit	Thermo Fisher Scientific	Cat#23227
CellTiter-Glo Luminescent Cell Viability Assay Kit	Promega	Cat#G7570
Fix & Perm Cell Permeabilization Kit	Thermo Fisher Scientific	Cat#GAS003
Human IL-6 ELISA MAX Standard Set	Thermo Fisher Scientific	Cat#430501
Human IL-10 ELISA MAX Standard Set	Thermo Fisher Scientific	Cat#430601
I-Blue Midi Plasmid Kit	IBI SCIENTIFIC	Cat#IB47180
Mouse IL-6 ELISA MAX Standard Set	BioLegend	Cat#431301; RRID:AB_2883997
Mouse IL-10 ELISA MAX Standard Set	BioLegend	Cat#431411
Odyssey Blocking Buffer	LI-COR	Cat#927-40000
Phosphopeptide Enrichment Kit	Thermo Fisher Scientific	Cat#A32993
QIA quick PCR Purification Kit	QIAGEN	Cat#28104
REVERT Total protein stain	LI-COR Biotech.	Cat#926-11011
SeaHorse XF Base Medium	Agilent Technologies, Inc.	Cat#103334-100
SeaHorse XFe96 FluxPak	Agilent Technologies, Inc.	Cat#102416-100
Zombie NIR Fixable Viability Kit	BioLegend	Cat#423105
Deposited data		
Affinity-based mass spectrometry performed with 5680 proteins (Proteomic analysis)	This paper	Accession number PXD042428, https://www.ebi.ac.uk/pride/
Affinity-based mass spectrometry performed with 19383 protein-sites (Phospho-proteomic analysis)	This paper	Accession number PXD042428, https://www.ebi.ac.uk/pride/
LC MS/MS analysis (Metabolomic analysis)	This paper	Accession number ST003516, https://www.metabolomicsworkbench.org/
Murine database for phosphopeptides	PhosphoSitePlus	https://www.phosphosite.org/staticDownloads
Experimental models: Cell lines		
Human: HEK293T-CAF40-null	DSMZ	Cat#ACC-872; RRID:CVCL_A5EE
Human: THP-1	DSMZ	Cat#ACC-16; RRID:CVCL_0006
Humanized mouse cells: hMB, strain 102		Leskov et al.[36]
Mouse: J774A.1	ATCC	Cat#TIB-67; RRID:CVCL_0358
Human: L-929	DSMZ	Cat#ACC-2; RRID:CVCL_0462

(*Continued on next page*)

Continued

REAGENT or RESOURCE	SOURCE	IDENTIFIER
Experimental models: Organisms/strains		
Mouse: C57BL/6J	Jackson laboratory	Cat#000664; RRID:IMSR_JAX:000664
Mouse: Wild-type NOD.Cg-Prkdc^{scid} Il2rg^{tm1Wjl}/SzJ (NSG)	Jackson laboratory	Cat#005557/NSG; RRID:IMSR_JAX:005557
Mouse: C57BL/6NJ-Acod1$^{em1(IMPC)J}$/J	Jackson laboratory	Cat#029340; RRID: IMSR_JAX:02 9340
Oligonucleotides		
6PGD_1	SIGMA-ALDRICH	Oligo#8810932277-000060
6PGD_2	SIGMA-ALDRICH	Oligo#8810932277-000070
TKT_1	SIGMA-ALDRICH	Oligo#8810932277-000040
TKT_2	SIGMA-ALDRICH	Oligo#8810932277-000050
Software and algorithms		
Enhanced Volcanoplot software (Figure 4)	Bioconductor	https://bioconductor.org/packages/release/bioc/html/EnhancedVolcano.html
FlowJo 10.7.1	FlowJo	https://www.flowjo.com/solutions/flowjo
GeneAnalytics	LifeMap Sciences	https://geneanalytics.genecards.org/
GraphPad Prism6	GraphPad Software	https://www.graphpad.com/
Image Studio Lite	LI-COR Biotechnology	https://www.licor.com
ImageJ	U.S. Department of Health & Human Services	https://imagej.nih.gov/ij/download.html
INKA (original and own mouse modification)	Molecular System Biology; this paper	Beekhof et al.[22]
MACSQuantify	Miltenyi Biotec	https://www.miltenyibiotec.com
MaxQuant	Max-Planck-Institute of Biochemistry	https://maxquant.net/maxquant/
NDP.view2 Plus Image viewing software U12388-02	Hamamatsu Photonics Deutschland GmbH	https://www.hamamatsu.com/eu/en/product/life-science-and-medical-systems/digital-slide-scanner/U12388-01.html
Perseus	Max-Planck-Institute of Biochemistry	https://maxquant.net/perseus/
PRIDE database	EMBL-EBI	https://www.ebi.ac.uk/pride/
StringAnalysis	STRING Consortium 2021	https://string-db.org

EXPERIMENTAL MODEL AND STUDY PARTICIPATION DETAILS

Mouse strains

Wild type NOD.Cg-Prkdcscid Il2rgtm1Wjl/SzJ (NSG) and C57BL/6 mice were from Jackson laboratory (ME, USA), Acod1eml(IMPC)J/1J mice were kindly provided by Paul Diefenhardt from AG Braehler (Uniklinik Köln, CECAD Research Center, AG Braehler, Joseph-Stelzmann-Str. 26, 50931 Cologne, Germany). NSG is an immune-deficient strain with compromised generation of lymphocytes, natural killer cells, macrophages, and immunoglobulins caused by lacking expression of PRKDC and the γ-chain of interleukin-2 receptor. Acod1eml(IMPC)J/1J is a mouse strain with global guide RNA mediated knockout of Acod1 (=Irg1) on background of C57BL/6 mice. C57BL/6 is a commonly used immune competent inbreeding strain. To generate the humanized double-hit lymphoma mouse model, 8–18 week old NSG mice got intravenous injection of 1×10^6 hMB cells in 100μL PBS.

Animals (female and male; 0–40 weeks) were maintained under specific pathogen free conditions in line with European Union regulations. Experiments were approved by local ethical review (LANUV (Landesamt für Natur, Umwelt und Verbraucherschutz Nordrhein-Westfalen)) and were carried out under the authority of Michael Michalik M. Sc., (Uniklinik Köln, Translational Research for Infectious Diseases and Oncology (TRIO), Robert-Koch-Straße 21, 50931 Cologne, Germany) project license.

Mice were kept under cage conditions at 20°C–22°C. Littermates of the same sex were randomly assigned to experimental groups. Adult mouse weight is around 23,4 g.

Cell lines

HEK293T-CAF40-null cells were from DSMZ, hMB cells were generated by Leskov et al.,[36] J774A.1 macrophages were from ATCC, THP1 monocytes were from DSMZ.

hMB cells represent a humanized mouse model of "double-hit" lymphoma by overexpression of c-MYC and BCL2 in human HSC-derived B-lineage cells. hMB cells express GFP and can be targeted by antibodies used in clinics. Like most double-hit lymphoma patient cells, hMB cells have a low expression of CD20.

All cell lines were cultured on 6 well plates or 10cm dishes from Corning and incubated with 5% CO_2 at 37,0°C. J774A.1 cells, hMB cells, and HEK293T cells were cultured in DMEM containing 10% fetal bovine serum and 1% penicillin/streptomycin. THP1 cells were cultured in RPMI 1640 medium containing 10% FBS and 1% penicillin/streptomycin.

Primary cells

Primary CLL patient cells and primary monocytes from healthy donors were collected from buffy coats donated by blood bank of University Hospital of Cologne. Cells were cultured on 6 well plates or 10cm dishes from Corning and incubated with 5% CO_2 at 37,0°C. The cells were cultured in RPMI 1640 medium containing 10% FBS and 1% penicillin/streptomycin.

Monocytes of buffy coats were separated by CD14 anti-human magnetically labeled MicroBeads from Miltenyi Biotec.

The study was approved by the ethical commission of the medical faculty of the University of Cologne (reference no. 13–091) and performed under the authority of Prof. Michael Hallek (Department I of Internal Medicine, Center for Integrated Oncology (CIO) Aachen-Bonn-Cologne-Duesseldorf, University of Cologne, Kerpener Str. 62, 50937 Cologne, Germany) project license.

Microbe strains

5-alpha competent E. coli from New England Biolabs Inc. were used for plasmid generation.

METHOD DETAILS

Antibody-dependent cellular phagocytosis assay (ADCP)

1×10^4 J774A.1 cells were plated out in 100μL media per well in a 96 well plate. After 24hrs of attachment, hMB cells were added in a macrophage:hMB ratio 1:15. Compounds were added in increasing concentration up to maximal non-toxic concentration. Alemtuzumab was added to every second well in a concentration of 10μg/mL. Wells were filled up with macrophage medium up to volume of 250μL. Each ADCP was performed with 5 technical replicates. After 18hrs of incubation, remaining hMB cells per well (GFP positive) were measured using Miltenyi MacsQuant VYB flow cytometer. Out of the absolute GFP positive cell count the antibody-dependent cellular phagocytosis rate was calculated with the formula

100-(100*(total GFP^+ antibody-treated well/total GFP^+ antibody-untreated well)).

The calculated ADCP rate was compared to basal ADCP rate of untreated control cells (set as 100%) by division of the calculated ADCP rates (= ADCP change). For ADCP assays performed with THP1 cells the amounts were subtracted to avoid bias as basal phagocytosis rate of THP1 cells is low (= ADCP difference).

For pre-treatment assays, macrophages respectively hMB cells were treated with increasing concentration of the compounds up to maximal non-toxic concentration. After 24hrs of incubation, the cells were washed three times and the assay was performed as described above without addition of the compounds to co-culture.

Performing the assay with THP1 cells, the antibody obinutuzumab was used in a concentration of 1 μg/mL.

Compounds and antibodies were diluted in media of used macrophage type respectively in hMB medium in case of hMB pre-treatment ADCP assays.

For ADCPs in hypoxia, cells were incubated under hypoxic conditions with 1.5% O_2 and 5% CO_2.

For ADCPs with CLL patient cells, CLL patient cells were used instead of hMB cells.

For ADCPs with primary human macrophages, 2×10^4 primary human macrophages and 3×10^5 hMB cells were used per well. As antibody daratumumab in a concentration of 10μg/mL was used.

For ADCPs with primary murine macrophages, 5×10^4 primary murine macrophages and $1,5 \times 10^5$ hMB cells were used per well. As antibody daratumumab in a concentration of 10μg/mL was used.

Antibody-independent cellular phagocytosis assay (AICP)

Experiment was performed like ADCP without the addition of antibody. Remaining hMB cells were compared to hMB mono-culture cell count under inhibitor treatment. After 18hrs of incubation, remaining hMB cells per well were measured using Miltenyi MacsQuant VYB flow cytometer. Out of the absolute GFP positive cell count the antibody-independent cellular phagocytosis rate was calculated with the formula

100-(100(total GFP^+ macrophage co-culture well/total GFP^+ hMB mono-culture well))*.

Bone marrow derived macrophage generation

Femur were flushed with DMEM media. Erythrocytes were lysed by addition of 2mL ACK lysis buffer to cells. Reaction was stopped by addition of 50mL cold PBS. Cells were re-suspended in media and plated out on 10cm cell culture plates for 24hrs. Non adherent cells were collected and plated out in a concentration of 6×10^5 cells/mL on 10cm cell culture plates in media and 15% feeder media 1 and 2. Feeder media was collected from L-929 cells after incubation with RPMI media for one week (feeder media 1) and three weeks (feeder media 2). On day three additional 4mL media with 15% feeder media 1 and 2 and 50ng murine recombinant M-CSF were added. On day seven media was replaced by 10mL media. On day eight the plates were washed two times and adherent macrophages were detached by scraping. Macrophages were plated out for further experiments and were incubated for 24hrs for recovering before further experiments were performed.

Please cite this article in press as: Beielstein et al., Macrophages are activated toward phagocytic lymphoma cell clearance by pentose phosphate pathway inhibition, Cell Reports Medicine (2024), https://doi.org/10.1016/j.xcrm.2024.101830

CLL patient cell co-culture

5×10^4 J774A.1 cells were plated out in 1mL media on a 24 well plate and were incubated for 5hrs. Three samples per condition were treated with the PPP inhibitors for macrophages pre-treatment. Cells were incubated for 24hrs. Pre-treated cells were washed three times. Viability of CLL patient cells was measured by 7AAD plus AnnexinV staining. Therefor, 2μL 7AAD stain, 2μL AnnexinV stain and 46μL 1% ABB were added to washed cells, cells were incubated for 20 min at 4°C and additionally 50μL 1% ABB was added. Readout was performed immediately using Miltenyi MacsQuant X flow cytometer. $7{,}5 \times 10^5$ viable CLL patient cells in 1mL media were added to the macrophages and CLL mono-culture wells were plated out under addition of 1mL DMEM. Three samples per condition were treated with PPP inhibitors for co-culture treatment. The co-culture was incubated for three days. CLL cells were re-suspended by pipetting and supernatant was transferred into eppies. On U-bottom plates 7AAD plus AnnexinV staining (see above) was performed and cell count was measured using Miltenyi MacsQuant X flow cytometer.

CLL patient cell chemotoxicity stain

CLL patient cells after CLL co-culture performance were transferred into 96 U-bottom plates. 25μL of each bendamustine concentration was added to one well of each condition. Cells were incubated for 48hrs. Cells were washed and 7AAD plus AnnexinV staining was performed (see above).

Chemotoxicity assay was also performed by adding the cells to 1×10^4 J774A.1 cells per well plated out the day before. After co-incubation for 48hrs, wells were mixed up and supernatant was transferred to a 96 U-bottom plate to perform 7AAD plus AnnexinV staining of the CLL patient cells (see above).

ELISA

7×10^5 J774A.1 cells in 2mL media per well were plated out on a 12 well plate and incubated for 24hrs. Each inhibitor was added to two wells and cells were incubated for 24hrs. 100ng/mL LPS was added to one well of each condition. After incubation of 16hrs, supernatant was transferred into Eppendorf tubes. The supernatant was centrifuged at 300g for 5min and transferred to new Eppendorf tubes. BioLegend ELISA kit for IL-10, and IL-6 was used and protocol performed as from BioLegend mentioned. Readout was performed by fluorescence intensity measurement using FLUOStar OPTIMA.

Immunofluorescent microscopy

Microscopy coverslips were washed three times in ethanol and autoclaved. Two microscopy coverslips per well were placed on a 6 well plate. 1×10^6 J774A.1 cells in 1mL media per well were plated out, treated with the PPP inhibitors and incubated for 24hrs. Cells were washed with 5mL DPBS for 5min. 2mL PFA was put on the cells and incubated for 10min. Cells were washed three times with 5mL DPBS for 5min. Cells were incubated with 2mL of DPBS with 0.25% Triton X- for 3min. Cells were incubated with 2mL of DPBS with 0.125% Triton X- plus 5% BSA for 1h. Coverslips were taken off the 12 well plate and dried on a paper towel. Mitochondrial antibody TOM20 F-10 was diluted 1:500 in DPBS plus 0.125% Triton X- plus 2.5% BSA, 100μL was pipetted on the coverslips and they were incubated for 2hrs. Coverslips were washed three times with 100μL DPBS with 0.125% Triton X-. 2^{nd} mitochondrial antibody (Alexa Fluor 647 α mouse) was diluted 1:1000 in DPBS plus 0.125% Triton X- plus 2.5% BSA, 100μL was pipetted on the coverslips and they were incubated for 1h. Coverslips were washed three times with 100μL DPBS with 0.125% Triton X-. Actin antibody (Phalloidin Alexa Fluor 568) was diluted 1:1000 in DPBS with 0.125% Triton X- plus 2.5% BSA, 100μL was pipetted on the coverslips and they were incubated for 1h. Coverslips were washed nine times with 100μL DPBS with 0.125% Triton X-. Nuclear antibody (DAPI) was diluted 1:10000 in DPBS and 100μL was pipetted on the coverslips. Coverslips were washed one time with 100μL H_2O. Coverslips were dried on a paper towel, one drop of mounting media was put on and the coverslips were placed on object plates. The probes were dried overnight at room temperature and then stored at 4°C until microscopy. Pictures were recorded using SP8 confocal microscope (Leica) and analyzed with ImageJ.

Immune phenotyping

1×10^6 J774A.1 cells in 1mL media were plated out on a 6 well plate and treated with PPP inhibitors. After 24hrs of incubation, cells were scraped off. Cells were washed with 1mL DPBS. Cells were re-suspended in 90μL DPBS and 10μL murine FcR-blocking agent. Cells were incubated for 10min at 4°C. 900μL DPBS were added and probes were split into 100μL portions. Master mixes of different stains were prepared and added to the cells. Cells were incubated for 20min at 4°C and washed with 1mL DPBS afterward. For washing, cells were incubated with DPBS for 5min and centrifuged at 300g for 5min afterward. Cells were re-suspended in 200μL DPBS and measured using Miltenyi MacsQuant X flow cytometer immediately after an initial multi-color compensation procedure.

For intracellular marker, Fix & Perm Cell Permeabilization kit was used following manufacturés protocol.

Primary murine macrophages were processed equally.

Immunohistochemical staining of murine spleen

After preparation of survival cohort of hMB transfected NSG mice after treatment with alemtuzumab and/or S3, a 2 × 2mm piece of spleen was fixated in formaldehyde. Histological sections were produced and immunohistochemical staining of CD19 and CD68 was performed. Whole slide scans were saved and analyzed with NDP.view2 Plus Image viewing software.

In vivo experiments

Survival analysis of hMB transfected NSG mice under treatment with alemtuzumab and/or S3

8-18 week old NSG mice got intravenous injection of 1 × 10^6 hMB cells in 100μL PBS.

Four cohorts were built:

(1) vehicle + vehicle
(2) vehicle + alemtuzumab
(3) vehicle + S3
(4) alemtuzumab + S3

Three days after tumor cell injection, cohort 3 and 4 were treated for ten days with 20mg/kg S3 in 200μL 30% PEG 400/0.5% Tween 80/5% propylene glycol (vehicle 200μL 30% PEG 400/0.5% Tween 80/5% propylene glycol) intraperitoneally. On day 8 after tumor cell injection alemtuzumab was applicated for three days intraperitoneally. On day 8 the mice were injected with alemtuzumab 1mg/kg, on day 9 and 10 with 5mg/kg, in a total volume of 50μL PBS (vehicle 50μL PBS). Mice were scored daily with a score sheet developed for hMB-transfected NSG mice.

Macrophage function analysis of primary murine macrophages of C57BL/6 after treatment with S3

8-18 week old C75BL/6 mice were treated for seven days with 20mg/kg S3 in 200μL 30% PEG 400/0.5% Tween 80/5% propylene glycol (vehicle 200μL 30% PEG 400/0.5% Tween 80/5% propylene glycol) intraperitoneally. Mice were scored daily and were sacrificed on day eight. Peritoneal macrophages were collected by peritoneal lavage with DMEM medium. Spleen and femurs were dissected. Spleen were mashed through a 30μM filter with DMEM medium and cell suspension was used for further analysis. Femurs got flushed with DMEM medium to collect bone marrow.

Knockdown cell production

Plasmid production

Target sequence oligonucleotides were produced by SIGMA-ALDRICH. For oligonucleotide cloning, 1μL of 1μM oligonucleotide, 2,5μL thermopol polymerase buffer, 2,5μL of 5μM primer EcoR1, 2,5μL of 5μM primer Xho1, 0,5μL dNTPs mix, 0,5μL vent polymerase and 14,5μL H_2O were mixed and polymerase chain reaction was performed. Oligonucleotides were selected by electrophoretic separation using FAE gel with 1.5% agarose and 5μL GELRed Nucleic Acid Gel stain 10000x. After cutting out oligonucleotide bands under UV-light, oligonucleotides were purified with QIAquick PCR purification kit (kit protocol followed). For oligonucleotide digest, 30μL oligonucleotide solution, 1μL primer EcoR1, 1μL primer Xho1 and 8μL NEBuffer 2 were incubated for 2hrs at 37°C. Oligonucleotides were purified again as described above, oligonucleotide concentration was determined with Quick-load 100bp DNA ladder on gel and oligonucleotides were solved in 30μL elution buffer. For ligation 2.92ng oligonucleotide and 97,08ng vector [MLP plasmid, 7893bp] with 1μL 10x T4 DNA Ligase Reaction Buffer and 1μL T4 DNA ligase were used and filled up with H_2O to 10μL. Probes were incubated for 1h at room temperature.

Transformation into competent bacteria

Competent E. coli were thawed on ice. 5μL plasmid per 50μL competent cells was added and incubated for 30min on ice. Heat shock for 110s at 42°C and recovery for 2min on ice was done. Cells were centrifuged at 6000rpm for 1min, supernatant was removed and 450μL fresh LB media (1% tryptone, 0.5% yeast extract, 1% NaCl, filled up with water) was added. Cells were recovered in shaker for 30min at 37°C and 100μL were plated out on LB media layer (1% tryptone, 0.5% yeast extract, 1% NaCl, 1.5% agar filled up with water) with 100μg/mL ampicillin in a 10cm dish.

Plasmid enrichment and purification

When colonies on bacteria plate were visible by eye, 4–5 colonies per plasmid were picked and expanded overnight in 50mL LB media with 100μg/mL ampicillin in shaker at 37°C. For later use, a probe of each colony was saved on a new bacteria plate. Plasmids were purified by using I-Blue Midi Plasmid Kit (following kit protocol).

For sequence verification, 10μL of 100ng plasmid with 4μL MSV-5 primer was sent to LGC Genomics GmbH.

Plasmids with correct sequence were picked from back up bacteria plate and expanded and purified again as described above.

Transfection with phoenix retroviral producer line

8 × 10^6 HEK293T cells were plated out on a 10cm dish and incubated overnight. Cells were washed and 10mL DMEM media without any supplements was put on the cells. 25μM cholorquine was added and cells were incubated for 10min at 37°C. 18,5μg plasmid, 3μg pMD2.G, 5μg psPax2 and 99μL 2M $CaCl_2$ were mixed and filled up with H_2O to 790μL. Under mixing with bubble formation, 790μL 2x HEPES buffered saline (280mM NaCl, 50mM HEPES, 1.5mM Na_2HPO_4, adjusted pH to 7,05) was added and mixture was added immediately dropwise to the HEK293T cells. Cells were incubated for 4hrs, then media was soaked off, cells were washed with 10mL DPBS and 10mL HEK293T cell media was added. 100μM sodium butyrate was added and cells were incubated. After 24hrs and 48hrs supernatant was collected and centrifuged at 1500rpm for 10min. Supernatant was filtered through a 45μm filter and flow through was used for further steps. New media and sodium butyrate was put on the HEK293T cells.

Virus production was verified with fluorescent microscopy and Lenti-X GoStix Plus.

Infection of J774A.1 macrophages

1×10^5 J774A.1 cells in 1mL media per well were plated out on a 12 well plate and incubated for 24hrs. 1mL of viral media per well was added and cells were spin at 800CF for 2hrs at 32°C. Cells were incubated for 48hrs. Cell media was changed and cell selection with 2μg/mL puromycin was started. Selection efficacy was verified using Miltenyi MacsQuant X flow cytometer. ≥ 95% GFP-positive macrophages were accepted as pure shRNA-transfected cells.

Metabolomics

Sample preparation

1×10^7 J774A.1 (wild-type, empty vector control, shRNA 6PGD knockdown or shRNA TKT knockdown) in 10mL media were plated out on 10cm dishes and incubated for 24hrs. Dishes were treated with PPP inhibitors (oxythiamine 520μM, physcion 9μM or 6-aminonicotinamide 11μM) and incubated for 24hrs. Cells were scraped, washed with DPBS and re-suspended in 1mL DPBS. The cells were counted using CASY cell counter and analyzer. Cells were centrifuged at 300g for 5min and supernatant was discarded. Cell pellet was crash frozen using liquid nitrogen.

The cell pellets were sent to the Center of Metabolomics and Bioanalysis (CEMBIO) at San Pablo CEU University in Madrid (Spain). The analysis of metabolites was performed in the laboratory of Dr. Coral Barbas following previous work.[31]

Macrophage pellet was resuspended in 50μL of cold MeOH, vortex-mixed for 2min and incubated on ice for 5min in order to precipitate the protein content. Samples were sonicated for 4min to break the cell membranes, and 50μL of water was added to extract and solubilize metabolites. Samples were vortex-mixed for 2min and centrifuged for 20min at 4°C at 12.000g. 60μL of the supernatant was transferred to a liquid chromatography (LC) vial for the analysis. 20μL of the remaining supernatant of each sample were taken to make a pool solution (named quality control, QC). The QC sample was used to estimate the concentration of the metabolites and these concentrations were selected as the intermediate point of external calibration curve (100%). The selected range for the external calibration curve was from 25 to 800%. The external calibration curve was prepared using equal volumes 1:1 (*v/v*) of the QC sample and level each of the standard levels leading to the final levels of 25%, 50%, 100%, 200%, 400%, and 800% (calibration curve levels L1-L6, respectively).

LC MS/MS analysis

Sample analysis was performed in an Agilent 1290 Infinity high-pressure liquid chromatography system (HPLC), consisting of a degasser and an autosampler, and using an Infinity Binary Pump (1200bar) and a 400bar 1260 Infinity Quaternary Pump (both from Agilent Technologies, Waldbronn, Germany). The HPLC system was coupled to an Agilent 6460 triple quadrupole mass spectrometer using an electrospray (ESI) source working in dynamic multiple reaction monitoring (dMRM) mode (Agilent Technologies, 465 Waldbronn, Germany). 6μL of sample supernatant was injected into a reverse-phase column (Zorbax Extend-C18 (1.8μm, 2.1 mm × 15 cm, Agilent Technologies, CA, USA) with a guard column (Zorbax Extend-C18 guard (1.8μm, 2.1 mm × 5 mm, Agilent Technologies, CA, USA), maintained at 50°C. LC-QqQ/MS mobile phases consisted of mobile phase A prepared by mixing 97% Milli-Q water (v/v) with 3% (v/v) MeOH, 10mM tributylamine (≥99.5%), and 15mM glacial acetic acid and mobile phase B, prepared by adding 10mM tributylamine and 15mM glacial acetic acid to MeOH. The LC-QqQ/MS mobile phase for the quaternary bump consisted of mobile phase C, identical to mobile phase A, and mobile phase D made of ACN. The chromatographic separation was based on gradient elution using a binary pump at a flow rate of 0.25mL/min with a composition of 0% B from time 0−2.5min, and then % B was progressively increased until 20% B at 7.5min, up to 45% B at 13.0min, and up to 99% B at 20.0min, which was held until 24.0min. Then, the equilibration step started and the flow of the binary pump was stopped at 24.05min while allowing a subsequent quaternary pump washing step. It started with 99% C at 24.0min with a flow rate of 0.2mL/min until 27.0min, and then the flow rate was gradually increased until 0.3mL/min at 27.5min and until 43.5min. Subsequently, % C was progressively decreased up to 0% C while returning the flow rate to 0.2mL/min at 52.25min. These conditions were held until 59.0min and returned to 99% C at 59.9min. Finally, the binary pump was activated at 0% B at 59.0min, with a flow rate of 0.2mL/min, and increased up to 0.25mL/min at 60.0min. The total method run time was 60min.

Metabolites were ionized in an ESI source operating in negative ionization mode. The drying gas flow rate was 13L/min at 225°C, and the nebulizer was set to 60psi. The sheath gas flow rate was set to 12L/min at 250°C; capillary and nozzle voltages were set to 3500V and 2000V, respectively. Data were acquired in dynamic MRM mode, using a cycle time of 1000ms. Transitions showing the highest signal-to-noise ratios were used for the quantification of the metabolites in samples. For those metabolites with two transitions with a good signal-to-noise ratio, the less intense transitions were used for identification and confirmation of the metabolite (see Table S6).

Sample quantitation and statistical analysis

Samples were analyzed in a randomized order, injecting the calibration curve from the lower to the higher concentrated ones in regular intervals. Output raw data files were reprocessed with Agilent MassHunter Workstation Software Quantitative Analysis for QQQ, from which a metabolite matrix containing the integrated area and retention time (RT) for specific transitions was obtained. The concentration of the metabolites in the samples were calculated by interpolation in calibration curves and normalized by the number of cells. Statistical analysis and graph representation was carried out using GraphPad Prism (v.9.5.0) software.

Maturation staining of primary murine macrophages

For LSK compartment analysis, ACK lysis buffer was added to bone marrow cells for 2min to lysate erythrocytes. Bone marrow cells were processed as described in section Immune phenotyping and stained with maturation antibody panel. Common myeloid progenitor cells: CD41, CD34. Monocytes: CD11b, CX3CR1, Ly6C. Macrophages: CD11b, F4/80, CD64. LSK compartment analysis was performed by Felix Picard (AG Holger Winkels, University of Cologne) with 5×10^6 cells per mice.

Phosphoproteomics

Sample preparation and lysis

Three dense 25cm dishes with J774A.1 cells were treated with PPP inhibitors. After 24hrs incubation, plates were washed with 20mL 4°C DPBS per plate. Cell dishes were placed on ice, 1mL RIPA buffer with 1% phosphatase and 1% protease inhibitor was added, cells were scraped off and transferred into 2mL Eppendorf tubes on ice. Cells were centrifuged at full speed for 30min at 4°C. DNA was sheared by sonication with Bioruptor for 10min at 4°C. Samples were centrifuged at full speed for 10min at 4°C and supernatant was transferred into new Eppendorf tubes. Protein concentration was determined by BCA assay. 3mg protein was used for further steps.

Acetone precipitation

Four times volume of cold 100% acetone was added and samples were incubated overnight at −20°C. Samples were centrifuged at 15000g for 10min at 4°C. Supernatant was discarded and pellet washed twice with 250μL 80–90% acetone under centrifugation at 15000*g* for 10min at 4°C. Uncapped tubes were left at room temperature for 5-10min to let remaining acetone evaporate without overdrying. Pellet was dissolved in 300μL 6M Urea/2M Thiourea.

In solution digest

1mM 1,4-Dithiothreit (DTT) was added and samples were incubated for 1h at room temperature. 5.5mM iodoacetic acid (IAA) was added and samples were incubated for 20-45min at room temperature in the dark. 60μL 0.5μg/μL endoprotease Lys-C was added and samples were incubated for 3hrs at room temperature. 900μL 50mM ammonium bicarbonate and 60μL 0.5μg/μL trypsin were added and samples were incubated overnight at room temperature. Samples were acidified with 1% trifluoroacetic acid and centrifuged for 10min at full speed. Supernatant was transferred to a new Eppendorf tube for further steps.

Sample purification by stage tips

C18 columns (200mg Sep Pak of capacity up to 10mg protein) were prepared. Columns were activated with 1mL 100% acetonitrile and washed twice with 1mL 0.1% trifluoroacetic acid. Flow through was discarded and samples were loaded on column. Flow through was discarded and column was washed twice with 1mL 0.1% trifluoroacetic acid. Peptides were eluted into Eppendorf tubes by adding two times 0.2mL elution buffer (60% acetonitrile, 0.1% formic acid).

Sample enrichment

Phosphopeptide samples were enriched using High select TiO_2 Phosphopeptide Enrichment Kit by following kit protocol.

Sample measurement

Label-free quantification of peptides was performed on mass spectrometer (Q Exactive Plus Hybrid Quadrupole-Orbitatrap Mass Spectrometer + EASY-nLC 1200 System) by cooperating CECAD proteomics facility, University of Cologne.

Analysis

Raw data acquired from CECAD proteomics facility were filtered and processed on MaxQuant software (v.1.5.3.8) and Perseus software (v.1.5.5.3).

Primary human macrophages

Isolation of CD14⁺ cells

Peripheral blood mononuclear cells (PBMCs) were isolated from buffy coats of healthy donors provided by blood bank of University Hospital of Cologne. 15mL Lymphoprep was added to a 50mL SepMateTM tube, buffy coats were diluted 1:1 in sterile room temperature DPBS and 20-25mL of it was layered on the top of the Lymphoprep through pipetting it to the walls of the SepMateTM tube. Tubes were centrifuged at 1200g for 15min at room temperature. PBMCs ring was harvested by pouring entire top layer in new 50mL falcon tube. Cells were washed three times with 50mL DPBS and centrifuged at 1300rpm for 8min. Cell pellet was re-suspended in 12mL 4°C MACS buffer (2mM EDTA +5% Bovine serum albumin (BSA) (PAA Laboratories)), transferred to 15mL tube, centrifuged at 1300rpm for 8min at 4°C and discarded. 200μL of CD14 anti-human magnetically labeled MicroBeads and 800μL of 4°C MACS buffer was added. Magnetic separation was performed by Miltenyi Biotec CD14 human microbead isolation protocol using Miltenyi MacsQuant X flow cytometer. $CD14^+$ cells were then re-suspended in RPMI 1640 media. Differentiation was started immediately.

Differentiation of human monocytes under PPP inhibition

1×10^6 $CD14^+$ cells in 2mL RPMI 1640 media per well were plated out on a 12 well plate. 10ng/mL M-CSF and oxythiamine were added at day 1, 3 and 5 without changing the medium. On day 7 the cells were scraped off and used for further experiments.

Proteomics

Sample preparation and lysis

1×10^7 J774A.1 cells ins 10mL media per 10cm dish were plated out and after 24hrs treated with PPP inhibitors. After another 24hrs, plates were washed with 10mL 4°C DPBS per plate. Cell dishes were placed on ice, 500μL RIPA buffer with 1% phosphatase and 1%

Please cite this article in press as: Beielstein et al., Macrophages are activated toward phagocytic lymphoma cell clearance by pentose phosphate pathway inhibition, Cell Reports Medicine (2024), https://doi.org/10.1016/j.xcrm.2024.101830

protease inhibitor was added, cells were scraped off and transferred into 2mL Eppendorf tubes on ice. Cells were centrifuged at full speed for 30min at 4°C. DNA was sheared by sonication with Bioruptor for 10min at 4°C. Samples were centrifuged at full speed for 10min at 4°C and supernatant was transferred into new Eppendorf tubes. Protein concentration was determined by BCA assay. 30μg protein was used for further steps.

Acetone precipitation

Four times volume of cold 100% acetone was added and samples were incubated overnight at −20°C. Samples were centrifuged at 15000g for 10min at 4°C. Supernatant was discarded and pellet washed twice with 250μL 80–90% acetone under centrifugation at 15000*g* for 10min at 4°C. Uncapped tubes were left at room temperature for 5-10min to let remaining acetone evaporate without overdrying. Pellet was dissolved in 60μL 6M urea/2M thiourea.

In solution digest

3μL 1M DTT was added and samples were incubated for 1h at room temperature. 3μL 550mM IAA was added and samples were incubated for 20-45min at room temperature in the dark. 0,6μL 0.5μg/μL endoprotease Lys-C was added and samples were incubated for 3hrs at room temperature. 180μL 50mM ammonium bicarbonate and 0,6μL 0.5μg/μL trypsin were added and samples were incubated overnight at room temperature. Samples were acidified with 1% trifluoroacetic acid and centrifuged for 10min at full speed. Supernatant was transferred to a new Eppendorf tube for further steps.

Sample purification by stage tips

Stage tips were prepared by stacking 2 layers of SDB-RPS material in a 200μL pipette tip. Stage tips were equilibrated with 20μL 100% methanol and centrifuged at 2600rpm for 2min. 20μL elution buffer (80% acetonitrile +0.1% trifluoroacetic acid) was added and tips were centrifuged at 2600rpm for 2min. 20μL washing buffer (0.1% trifluoroacetic acid) was added and tips were centrifuged at 2600rpm for 1min. 100μL of the sample was added and tips were centrifuged at 2600 rpm for 5min. Tips were washed with 100μL washing buffer and centrifuged at 2600rpm for 3min once and two times with elution buffer. Stage tips were dried with a syringe and stored at −4°C.

Sample measurement

Peptides were eluted with 30μL 1% ammonia in 60% acetonitrile into 96 well plate and dried using SpeedVac concentrator. Label-free quantification of peptides was performed on a mass spectrometer (Q Exactive Plus Hybrid Quadrupole-Orbitatrap Mass Spectrometer + EASY-nLC 1200 System) by cooperating CECAD proteomics facility, University of Cologne.

Analysis

Raw data acquired from CECAD proteomics facility were filtered and processed on MaxQuant software (v.1.5.3.8) and Perseus software (v.1.5.5.3).

SeaHorse analysis

1×10^5 J774A.1 cells in 100μL media per well were plated out in the XFe96 cell culture microplate. PPP inhibitors were added and cells were incubated for 24hrs. Agilent Seahorse XFe96 Sensor Cartridge was prepared (following Agilent user guide) and cell culture microplate and sensor cartridge preparation for measurement were done (following Agilent protocol). Sensor cartridge injection ports were filled with 20μL of 1μM oligomycin (port A), 22μL of 0.5μM Carbonyl cyanide-*4*-(trifluoromethoxy)phenylhydrazone (FCCP) (port B), and 25μL of 1μM antimycin A plus 100μM rotenone (port C). Four measurement cycles of basal activity of the cells and three cycles of measurement after each injection were performed by Agilent Seahorse XF Analyzer.

Viability stain

7AAD staining was performed for hMB cells and Zombie-NIR staining was performed for J774A.1 cells.

For 7AAD staining, $1{,}5 \times 10^5$ hMB cells were plated out in 100μL media per well on a 96 well plate. At least duplicates were treated with one concentration of the tested inhibitor. As positive control 10% dimethylsulphoxide (DMSO) was used. After 24hrs of incubation, cells were transferred into a 96 well U-bottom plate, washed and 7AAD staining was performed. Therefore, 2μL 7AAD stain and 48μL 1x ABB were added per well, cells were incubated for 20min at 4°C and additionally 50μL 1% ABB was added. Readout was performed immediately using Miltenyi MacsQuant X flow cytometer. Inhibitor concentrations with an amount of viable cells ≥90% compared to untreated control were accepted as non-toxic concentration.

For Zombie-NIR staining, $1{,}2 \times 10^6$ J774A.1 cells were plated out in 1mL media on a 12 well plate. Duplicates were treated with one concentration of the tested inhibitor. As positive control 10% DMSO was used. After 24hrs of incubation, cells were scraped off, transferred into FACS tubes and Zombie-NIR staining was performed. A dilution of Zombie-NIR staining solution 1:100 in DPBS was used. Readout was performed using Miltenyi MacsQuant X flow cytometer. Inhibitor concentrations with an amount of viable cells ≥90% compared to untreated control were accepted as non-toxic concentration.

Additionally, Cell titer glo assay was used to measure viability of J774A.1, THP1 and hMB cells. 1×10^4 J774A.1 cells or THP1 cells respectively $1{,}5 \times 10^5$ hMB cells were plated out in 100μL media per well on a 96 well plate. Triplets were treated with one concentration of the tested inhibitor. As positive control 10% DMSO was used. After 18hrs, cells were washed two times, were transferred to white 96 well plate and Cell titer glo staining was performed. Readout was performed by fluorescence intensity measurement with FLUOStar OPTIMA. Inhibitor concentrations with an ATP amount of the cells ≥90% compared to untreated control were accepted as non-toxic concentration.

Please cite this article in press as: Beielstein et al., Macrophages are activated toward phagocytic lymphoma cell clearance by pentose phosphate pathway inhibition, Cell Reports Medicine (2024), https://doi.org/10.1016/j.xcrm.2024.101830

Western Blot analysis

3×10^6 J774A.1 respectively $4,5 \times 10^6$ hMB cells were plated out on a six well plate. The cells were treated and incubated for 18hrs. The cells were washed with 1mL DPBS, discarded and stored on ice. 30μL of RIPA buffer (50mM Tris-HCl pH8, 150mM NaCl, 0.1% SDS, 0.5% DOC, 1% NP-40, filled up with ddH2O) with 1x Phosphatase Inhibitor Cocktail 2 and 1x Protease Inhibitor Cocktail were added and probes centrifuged for 30min at full speed at 4°C. Supernatant was used for the experiments. BCA-Assay was performed to evaluate protein concentration, measured with FLUOStar OPTIMA. 60μg protein per condition was used, volume filled up with RIPA to 5μL and 5μL Urea added. Probes were incubated at 37°C for 10min. A 10% separating gel (1.85mL Buffer (1.5mM Tris HCL pH8.8, 0.4% SDS, ddH_2O), 1.66mL 30% Rotiphorese, 1.5mL ddH_2O, 40.6μL APS and 4.06μL Temed) and a 5% stacking gel (0.31mL Buffer (0.5M Tris HCl pH6.8, 0.4% SDS, ddH_2O), 0.42mL 30% Rotiphorese, 1.75mL ddH_2O, 12.5μL APS and 1.25μL Temed) were produced. 3.5μL Page Ruler Prestained NIR Protein Ladder was used. Western Blot run was performed in Running Buffer (25mM Tris, 192mM glycine, 3.5mM SDS in ddH_2O) at constant 80V until stacking gel was passed and at constant 150V in separating gel. Gel was blotted on nitrocellulose membrane Hybind-C at constant 400mA for 1h in transfer Buffer (25mM Tris, 192mM glycine, ddH_2O). Total Protein stain was performed with REVERT Total protein stain and membrane was blocked with 10mL TBS-T (10mM Tris, 250mM NaCl, HCl pH7.6, 0.05% Tween 20, ddH_2O) + 5% BSA for 1h. First antibody was diluted in 5mL TBS-T + 5% BSA and membrane was incubated overnight at 4°C in the dark. Membrane was washed to times with 2mL TBS-T for 10min and one time with 2mL TBS (10mM Tris, 250mM NaCl, HCl pH7.6, ddH_2O) for 10min. Second antibody was diluted in 2.5mL TBS + 2.5mL Odyssey Blocking Buffer. Membrane was incubated with second antibody for 1h at room temperature. Membrane was washed three times with TBS for 10min. Membrane fluorescence was measured with ODYSSEY CLx. Fluorescence intensity was calculated with Image Studio Lite Vers. 5.2.

QUANTIFICATION AND STATISTICAL ANALYSIS

Statistical analysis

Statistical analysis was performed using GraphPad Prism software. Significance was calculated using unpaired t-test (Figures 1B–1D and 5F–5H), multiple comparison one-way ANOVA (Figures 2, 3A, 3B, 3E–3G, 4, 5A, 5B, 5D–5E, and 6A–6G), two-way ANOVA (Figure 3D), RM one-way ANOVA (Figure 6H), paired t-test (Figures 6I–6L), student's t-test (Figure 5E), unpaired t-test (Figures 7A–7E), Benjamini-Hochberg test (Figure 7F).

In Figures 1, 2, 4G, 5A, 5B, 5F–5H, 6A–6H, 7A–7C, and 7E data are shown as mean ± SEM. In Figure 3 surface marker stain is shown as mean of four replicates, SeaHorse analysis over time is shown as one representative example mean ± SD, calculated parameters of SeaHorse analysis are shown as mean ± 5–95 percentile. In Figures 5D–5E metabolite amount is shown as minimum to maximum and protein expression is shown as calculated –Log2 fold change of control and knockdown macrophages. In Figures 6I–6L data are shown as minimum to maximum. In Figure 7D surface marker stain is shown as mean of ten replicates.

Statistical values, including technical and biological number of replicates (n), are named in the figure legends. *$p < 0.05$; **$p < 0.01$; ***$p < 0.001$; ****$p < 0.0001$.

Proteomic and phosphoproteomic analysis

Raw data acquired from CECAD proteomics facility were filtered and processed on MaxQuant software (v.1.5.3.8) and Perseus software (v.1.5.5.3). Data are generated out of one experiment with three replicates per condition.

Volcano plots of proteomics were generated with software of Bioconductor. The mean of the different inhibitor treatments respectively PPP enzyme knockdowns was calculated and compared to the untreated control. Significance was defined as mean Log_2 fold change >0.5 or < −0.5 and q value <0.05. Circle size represents the number of significant occurrence in the different treatment conditions.

For circle plot analysis, significant genes were extracted from proteomic- and phosphoproteomic analysis. Significance was defined as mean Log_2 fold change >0.5 or < −0.5 and q value <0.05 for proteomic analysis and as mean Log_2 fold change >0.5 or < −0.5 and p value >1.3 for phosphoproteomic analysis. Significant genes were clustered with String analysis. The ten biggest clusters were used for further analysis. Clusters were named by using GeneAnalytics and similar clusters were merged in one heading. Mean of $-\log_{10} p$ value of the clusters was calculated and is represented in heat color, count of genes per cluster is represented in circle size.

Normalized upstream kinase score out of phosphoproteomic analysis was calculated by adapted code of INKA analysis. On basis of the work of Beekhof et al.,[22] we calculated a simplified upstream kinase score analysis, using the murine data available from the PhosphoSitePlus (PSP) database:

$$\textit{Upstream Kinase Score} = \sqrt{\sum_{\text{Kin}}} \times \sum_{\text{PSP}}$$

With $\sum_{\text{Kin}}$ representing the sum of all phosphopeptides observed in the experiment per kinase found in the murine PSP database, whilst $\sum_{\text{PSP}}$ representing the sum of all substrate phosphopeptides observed in the experiment associated with each kinase found in the murine PSP database. These scores were calculated for each replicate per condition, with the normalized upstream kinase score (NUKS) representing the mean difference in upstream kinase scores between untreated control and treatment with PPP inhibitors and macrophage wild-type and PPP knockdown macrophages respectively.

Cell Reports Medicine, Volume *5*

Supplemental information

Macrophages are activated toward phagocytic lymphoma cell clearance by pentose phosphate pathway inhibition

Anna C. Beielstein, Elena Izquierdo, Stuart Blakemore, Nadine Nickel, Michael Michalik, Samruddhi Chawan, Reinhild Brinker, Hans-Henrik Bartel, Daniela Vorholt, Lukas Albert, Janica L. Nolte, Rebecca Linke, Carolina Raíssa Costa Picossi, Jorge Sáiz, Felix Picard, Alexandra Florin, Jörn Meinel, Reinhard Büttner, Paul Diefenhardt, Sebastian Brähler, Alma Villaseñor, Holger Winkels, Michael Hallek, Marcus Krüger, Coral Barbas, and Christian P. Pallasch

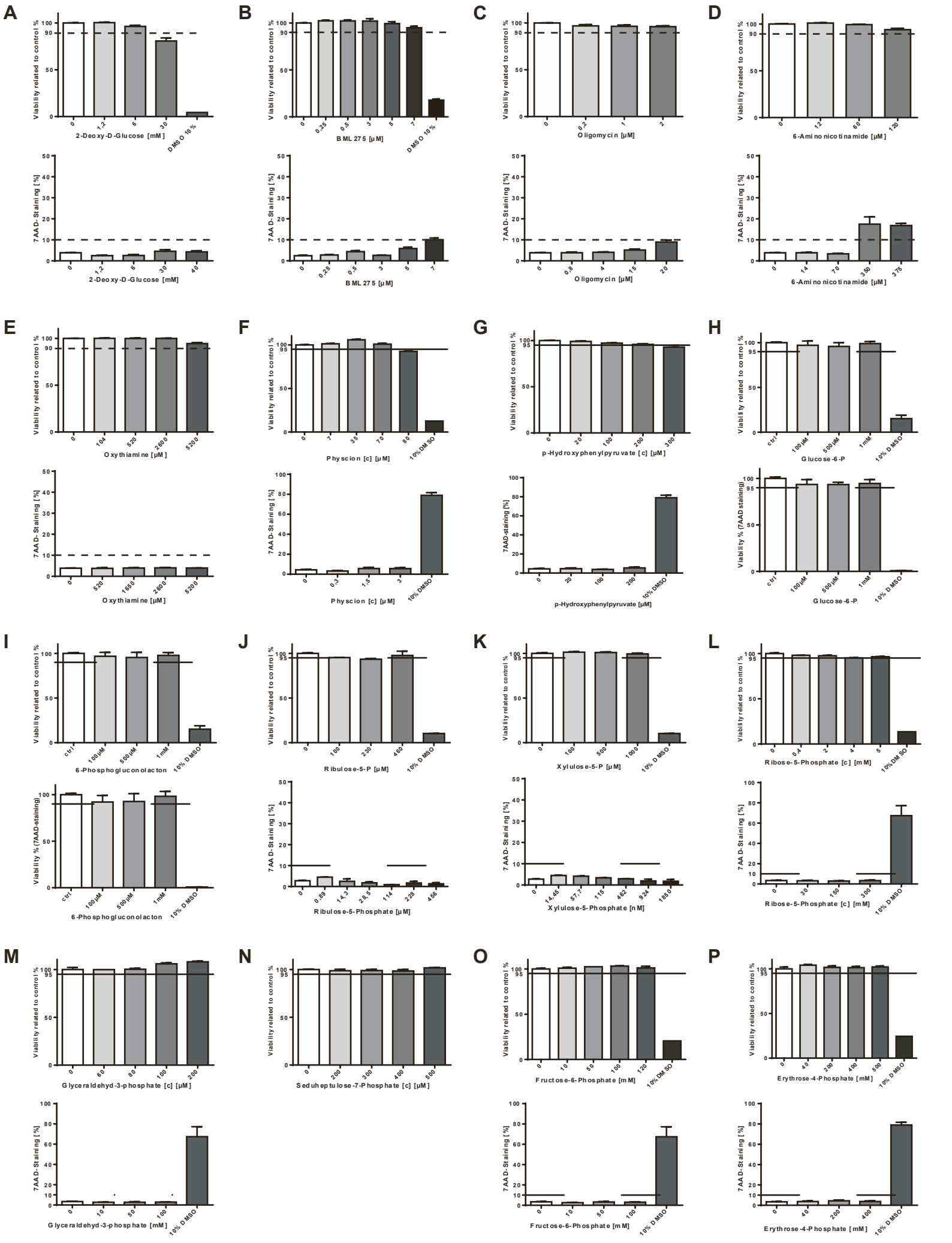
A
Viability related to control %
2-Deoxy-D-Glucose [mM]
DMSO 10%
7AAD-Staining [%]
2-Deoxy-D-Glucose [mM]
B
Viability related to control %
BML 275 [µM]
DMSO 10%
7AAD-Staining [%]
BML 275 [µM]
C
Viability related to control %
Oligomycin [µM]
7AAD-Staining [%]
Oligomycin [µM]
D
Viability related to control %
6-Aminonicotinamide [µM]
7AAD-Staining [%]
6-Aminonicotinamide [µM]
E
Viability related to control %
Oxythiamine [µM]
7AAD-Staining [%]
Oxythiamine [µM]
F
Viability related to control %
Physcion [c] [µM]
10% DMSO
7AAD-Staining [%]
Physcion [c] [µM]
G
Viability related to control %
p-Hydroxyphenylpyruvate [c] [µM]
7AAD-staining [%]
p-Hydroxyphenylpyruvate [µM]
H
Viability related to control %
ctrl
100µM
500µM
1mM
10% DMSO
Glucose-6-P
Viability % (7AAD staining)
Glucose-6-P
I
Viability related to control %
ctrl
100µM
500µM
1mM
10% DMSO
6-Phosphogluconolacton
Viability % (7AAD-staining)
6-Phosphogluconolacton
J
Viability related to control %
Ribulose-5-P [µM]
10% DMSO
7AAD-Staining [%]
Ribulose-5-Phosphate [µM]
K
Viability related to control %
Xylulose-5-P [µM]
10% DMSO
7AAD-Staining [%]
Xylulose-5-Phosphate [nM]
L
Viability related to control %
Ribose-5-Phosphate [c] [mM]
10% DMSO
7AAD-Staining [%]
Ribose-5-Phosphate [c] [mM]
M
Viability related to control %
Glyceraldehyd-3-phosphate [c] [µM]
7AAD-Staining [%]
Glyceraldehyd-3-phosphate [mM]
10% DMSO
N
Viability related to control %
Seduheptulose-7-Phosphate [c] [µM]
O
Viability related to control %
Fructose-6-Phosphate [mM]
10% DMSO
7AAD-Staining [%]
Fructose-6-Phosphate [mM]
10% DMSO
P
Viability related to control %
Erythrose-4-Phosphate [mM]
10% DMSO
7AAD-Staining [%]
Erythrose-4-Phosphate [mM]
10% DMSO

Figure S1. Evaluation of cytotoxicity of used compounds in J774A.1 macrophages and hMB cells. Related to Figures 1-2.

(A-P) Measurement of viable cells under treatment with different inhibitors. Treatment with 10% DMSO used as positive control. Viability of J774A.1 cells (upper plots) was determined by Zombie staining, viability of hMB cells was determined by 7AAD staining. Viability under inhibition was compared to viability of untreated control cells. Used Inhibitors **A** 2-deoxy-D-glucose, **B** BML275, **C** oligomycin, **D** 6-aminonicotinamide, **E** oxythiamine, **F** physcion, **G** p-hydroxyphenylpyruvate, **H** glucose-6-phosphate, **I** 6-phosphogluconolactone, **J** ribulose-6-phosphate, **K** xylulose-5-phosphate, **L** ribose-5-phosphate, **M** glyceraldehyde-3-phosphate, **N** sedoheptulose-7-phosphate, **O** fructose-6-phosphate, **P** erythrose-4-phosphate.

Technical replicates n=4-12; biological replicates n=2-6. Data are shown as mean ± SEM. *P* values were calculated using one-way ANOVA. *$p < 0.05$; **$p < 0.01$; ***$p < 0.001$; ****$p < 0.0001$.

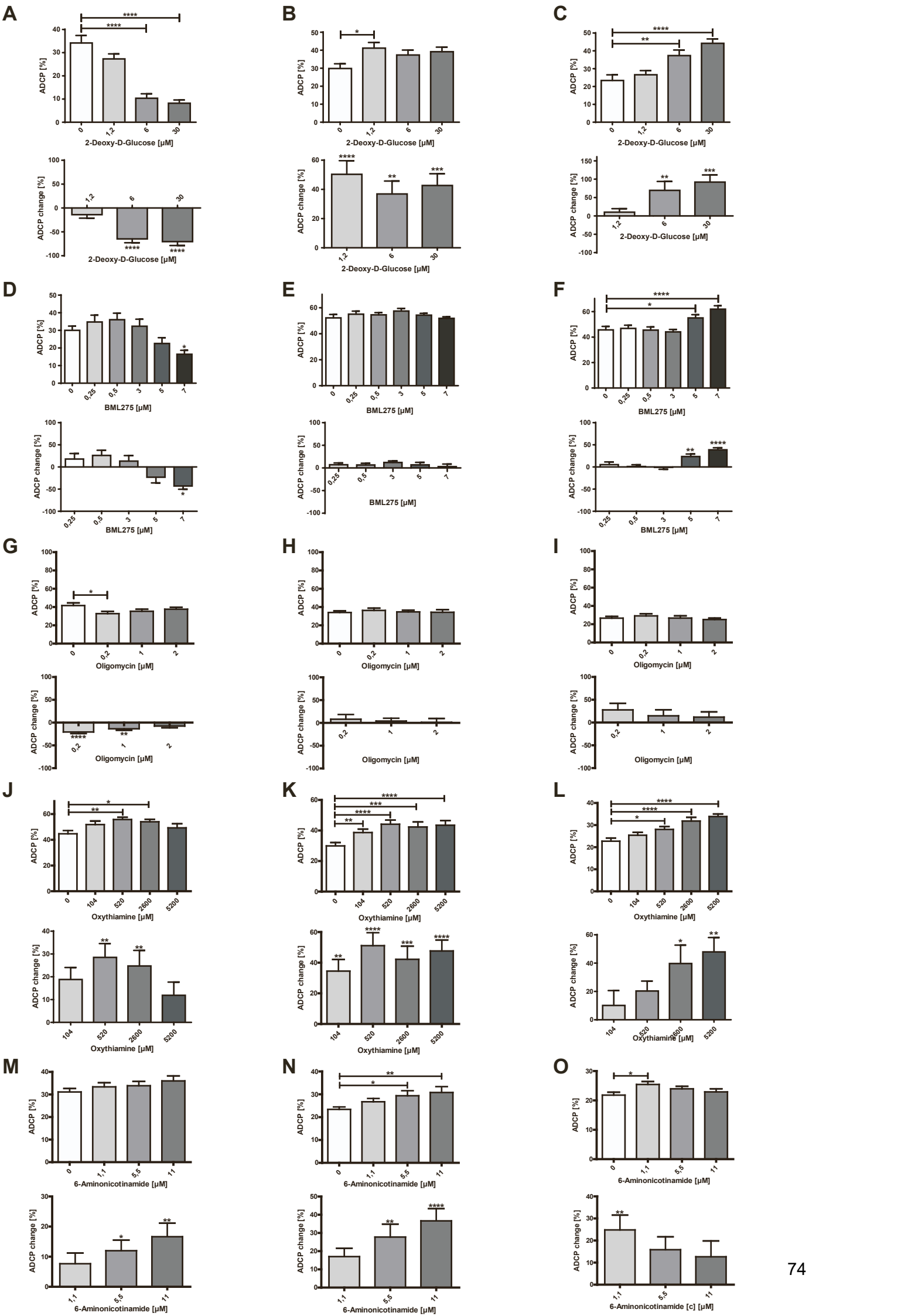
A
B
C
D
E
F
G
H
I
J
K
L
M
N
O
ADCP [%]
ADCP change [%]
2-Deoxy-D-Glucose [µM]
BML275 [µM]
Oligomycin [µM]
Oxythiamine [µM]
6-Aminonicotinamide [µM]
6-Aminonicotinamide [c] [µM]

Figure S2. Metabolic modulation changes antibody-dependent cellular phagocytosis (ADCP) of hMB cells by macrophages.

Related to Figure 1.

(A-O) ADCP rate and ADCP rate compared to basal phagocytosis rate (=ADCP change) under treatment with metabolic inhibitors in a co-culture of J774A.1 macrophages and hMB cells under antibody treatment with alemtuzumab. **A, D, G, J, M** J774A.1 macrophages pre-treated with metabolic inhibitor, **B, E, H, K, N** inhibitor treatment of the co-culture, **C, F, I, L, O** hMB cells pre-treated with metabolic inhibitor. Used inhibitors **A-C** 2-deoxy-D-glucose, **D-F** BML275, **G-I** oligomycin, **J-L** oxythiamine, **M-O** 6-aminonicotinamide.

Technical replicates n=15-58, biological replicates n=3-12. Data are shown as mean ± SEM. *P* values were calculated using one-way ANOVA. *$p < 0.05$; **$p < 0.01$; ***$p < 0.001$; ****$p < 0.0001$.

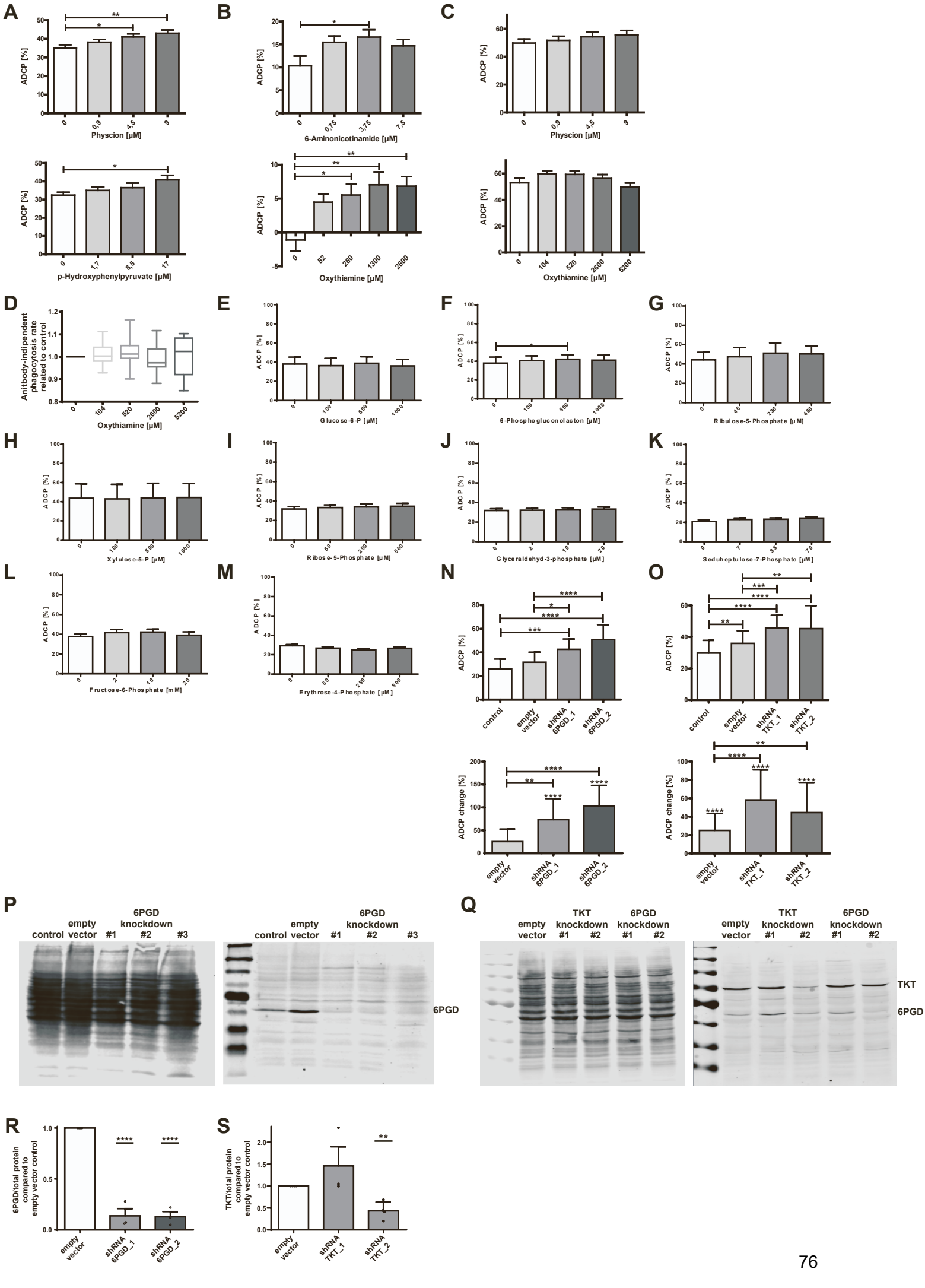
A
ADCP [%]
Physcion [µM]
p-Hydroxyphenylpyruvate [µM]
B
ADCP [%]
6-Aminonicotinamide [µM]
Oxythiamine [µM]
C
ADCP [%]
Physcion [µM]
Oxythiamine [µM]
D
Anitbody-indipendent phagocytosis rate related to control
Oxythiamine [µM]
E
ADCP [%]
Glucose-6-P [µM]
F
ADCP [%]
6-Phosphogluconolacton [µM]
G
ADCP [%]
Ribulose-5-Phosphate [µM]
H
ADCP [%]
Xylulose-5-P [µM]
I
ADCP [%]
Ribose-5-Phosphate [µM]
J
ADCP [%]
Glyceraldehyd-3-phosphate [µM]
K
ADCP [%]
Seduheptulose-7-Phosphate [µM]
L
ADCP [%]
Fructose-6-Phosphate [mM]
M
ADCP [%]
Erythrose-4-Phosphate [µM]
N
ADCP [%]
control
empty vector
shRNA 6PGD_1
shRNA 6PGD_2
ADCP change [%]
O
ADCP [%]
control
empty vector
shRNA TKT_1
shRNA TKT_2
ADCP change [%]
P
control
empty vector
6PGD knockdown
#1
#2
#3
6PGD
Q
empty vector
TKT knockdown
6PGD knockdown
#1
#2
TKT
6PGD
R
6PGD/total protein compared to empty vector control
empty vector
shRNA 6PGD_1
shRNA 6PGD_2
S
TKT/total protein compared to empty vector control
empty vector
shRNA TKT_1
shRNA TKT_2

Figure S3. PPP modulation changes ADCP of hMB cells by macrophages.

Related to Figure 2.

(A, C) ADCP rate and ADCP rate compared to basal phagocytosis rate (=ADCP change) under treatment with metabolic inhibitors in a co-culture of J774A.1 macrophages and hMB cells under antibody treatment with alemtuzumab. **A** ADCP performed under PPP inhibition with physcion or p-hydroxyphenylpyruvate, **B** ADCP performed with THP1 monocytes and hMB cells under antibody treatment with obinutuzumab and PPP inhibition with 6-aminonicotinamide or oxythiamine. **C** ADCP assay performed in hypoxia under PPP inhibition with physcion or oxythiamine. **D** antibody-independent cellular phagocytosis (AiCP) rate of hMB cells by J744A.1 macrophages under treatment with oxythiamine. **(E-M)** ADCP rate under supplementation of PPP intermediates. **E** glucose-6-phosphate, **F** 6-phosphogluconolactone, **G** ribulose-5-phosphate, **H** xylulose-5-phosphate, **I** ribose-5-phosphate, **J** glyceraldehyde-3-phosphate, **K** sedoheptulose-7-phosphate, **L** fructose-6-phosphate, **M** erythrose-4-phosphate. **(N-O)** ADCP rate and ADCP rate compared to basal phagocytosis rate (=ADCP change) of hMB cells by shRNA mediates PPP knockdown macrophages**. N** shRNA mediated knockdown of 6-phosphogluconate dehydrogenase, **O** shRNA mediated knockdown of transketolase. **(P)** One representative example of western blot analysis of J744A.1 macrophages transfected with empty vector control and shRNA targeting 6-phosphogluconate dehydrogenase. Total protein stain and staining of 6-phosphogluconate dehydrogenase. **(Q)** One representative example of western blot analysis of J744A.1 macrophages transfected with empty vector control and shRNA targeting transketolase. Total protein stain and staining of transketolase. **(R)** Western blot analysis of 6pgd expression in J774A.1 macrophages under shRNA mediated PPP knockdown of 6Pgd compared to empty vector control. **(S)** Western blot analysis of Tkt expression in J774A.1 macrophages under shRNA mediated PPP knockdown of 6Pgd compared to empty vector control.

Technical replicates n=13-30; biological replicates n=3-6. In **A-O, R-S** data are shown as mean ± SEM. *P* values were calculated in **A-O** using one-way ANOVA, in **R-S** using Unpaired t-test. *$p < 0.05$; **$p < 0.01$; ***$p < 0.001$; ****$p < 0.0001$.

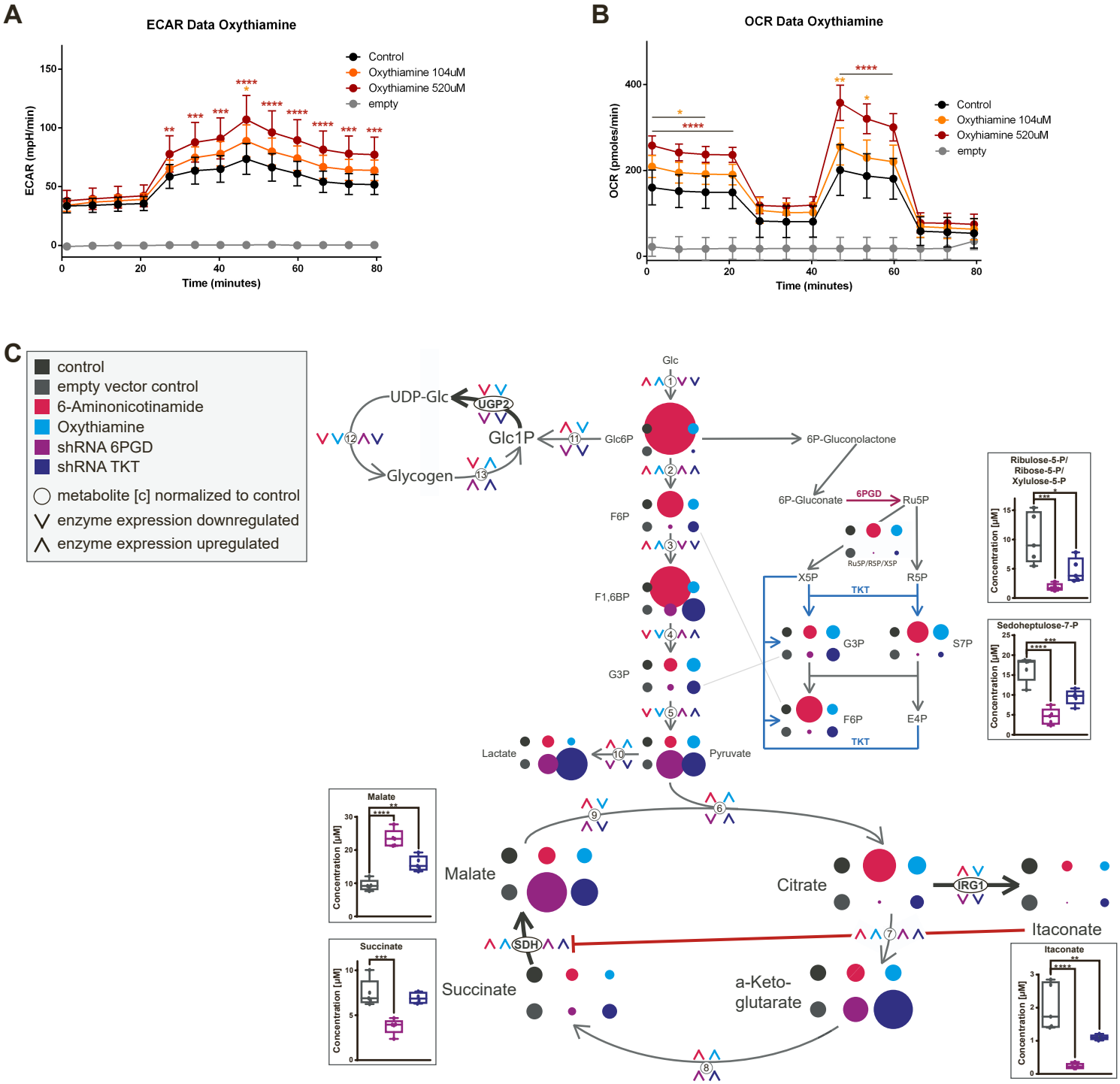
A
ECAR Data Oxythiamine
ECAR (mpH/min)
Time (minutes)
Control
Oxythiamine 104uM
Oxythiamine 520uM
empty
B
OCR Data Oxythiamine
OCR (pmoles/min)
Time (minutes)
Control
Oxythiamine 104uM
Oxythiamine 520uM
empty
C
control
empty vector control
6-Aminonicotinamide
Oxythiamine
shRNA 6PGD
shRNA TKT
metabolite [c] normalized to control
enzyme expression downregulated
enzyme expression upregulated
Glc
UDP-Glc
UGP2
Glc1P
Glycogen
Glc6P
6P-Gluconolactone
6P-Gluconate
6PGD
Ru5P
Ribulose-5-P/
Ribose-5-P/
Xylulose-5-P
Ru5P/R5P/X5P
X5P
R5P
TKT
F6P
F1,6BP
G3P
S7P
E4P
Sedoheptulose-7-P
Lactate
Pyruvate
Malate
Succinate
Citrate
IRG1
Itaconate
SDH
a-Keto-
glutarate
Concentration [µM]

Figure S4. PPP modulation changes metabolic activity in macrophages.

Related to Figures 3 and 5.

(A-B) Measurement of metabolic activity of J774A.1 macrophages under drug mediated PPP inhibition with oxythiamine by SeaHorse analysis. **A** one representative example of MitoStress test measurement of ECAR, **B** one representative example of MitoStress test measurement of OCR. **C** Metabolomic analysis of central metabolic pathways with overlay of proteomics data under compound mediated PPP inhibition compared to untreated J774A.1 macrophages and shRNA mediated PPP knockdown of 6Pgd and Tkt compared to empty vector control J774A.1 macrophages. Relative metabolite abundance compared to respective control represented in circle size. Absolute amount of metabolites of interest displayed in bar graphs. Change in enzyme expression assessed by proteomics displayed in arrow direction. Arrow upwards: increased enzyme expression compared to respective control; arrow downwards: decreased enzyme expression compared to respective control. Inhibited enzyme reactions by compounds or shRNA mediated knockdown coloured in violet (6Pgd) and blue (Tkt). *Metabolites: E4P* erythrose-4-phosphate, *F1,6BP* fructose-1,6-bisphosphate, *F6P* fructose-6-phosphate, *G3P* glyceraldehyde-3-phosphate, *Glc* glucose, *Glc1P g*lucose-1-phosphate, *Glc6P* glucose-6-phosphate, *R5P* ribose-5-phosphate, *Ru5P* ribulose-5-phosphate, *S7P* sedoheptulose-7-phosphate, *UDP-Glc* UDP-glucose, *X5P* xylulose-5-phosphate. *Enzymes: Irg1* immune-regulatory gene 1, *Sdh* succinate dehydrogenase, *Ugp2* UDP-glucose pyrophosphorylase 2, *1)* hexokinase, *2)* glucose-6-phosphate isomerase, *3)* phosphofructokinase, *4)* aldolase, *5)* sum up of glycerinaldehyde-3-phosphate dehydrogenase, phosphoglycerate kinase, enolase, pyruvate kinase, *6)* citrate synthase, *7)* sum up of aconitase, isocitrate dehydrogenase, *8)* sum up of a-ketoglutarate dehydrogenase, succinyl-CoA synthetase, *9)* malate dehydrogenase, *10)* lactate dehydrogenase, *11)* phosphoglucomutase 1, *12)* UTP-glucose-1-phosphate uridyltransferase, *13)* glycogen phosphorylase.

Technical replicates **A**-**B** n=6-27, **C** n=3; biological replicates **A**-**B** n=1-9, **C** n=3. In **A**-**B** data are shown as mean of six replicates in one experiment ± SD, n=6, in **C** data are shown as Min. to Max, n=3. *P* values were calculated using one-way ANOVA. *$p < 0.05$; **$p < 0.01$; ***$p < 0.001$; ****$p < 0.0001$.

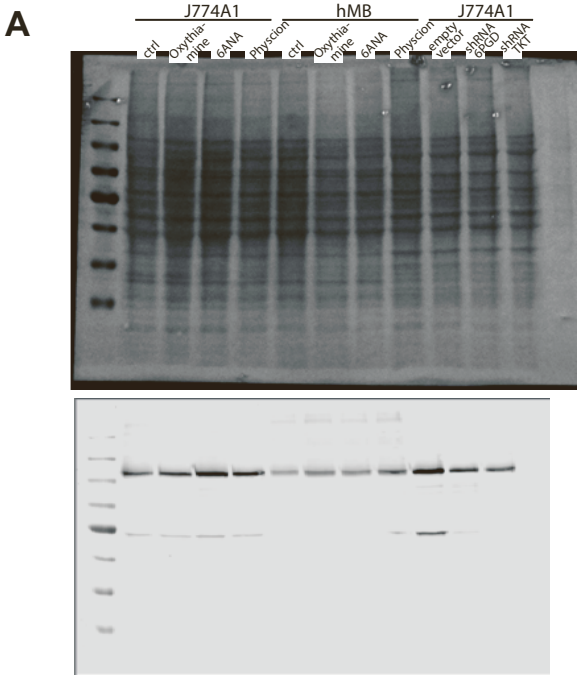
A
J774A1
hMB
J774A1
ctrl
Oxythia-mine
6ANA
Physcion
ctrl
Oxythia-mine
6ANA
Physcion
empty vector
shRNA 6PGD
shRNA TKT

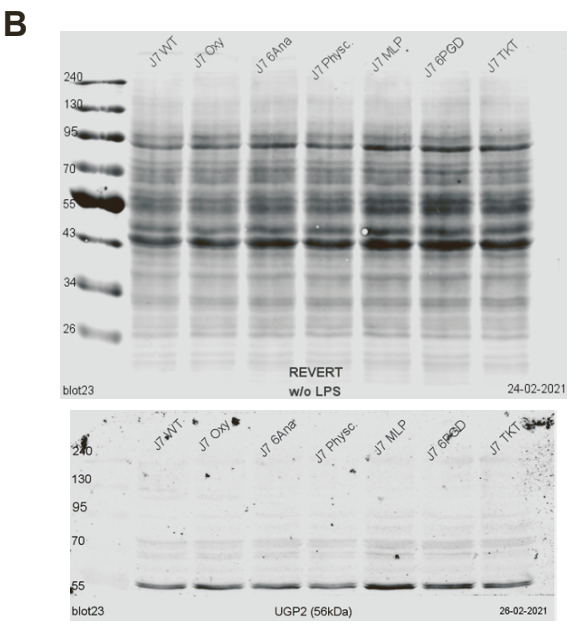
B
J7 WT
J7 Oxy
J7 6Ana
J7 Physc.
J7 MLP
J7 6PGD
J7 TKT
240
130
95
70
55
43
34
26
REVERT
w/o LPS
blot23
24-02-2021
UGP2 (56kDa)
26-02-2021

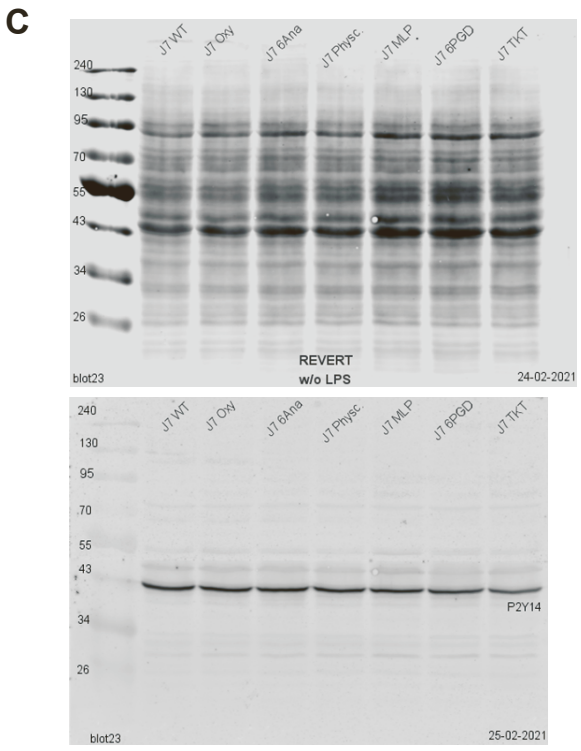
C
J7 WT
J7 Oxy
J7 6Ana
J7 Physc.
J7 MLP
J7 6PGD
J7 TKT
240
130
95
70
55
43
34
26
REVERT
w/o LPS
blot23
24-02-2021
P2Y14
25-02-2021

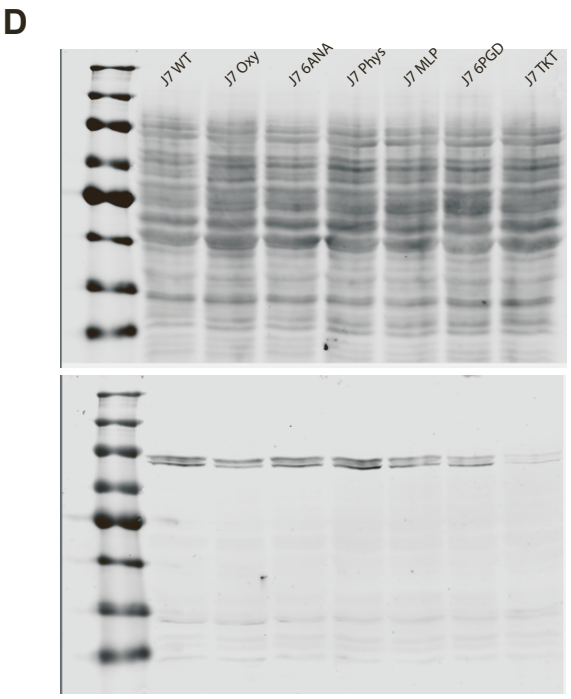
D
J7 WT
J7 Oxy
J7 6ANA
J7 Phys
J7 MLP
J7 6PGD
J7 TKT

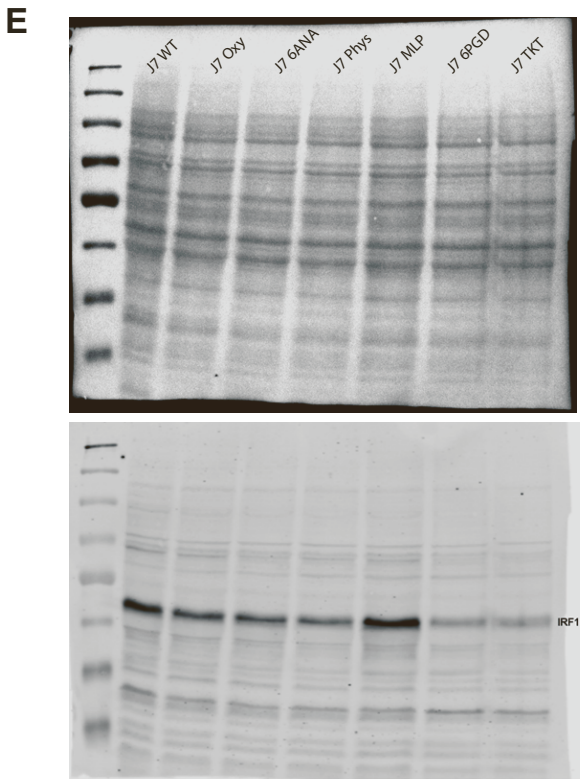
E
J7 WT
J7 Oxy
J7 6ANA
J7 Phys
J7 MLP
J7 6PGD
J7 TKT
IRF1

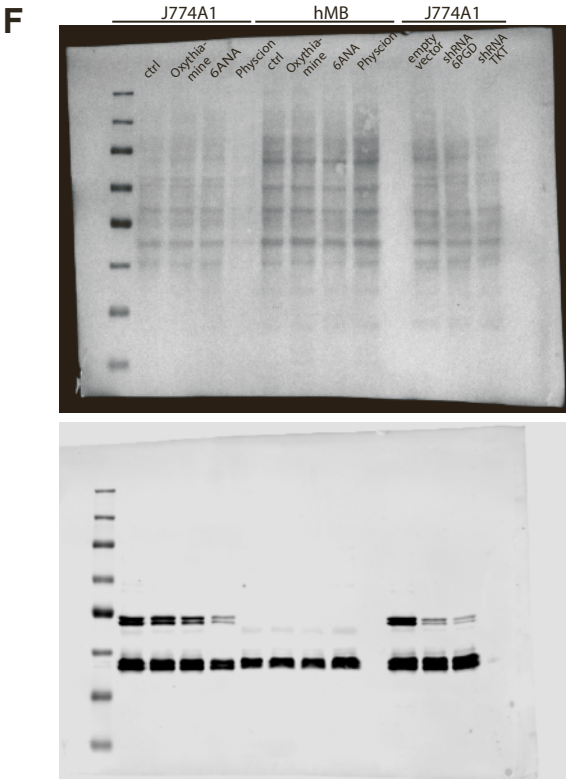
F
J774A1
hMB
J774A1
ctrl
Oxythia-mine
6ANA
Physcion
ctrl
Oxythia-mine
6ANA
Physcion
empty vector
shRNA 6PGD
shRNA TKT

Figure S5. PPP inhibition changes the protein expression of hypothesized metabolic-immune response axis in macrophages.

Related to Figures 4 and 5.

(A-F) One representative example of western blot analysis of J744A.1 macrophages after drug mediated inhibition of the PPP or shRNA mediated knockdown of the PPP. Total protein stain and staining of protein of interest are shown. In **A** and **F** also hMB cells under PPP inhibition has been tested. **A** PYK2 staining, **B** UGP2 staining, **C** P2Y14 staining, **D** STAT1 staining, **E** IRF1 staining, **F** IRG1 staining.

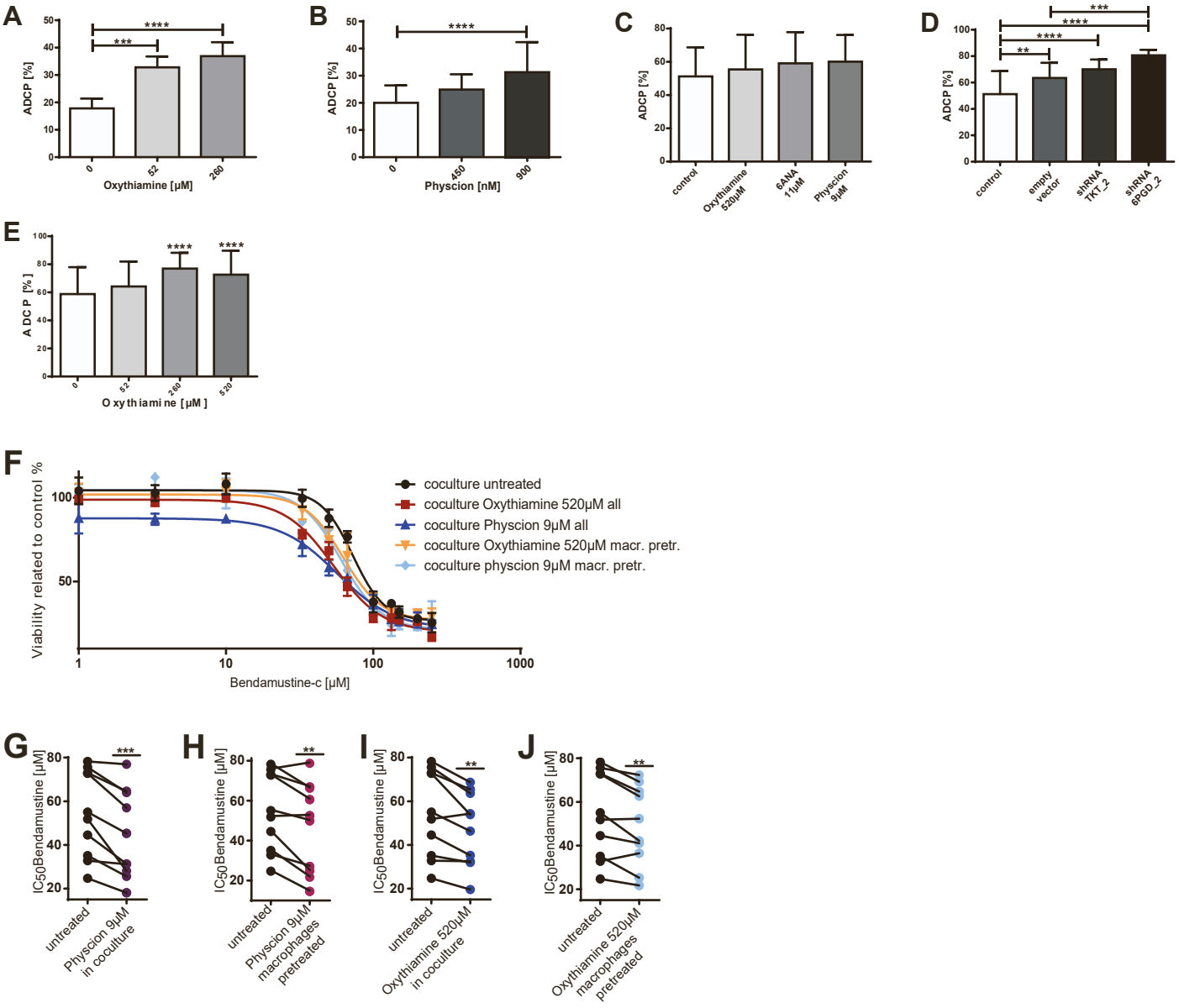
A
ADCP [%]
Oxythiamine [µM]
B
ADCP [%]
Physcion [nM]
C
ADCP [%]
control
Oxythiamine 520µM
6ANA 1µM
Physcion 9µM
D
ADCP [%]
control
empty vector
shRNA TKT_2
shRNA 6PGD_2
E
ADCP [%]
Oxythiamine [µM]
F
Viability related to control %
Bendamustine-c [µM]
coculture untreated
coculture Oxythiamine 520µM all
coculture Physcion 9µM all
coculture Oxythiamine 520µM macr. pretr.
coculture physcion 9µM macr. pretr.
G
IC50Bendamustine [µM]
untreated
Physcion 9µM in coculture
H
IC50Bendamustine [µM]
untreated
Physcion 9µM macrophages pretreated
I
IC50Bendamustine [µM]
untreated
Oxythiamine 520µM in coculture
J
IC50Bendamustine [µM]
untreated
Oxythiamine 520µM macrophages pretreated

Figure S6. PPP inhibition in primary human environment increases phagocytic capacity of macrophages and favours primary CLL cells chemotherapy sensitivity.

Related to Figure 6.

(A-B) ADCP rate of primary human monocyte derived macrophages differentiated in the presence of PPP inhibitors. **A** ADCP change by primary monocyte derived macrophages differentiated in the presence of physcion and M-CSF **B** ADCP change by primary monocyte derived macrophages differentiated in the presence of oxythiamine and M-CSF. **(C-D)** ADCP rate of primary CLL patient cells by J774A.1 macrophages. **C** ADCP rate under drug mediated PPP inhibition, **D** ADCP rate under shRNA mediated PPP knockdown. **(E)** ADCP rate of primary CLL patient cells by primary human monocyte derived macrophages differentiated in the presence of oxythiamine and M-CSF. **(F)** One representative example of dose response curve of individual orimary CLL patient cell samples towards bendamustine treatment. Cells were incubated with bendamustine after protective macrophage co-culture with untreated J774A.1 macrophages vs. PPP inhibition. **(G-J)** Dose-response curve (IC_{50}) for individual primary CLL patient cell samples to bendamustine treatment. Cells were incubated with bendamustine after protective macrophage co-culture with untreated J774A.1 macrophages vs. PPP inhibition. **G-H** Inhibition of 6Pgd in oxidative part of PPP by physcion, **G** co-culture treatment, **H** macrophage pre-treatment. **I-J** Inhibition of Tkt in non-oxidative part of PPP by oxythiamine, **I** co-culture treatment, **J** macrophage pre-treatment.

Technical replicates **A** n=28, **B** n=20, **C-D** n=20, **E** n=65, **F** n=30, **G-J** n=30; biological replicates **A** n=6, **B** n=4, **C-D** n=5, **E** n=12, **F** n=10, **G-J** n=10. Data are shown as mean ± SEM. *P* values were calculated in **A-E** by using one-way ANOVA, in **G-J** using paired t-test. *$p < 0.05$; **$p < 0.01$; ***$p < 0.001$; ****$p < 0.0001$.

A

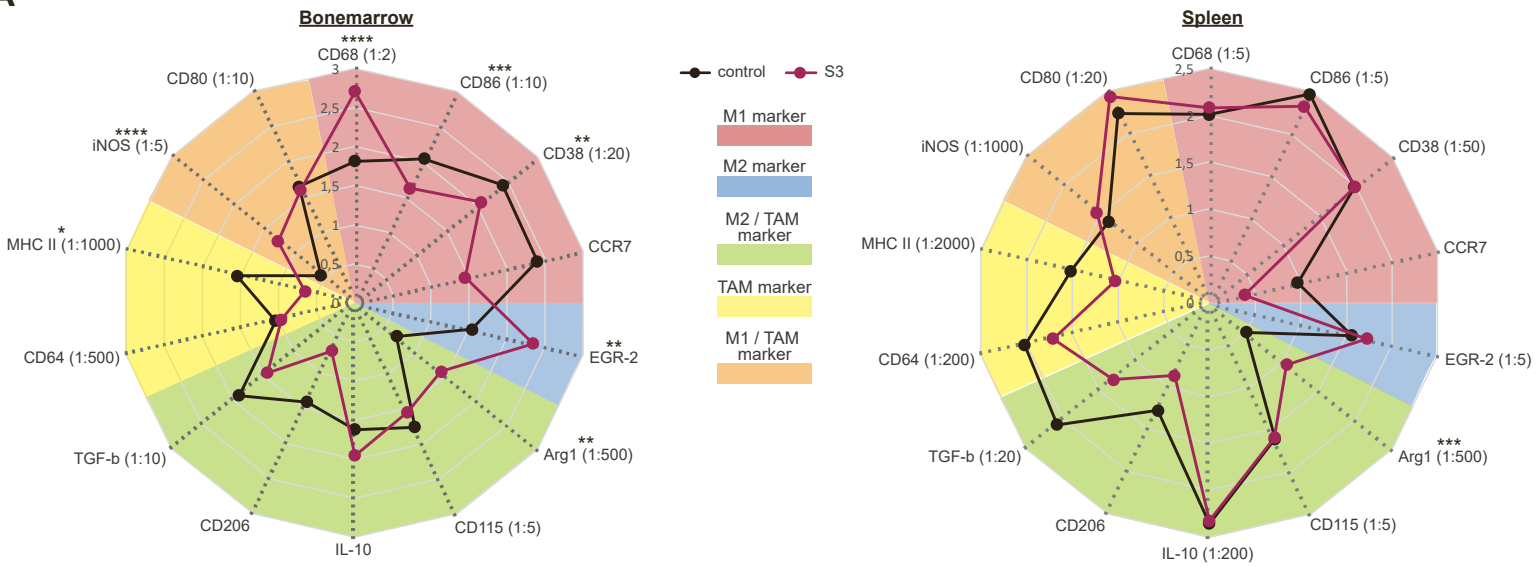

B

Benjamini-Hochberg-analysis

	vehicle	alemtuzumab	S3 + alemtuzumab
vehicle	--	**1.4e-05**	--
S3	**0.6159**	**5.5e-05**	**1.0e-07**
S3 + alemtuzumab	**3.4e-09**	**0.0059**	--

C

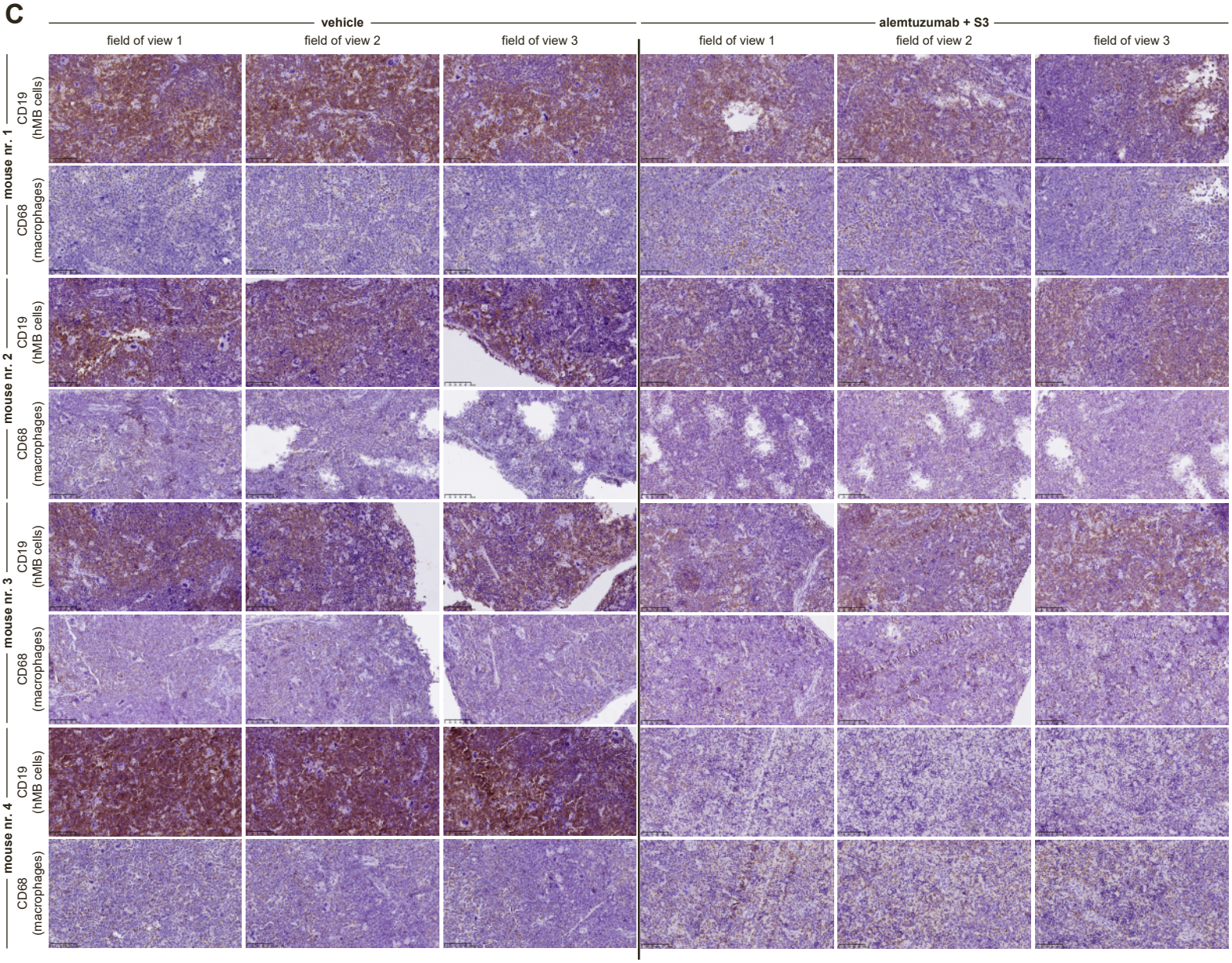

Figure S7. PPP inhibition increases myelopoiesis and macrophages´ activity *in vivo* and improves treatment response in an aggressive humanized lymphoma mouse model.

Related to Figure 7.

(A) Expression of characteristic surface marker for different macrophage subtypes on macrophages in bone marrow and spleen. C57BL/6 mice treated with vehicle (control) or S3 i.p. for 7 days. **(B)** Significance testing by using Benjamini-Hochberg-analysis of survival curves of NSG mice transfected with hMB and treated after three days of engraftment with vehicle, alemtuzumab and/or PPP inhibitor S3 for 12 days. **(C)** Immunohistochemical staining of hMB cells ($CD19^+$) and macrophages ($CD68^+$) in spleen of NSG mice transfected with hMB and treated after three days of engraftment with vehicle or alemtuzumab + S3 for 12 days.

Technical replicates **A** n=9-10, **B** n=21-25, **C** n=4; biological replicates **A** n=9-10, **B** n=21-25, **C** n=4. In **A** data are shown as mean of ten replicates. In **A** *P* values were calculated by using one-way ANOVA. *$p < 0.05$; **$p < 0.01$; ***$p < 0.001$; ****$p < 0.0001$.

Table S6. Qualifier and quantifier transition of metabolites measured by targeted LC-QqQ/MS analysis. Related to Figure 5.

Compound name	Transition (m/z)	Transition type	Fragmentor (V)	Collision Energy (eV)	Cell accelerator (V)	RT (min)
Succinic acid D6 (ISTD)	121 → 77	quantifier	77	10	4	11.9
Glutathione - glycine-$^{13}C_2$,^{15}N trifluor (ISTD)	309 → 146	quantifier	119	14	4	12.3
	309 → 128	qualifier	119	14	4	12.3
Adenosine 5-diphosphate	426 → 328	quantifier	56	16	4	17.9
	426 → 159	qualifier	56	28	4	17.9
Adenosine 5-triphosphate	506 → 408	quantifier	122	22	4	20.5
	506 → 159	qualifier	122	38	4	20.5
Lactic acid	89 → 45	qualifier	48	9	4	3.0
	89 → 43	quantifier	48	10	4	3.0
Pyruvic Acid	87 → 43	quantifier	48	4	4	2.2
alpha - ketoglutaric acid	145 → 101	quantifier	70	5	4	10.6
	145 → 57	qualifier	70	9	4	10.6
NAD	662 → 540	quantifier	70	12	4	14.4
	662 → 328	qualifier	70	36	4	14.4
D-Fructose 6-phosphate	259 → 97	quantifier	102	14	4	16.3
	259 → 79	qualifier	102	48	4	16.3
D-Glucose-6-phosphate	259 → 79	quantifier	102	48	4	18.5
	259 → 97	qualifier	102	14	4	18.5
Ribose 5-phosphate / Ribulose 5-phosphate	229 → 97	qualifier	96	10	4	14.3
	229 →79	quantifier	96	48	4	14.3
D-Xylulose 5-phosphate / Ribose 5-phosphate / Ribulose 5-phosphate	229 → 139	qualifier	86	8	4	15.3
	229 → 79	quantifier	96	48	4	15.3
D-Sedoheptulose 7-phosphate	289 → 97	quantifier	104	18	4	17.0
	289 → 79	qualifier	104	48	4	17.0
Glutathione Reduced	306 → 143	quantifier	109	14	4	12.3
	306 → 128	qualifier	109	14	4	12.3
NADP	742 → 620	quantifier	79	10	4	24.9
	742 → 408	qualifier	79	38	4	24.9
Succinic acid	117 → 99	qualifier	62	8	4	11.9
	117 → 73	quantifier	62	10		11.9
Itaconic acid	129 → 85	quantifier	68	6	4	8.4
	129 → 41	qualifier	68	12	4	8.4
L-Malic acid	133 → 115	quantifier	76	8	4	12.8
	133 → 71.1	qualifier	76	14	4	12.8
Citric acid	191 → 111	quantifier	78	10	4	17.5
	191 → 87	qualifier	78	16	4	17.5

NADH	664 → 408	qualifier	190	29	4	11.7
	664 → 79	quantifier	190	49	4	11.7
DL-Glyceraldehyde 3-phosphate	169 → 97	quantifier	130	4	4	14.7
	169 → 79	qualifier	130	28	4	14.7
D-Fructose 1,6-biphosphate	339 → 241	qualifier	90	12	4	25.9
	339 → 97	quantifier	90	22	4	25.9
6-phosphogluconic acid	275 → 79	quantifier	109	49	4	21.7
D-erytrose 4-phosphate	199 → 97	quantifier	151	6	4	13.9
	199 → 79	qualifier	151	30	4	13.9

5. DISCUSSION

The ability of metabolism to determine macrophage polarization and activity has been recently established and is a central principle of immune regulation.[13,14] The influence of glucose and mitochondrial metabolism on this polarization is widely explored and reviewed, also in the context of TAMs.[13,14,63,79] While it has been shown that PPP has impact on the successful clearance of apoptotic cells, immune tolerance, and granuloma formation in the context of the diseases systemic lupus erythematosus and sarcoidosis,[112,113] the influence of the PPP on TAMs and on immune regulation got rarely attention up to now. The observation that TAMs are not that phagocytic active in the lymphoma microenvironment – a microenvironment with special nutrient supply and metabolic influence – in the context of chemo-immunotherapy while they are the most important cells for clearance of antibody-labeled lymphoma cells[9] and the poor prognosis of relapsed or refractory DLBCL,[18] constitutes the need to investigate possibilities to increase treatment efficacy.

In this study, we have demonstrated that inhibition of the PPP in TAMs can be used to increase macrophages´ anti-tumor function by increasing their phagocytic activity and decreasing their pro-tumoral bystander function. By that also a significant increase in overall survival in an aggressive B cell lymphoma mouse model was achieved by adding the PPP inhibitor S3 to antibody therapy.

5.1 Metabolic screening assays unveil the ability to influence macrophages´ phagocytic activity

5.1.1. Benefits and limitations of the phagocytosis assay design

To investigate the changes in macrophage activity in the context of antibody-based lymphoma therapy, we utilized a macrophage lymphoma co-culture system, with which we elucidated other cellular and microenvironmental interactions for first analyses. As a therapeutic antibody, alemtuzumab, an anti-CD52 antibody, was used. Alemtuzumab was originally used in B cell non-Hodgkin lymphoma and CLL,[114] but has been replaced by more efficient and less toxic newer antibodies targeting other epitopes like rituximab (anti-CD20) or obinutuzumab (anti-CD20). Nowadays, alemtuzumab is used for the treatment of refractory cutaneous T cell lymphoma (Sézary syndrome) and relapsed multiple sclerosis.[115] We, however, decided to use it for initial screening approach as several types of lymphoma downregulate the epitope of the newer antibodies CD20 but not the CD52 epitope including our humanized double-hit lymphoma cell model hMB. To dissolve possible limitations of the results by using alemtuzumab, we recapitulated our findings of interest with several other antibodies currently used in clinics (e.g. daratumumab, obinutuzumab). Nevertheless, in our aggressive lymphoma mouse model, where mice receive injection of hMB cells, we had to use alemtuzumab again,

which has to be seen as a possible point of uncertainty for efficacy in clinical settings. Therefore, the replication of the *in vivo* experiments with PPP inhibition added to antibody therapy is actually in preparation with other lymphoma mouse models and antibodies currently used in clinics. Nevertheless, expansion of the cell line experiments to primary human cells and to immune-competent mice, gave us the opportunity to study the effects of PPP inhibition in a human context and an immune-competent whole *in vivo* setting, which could have a great influence on the results as there is a brought spectrum of possible interferences by e.g. the body metabolism, the TME, other immune cells, and further aspects. Still achieving effective activation and increased phagocytosis of macrophages in these contexts, underlines the robustness and possible clinical relevance of PPP inhibition.

With the compound-mediated metabolism profiling, distinct regulation of the phagocytosis by inhibition of different metabolic pathways was explored. Complex effects toward target cells or effector cells and their respective interaction were dissected by comparing the effects of metabolic inhibition in the co-culture assay in comparison to pre-treatment of the effector cells (macrophages) or of the target cells (hMB cells). The screening was performed using non-toxic concentrations (Toxicity screening see Suppl. Figure 1) of the different inhibitors to prevent influence on phagocytic activity by macrophages through cell death programs or others in the target cells or the effector cells.

5.1.2. Metabolic modulation in macrophages and in lymphoma cells has influence on macrophages´ phagocytic activity

In the metabolism profiling, inhibition of glycolysis was identified to increase the susceptibility of lymphoma cells to be phagocytosed, even though an inhibitory effect on macrophage phagocytic function itself was seen. This finding is consistent with the 'Warburg effect' prevalent in tumor and lymphoma cells – affecting the overall viability of malignant cells once glycolysis is inhibited – causing higher susceptibility of these impaired lymphoma cells to phagocytic removal.[116] However, the inhibition of glycolysis solely in macrophages rendered antagonistic effects, being in line with the need of glycolysis for pro-inflammatory macrophage polarization.[63] In total, seen in co-culture treatment, the negative effect on target cells seems to predominate the negative effects on macrophages so that an increase of the phagocytic activity of macrophages was achieved in co-culture treatment. This points toward a higher dependency of lymphoma cells on glycolysis than of macrophages. Besides that, also the inhibition of mitochondrial ATP production by oligomycin and the inhibition of energy-regulating AMPK by BML-275 in macrophages significantly decreased their phagocytic capacity pointing toward important metabolic pathways to ensure phagocytic activity.

Only the inhibition of the PPP in macrophages showed a significant increase in phagocytosis. This increase was achieved in all treatment conditions. Both, the inhibition of the oxidative or the non-oxidative part of the PPP showed a synergistic effect on effector and target cells, which

causes the highest increase in phagocytosis of lymphoma cells in this screening approach. The inhibition of TKT via oxythiamine led to the highest increase of phagocytosis in all treatment conditions. Moreover, the phagocytosis of lymphoma cells was increased by inhibition of the non-oxidative part of the PPP in lymphoma cells, pointing to a higher susceptibility of lymphoma cells toward phagocytosis under PPP inhibition. As this project was conducted to study phagocytic modulation of macrophages to improve chemo-immunotherapy, we went on to focus on that cell type. Further investigations should focus on the effect of PPP inhibition on lymphoma cells to elucidate the mechanism behind the increased susceptibility for phagocytosis seen in this screening approach and make it potentially usable for lymphoma treatment.

5.1.3. PPP is a robust inductor of phagocytosis in macrophages

To prove the robustness of the effect of PPP inhibition on the phagocytic activity of macrophages, we validated our primary findings in several ways. By that, possible unique effects due to artifacts of used cell lines or inhibitors have been made more unlikely. The increase of phagocytosis was reproducible with independent inhibitors of the two PPP enzymes in focus, 6PGD and TKT, and in a variety of macrophage cell lines as well as primary human macrophages. Furthermore, PPP inhibition led to increased phagocytosis by use of several independent therapeutic antibodies currently used in clinics. Potential off-targets effects of used inhibitors driving the observed phenotype, were allayed by the generation of shRNA-mediated 6PGD- and TKT-knockdown macrophages, which achieved a strongly significant increased phagocytic activity. By that we have proven the effect of PPP inhibition using a genetic approach. The genetic targeting of the PPP enzymes demonstrated that the effect of PPP inhibition is not time-dependent. Chemical agents normally lead to a shorter distinct effect on metabolism as the cells can adapt to the inhibition and, for example, can produce a higher amount of the enzyme or induce other short-term compensatory mechanisms to overcome the inhibition. By continuously genetic targeting these compensatory mechanisms are not feasible. Nevertheless, we observed an equal phenotype so that it is more likely that the PPP inhibition itself and not a compensatory effect is leading to the observed changes.

An increase of phagocytosis without the targeting of tumor cells by therapeutic antibodies was observed under PPP inhibition also, which indicates a potential anti-tumor effect independent of antibody-based immunotherapy. This opens up a perspective for implementing the metabolic modulation to other therapeutic regimes.

A metabolic feature of the refractory niches of lymphoma – the lymph nodes and the bone marrow – can be hypoxia,[117,118] which has the potential to influence the efficacy of therapeutics and to alter the metabolism of macrophages. Therefore, we also performed the ADCP assays with PPP inhibitors under hypoxic conditions and could demonstrate that the positive effect of PPP inhibition also remains under that lymphoma-supportive condition.

All these validation experiments showed a very robust effect of chemical and genetic PPP inhibition on macrophages´ phagocytic activity and turns it into a promising target for improving chemo-immunotherapy and reaching the therapy refractory niches.

5.1.4. PPP enzyme inhibition is the driving force of increased phagocytosis in macrophages

For a deeper understanding of the metabolic effect PPP enzyme inhibition has on macrophages, we supplemented the intermediates of PPP and performed ADCP assays. With this approach, we were able to demonstrate that the increase of phagocytosis is driven by the enzyme inhibition itself rather than metabolite accumulation due to less enzyme activity. Non-exclusive PPP intermediates did not influence the phagocytosis, possibly due to their alternative metabolism via glycolysis (glyceraldehyde-3-phosphate, fructose-6-phosphate) or nucleotide synthesis (ribose-5-phosphate) before they could enter PPP flux. In contrast, the PPP-exclusive intermediates change the phagocytic activity with an increase of phagocytosis under supplementation of the glucose-6-phosphate dehydrogenase (G6PD) product 6-phosphogluconate, the 6PGD product ribulose-5-phosphate, and the TKT product sedoheptulose-7-phosphate and a decrease of phagocytosis by adding the TKT educt erythrose-4-phosphate. A lot of enzymes underlie a regulation via feedback inhibition. This describes the mechanism that an increase of educts of an enzyme increases its enzymatic activity while an accumulation of products decreases it. The observed increased phagocytosis rate under product supplementation points to that feedback inhibition of the respective PPP enzymes and emphasizes the enzyme inhibition as the driving force for increased phagocytosis while the educt accumulation under pharmacological enzyme inhibition was eliminated as a possible cause. To further validate this observation, ADCP assays with induction of the respective enzymes under observation if the phagocytic activity of macrophages decreases, could be performed.

5.2 6PGD and TKT modulation also has great impact on several cancer types and immune cells while it shows little side effects

Regarding the inhibited PPP enzymes in this work – 6PGD and TKT – in cancer cells, an altered expression has been described. Several publications refer to 6PGD upregulation in different cancer types, including colon cancer, hepatocellular cancer, pancreatic cancer, thyroid cancer, lung cancer, breast cancer, ovarian cancer, prostate cancer, and leukemia.[119–125] Enzyme upregulation in tumor cells was shown to be driven by common signaling alterations like phosphoinositide 3-kinase/Rho family-alpha serine/threonine-protein kinase (PI3K/Akt), breaking cluster region protein/Abelson kinase (Bcr/Abl), HIF1α, mammalian target of rapamycin (mTOR), p53, and epidermal growth factor receptor (EGFR) signaling,[126–133] whose shared interaction partner is the nuclear factor erythroid 2-related factor 2 (NRF2) and whose

are targets for different already established therapeutic agents. Overexpression of TKT was closely associated with aggressive clinic-pathological hepatocellular carcinoma features,[134] and 6PGD activity regulates metastasis by promoting phosphorylation of c-Met[135] and leads to cisplatin resistance.[136] By contrast, it was shown that suppression of 6PGD attenuates cell proliferation and tumor growth[137] and overcomes cisplatin resistance,[136] and TKT inhibition sensitized cancer cells to existing targeted therapy.[134] PPP inhibition by physcion, S3 or 6-aminonicotinamide has achieved anti-tumorigenic effects in leukemia, glioblastoma, and lung cancer cells,[138–140] without affecting the proliferation of non-malignant cells including mononucleocytes.[137] This antitumor effect was also reached in already chemotherapeutic-resistant acute myeloid leukemia cells.[125] In *in vivo* experiments, a very low rate of side effects by these inhibitors was demonstrated.[138–140] Knockdown of TKT profoundly reduced the growth of metastatic lesions, whereby TKT inhibition in normal cells did not have negative effects.[134] Besides its effect on cancer cells, 6PGD modulation has also been seen to influence the activity of other immune cells. Daneshmandi et al. described that 6PGD inhibition in $CD8^+$ T cells leads to an increased effector function with higher tumoricidal activity.[141] This opens up a new field for the use of PPP inhibition as a possible improver of adaptive immunity and T cell-based therapeutic regimes. Experimental analysis of PPP inhibition in T cells and the functional and therapeutic consequences has to be performed as well as further research in several cancer types.

5.3 PPP inhibition changes the characteristics of macrophages in different ways toward pro-inflammatory activity

For a deeper understanding of the observed changes in macrophages under PPP inhibition, we characterized the cells in several ways.

5.3.1. PPP inhibition shifts macrophage polarization toward M1-like phenotype

As described in the introduction, the polarization of macrophages mainly influences their activation and phagocytic activity. We therefore determined their polarization status by surface marker staining. Here, it was demonstrated that PPP inhibition decreases the expression of markers associated with M2- and TAM-like macrophages, which represent an immune-suppressive and tumor-promoting macrophage subtype,[6,142,143] while exclusive M1-marker, expressed on pro-inflammatory macrophages, were increased.[144–147] This tendency was even more present in the PPP-knockdown macrophages although there was no clear significant change in any of the markers under any treatment condition. As there is no black and white in the macrophage polarization and it is a brought spectrum, these data still show good hints for a changed tendency in polarization toward M1. A possible restriction of this polarization itemization causing the non-significant difference between the conditions might be the fact that we used already mature macrophages in these experiments. As we have demonstrated in

experiments with primary human macrophages, they have to be exposed to the PPP inhibition already under differentiation from monocytes into macrophages to develop a pro-phagocytic phenotype. Possibly, the treatment of an already mature macrophage cell line can push the cells into this direction but is not able to completely repolarize them even though it is able to significantly change several other characteristics of the macrophages including increased phagocytic activity. By treating macrophages in mice *in vivo*, we were able to demonstrate a much clearer shift away from the M2- and TAM-like phenotype and toward the M1-like phenotype with a significantly changed surface marker expression, supporting the first seen tendency of polarization in macrophages. In mice there is an ongoing renewal of macrophages, so it is likely that we treat immature macrophages with the PPP inhibitor during their maturation leading to the observation of the stronger change in polarization phenotype.

5.3.2. PPP inhibition leads to a phagocytic active morphological macrophage phenotype

Under different polarization, macrophages achieve very distinct morphological phenotypes to fulfil their tasks. We observed changes in cytoskeletal organization under pharmacological and shRNA-mediated PPP inhibition. The macrophages enlarge their cell size and achieve a widespread cytosol protrusion with formation of lamellipodia and filopodia. This reflects an activated state of macrophages and points to a higher disposition for phagocytosis, as lamellipodia and filopodia are used to initiate phagocytosis by approaching the targets prior engulfment.[148] This observation indicates that PPP activity also have influence on the actin organization and the activation status of macrophages.

5.3.3. PPP inhibition increases the metabolic activity of macrophages

The PPP is a central metabolic pathway as it is a linker between glucose metabolism, amino acid biosynthesis, fatty acid metabolism and redox homeostasis.[119] To investigate the metabolic status of macrophages under PPP inhibition, we performed a Seahorse XF Mito Stress test with which the glycolytic and mitochondrial activity, two very central metabolic pathways for the macrophage polarization and energy production, of cells can be measured. A general gain in metabolic activity of macrophages was observed under PPP inhibition with an increased glycolytic and mitochondrial capacity causing a significant enhanced ATP production. This might fuel macrophages´ activation. An increase of glycolysis is well described within the phenotypical switch to M1-like macrophages.[60] In line with our observations, 6PGD inhibition by physcion has been described to increase lactate and ATP production.[137]

In total, the restriction of one metabolic pathway – the PPP – gives rise to numerous paths of activation which renders a profound alteration of the phenotype and particular the phagocytic activity in macrophages whereby the anti-tumor function could be improved from several points of action.

5.3.4. Possible further advantages of PPP inhibition in macrophages and cancer cells

Regarding cancer cells, great changes in metabolism are seen to fuel their proliferation and survival.[149] The PPP promotes tumor cell growth by providing substrates for nucleotide biosynthesis and redox homeostasis.[119,126] By PPP inhibition a diminished tumor cell growth might be achieved. Further investigation on this has to be done.

Furthermore, PPP is the key resource for cytosolic NADPH needed for fatty acid synthesis. Therefore, a decreased fatty acid level under PPP inhibition has to be assumed. In macrophages this loss in fatty acids might be compensated by phagocytosis fueling fatty acid influx. To analyze this potential influence on fatty acid metabolism, a ^{13}C-glucose- and ^{13}C-glutamine supplementation with subsequent ^{13}C metabolic flux analysis via gas chromatography to quantify fatty acids under PPP inhibition can be performed. The hypothesized decreased intrinsic fatty acid generation might protect the macrophages to undergo lipid dense “foam cells” development[150,151] causing an increased and prolonged phagocytic function and a protection against the development of atherosclerosis. It was shown, that M2-like macrophages have a higher susceptibility to develop into “foam cells” than M1-like macrophages. Therefore, the observed phenotypic shift toward M1-like macrophages also reduces the possible atherosclerotic function.

5.4 PPP inhibition causes increased macrophage activity by modulation of the UDPG-STAT1-IRG1-itaconate axis

To understand the underlying mechanism behind the observed phenotypic changes of macrophages under PPP inhibition, we performed a multi-omic approach including proteomics, phosphoproteomics, and metabolomics. By using these different analyses of expression profiles, a distinct picture of cell regulation on different levels can be depicted.

5.4.1. Phospho-/proteomics unveil the CSF1R-PTK2B-HMOX-1-IRG1 signaling pathway as possible driver for the changed macrophage phenotype

The proteomic and phosphoproteomic analyses and pathway enrichment analysis confirmed the observed phenotypic changes. Expression pattern of changed phagocytic and immune activity were enriched as well as pattern of cytoskeletal organization. Moreover, changed expression pattern of glycolysis and mitochondrial activity as well as of central signaling pathways for metabolic regulation like HIF1α, PI3K, and mitogen-activated protein kinase (MAPK) were seen.

Deeper analysis of protein activity by calculation of the normalized upstream kinase score (NUKS) highlighted one possible signaling axis as major regulator of macrophages´ activated phenotype. A significantly reduced colony stimulating factor 1 receptor (CSF1R) expression and activity was detected and also seen in surface marker staining (Suppl. table 1) and

proteomic analysis. CSF1R activation leads to protein tyrosine kinase 2 beta (PTK2B) activation (also known as PYK2),[152] which itself can induce heme-oxygenase-1 (HMOX-1) expression via cytochrome b beta/MAPK1 (CYBB/MAPK1) signaling.[153] The expression of HMOX-1 in turn induces immune-responsive gene 1 (IRG1; also known as ACOD1) expression,[154] a central inhibitory regulator of macrophage activation.[25] With exception of HMOX-1, all named participants of this pathway were shown to be downregulated in proteomic screening. The PTK2B downregulation under PPP inhibition and knockdown was proven in the combined NUKS analysis and by western blot analysis, strengthening the hypothesized downregulation of the CSF1R signaling pathway as PTK2B is the first downstream kinase of CSF1R. Via CSF1R signaling, macrophages are polarized toward a M2- or TAM-like phenotype with increased M2-marker and –cytokine/chemokine expression by also direct activation of MAPK1/2 (also known as ERK1/2) and hematopoietic cell kinase (HCK) signaling.[155–160] Inhibition of HCK activity is known to reduce the amount of TAMs, colon cancer growth and tumor cell invasion.[161] Both, MAPK1 and HCK activity was detected as decreased under shRNA-mediated PPP inhibition in upstream kinase analysis. Beside these signaling pathways, also an interaction between CSF1R and interferon regulatory factor 1 (IRF1) and signal transducer and activator of transcription 1 (STAT1) is known.[162,163] Considering the pivotal role of CSF1R in macrophage activation and polarization, reduction in CSF1R expression might be the driving force of macrophage activation under PPP inhibition. Although, CSF1R activity is known to be essential especially in development, targeted inhibition of CSF1R is tolerable in adult mice.[164] Thereby, CSF1R blockade might also be a promising target for increasing macrophages´ efficacy in the context of tumor therapy. Several CSF1/CSF1R inhibitors are currently under clinical investigation.[165] Although CSF1R might be an auspicious target, it can only lead to effects in macrophages, as it is a macrophage-exclusive receptor. In contrast, 6PGD or TKT inhibition has the potential to have multicellular effects including the CSF1R regulation in macrophages as just one consequence of others as discussed above and might thereby have broader and more intensive effects in total.

5.4.2. PPP inhibition links metabolism and immune response via UDPG-STAT1-IRG1-itaconate axis

Ma et al. discovered another possible link between PPP activity and immune signaling. They have shown that PPP inhibition leads to inhibition of glycogenolysis leading to decreased uridine diphosphate glucose (UDPG) production.[22] UDPG is also a signaling molecule, which activates the purinergic receptor P2Y14 (P2Y14R) in autocrine and paracrine manner, whose activation in turn increases STAT1 expression and MAPK1 phosphorylation.[166] Considering STAT1 as major regulator of IRF1 expression,[23] an impact of PPP inhibition on IRG1 expression, whose expression is mainly regulated by IRF1,[24] is probable. IRG1 is almost exclusively expressed in activated immune cells, mostly in macrophages, and a key driver of

immune inhibition via itaconate production.[167] IRG1 is the exclusive enzyme for itaconate production. Itaconate inhibits the glycolysis and the mitochondrial activity by SDH inhibition,[71,168,169] promotes an anti-inflammatory macrophage phenotype by induction of NRF2 and activation transcription factor 3 (ATF3),[170] and promotes tumor growth via increased ROS secretion of macrophages, which activates MAPK in the tumor cells.[171] In contrast to the publication of Ma et al.,[22] we observed decreased glycogen amounts in macrophages under PPP inhibition. But concurrently, we observed an increase in glycolytic activity, which possibly leads to less glucose-6-phosphate flux into glycogen synthesis with subsequent less glycogenolysis caused by decreased glycogen amount. To prove this hypothesis, further analysis of the glycogen pathway should be performed. With a ^{13}C-glucose supplementation with subsequent ^{13}C-metabolic flux analysis via mass spectrometry analysis, the flux of glucose into the glycogen pathway and others can be detected. This analysis in macrophages under PPP inhibition and knockdown is planned and may give a deeper insight into regulation of the glycogen metabolism under PPP inhibition.

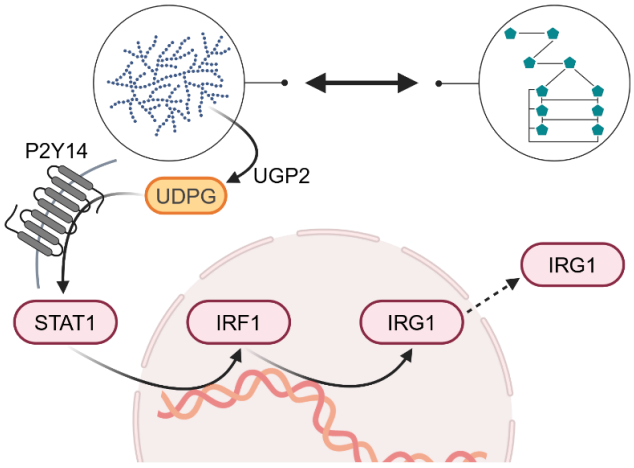

Fig. 5.1 **PPP inhibition is linked to macrophage immune response via UDPG-STAT1-IRG1 signaling axis.** Scheme of the hypothesized pathway causing changed macrophage phenotype. PPP activity and glycogen activity are coupled. Through glycogenolysis the P2Y14 receptor is activated by the glycogen pathway intermediate UDPG. By P2Y14R activation the STAT1 signaling axis is activated, which - beside others - leads to IRF1 and by that to IRG1 expression. IRG1 is the exclusive enzyme for itaconate production, which has a high impact on immunosuppressive polarization of macrophages. By PPP inhibition this signaling network is downregulated with concomitant more pro-inflammatory macrophage polarization. Figure modified from Beielstein et al.[3]

Following the above described hypothesized signaling pathway based on decreased glycogenolysis, we observed decreased expression of the UDPG-STAT1-IRG1 pathway proteins under PPP inhibition, subsequent lower amounts of itaconate, and an increased SDH activity. In line with the decreased itaconate amount, we observed a pro-inflammatory cytokine

switch with increase of IL-6 and decrease of IL-10 expression and a phenotypic shift toward M1-like polarization.

The importance of IRG1 as central linking point was highlighted by the use of an IRG1-knockout mouse model. Macrophages of these knockout mice showed a significantly higher phagocytic activity than macrophages of wild type mice. This strengthens the hypothesis that the link between PPP inhibition and IRG1 by the UDPG-STAT1-IRG1 axis is the driving force of the observed activated macrophage phenotype with higher phagocytic activity.

5.4.3. Possible functional consequences of UDPG-STAT1-IRG1-itaconate axis modulation

Itaconate is an inducer of NRF2, which suppresses pro-inflammatory macrophage function by blocking cytokine transcription[170,172] and increases HMOX-1, G6PD, 6PGD, TKT activity, and NADPH production.[173] This correlation between NRF2, itaconate and the PPP enzymes underlines the possible PPP inhibition effect on macrophages´ effector function. Furthermore, NRF2 is known to be essential for atherosclerosis development and is activated by cholesterol,[173] whose production is dependent on PPP-derived NADPH. Increased NRF2 expression has been described in several cancer types as origin of anti-inflammatory signaling and chemoresistance.[174] It has been shown that NRF2 is unable to lead to these pro-tumorigenic effects when the PPP is inhibited.[127] This points to a further multicellular effect of PPP inhibition causing decreased cancer cell support.

Besides its role in IRG1 expression, IRF1 is also known to induce iNOS expression,[24,175,176] consistent with the decreased iNOS expression under PPP inhibition we depicted. High iNOS expression and activity has been correlated with malignancy and poor survival in several solid tumors and leukemia.[177]

Moreover, it was shown that the IRG1 metabolite itaconate acts tumor-supportive by potentiating tumor growth.[75]

P2Y14R expression in T lymphocytes was shown to inhibit T cell proliferation and activation.[178] This strengthens the hypothesis that PPP inhibition is also able to be a regulator of tumor cell activity and adaptive immune responses.

Despite the known pro-inflammatory transcriptional function of STAT1 in LPS-stimulated macrophages, in this study we have shown an alternative mechanism of macrophage activation by metabolic depression of the anti-inflammatory properties of STAT1 via itaconate regulation leading to a pro-phagocytic phenotype of macrophages. In TAMs, STAT1 has been shown to be the generator of the blended M1/M2 phenotype and supporter of the anti-inflammatory and pro-tumorigenic properties.[10,179] Under PPP inhibition this tumor-supportive polarization of macrophages is diminished.

As the reduced expression of IRF1 under PPP inhibition also influences STAT1 and CSF1R expression,[180] IRF1 can be seen as the junction between all recapitulated pathways, which are leading to the changed macrophage activity and polarization we observed.

5.5 PPP inhibition diminishes macrophages´ pro-tumoral properties

Beside their needed activity for tumor cell elimination, the pro-tumoral function of TAMs for several tumor entities was mentioned before. Especially in CLL, macrophages play a pivotal role as supportive bystander cells in the TME. Without the appearance of these TAMs, CLL cells would undergo spontaneous apoptosis.[26] This depicts another pro-tumoral function of macrophages. We have demonstrated that PPP inhibition also diminishes this pro-survival bystander function. As a decrease of viable CLL cells was also observed in monoculture PPP inhibition, a direct negative effect on CLL cell survival could be expected and should be further analyzed. In line with that, a higher susceptibility to chemotherapeutic treatment under PPP inhibition in macrophage co-culture and under PPP-inhibited macrophage co-culture was demonstrated. This indicates PPP inhibition as a CLL sensitizer to conventional chemotherapeutic regimes by cellular effects on CLL cells and macrophages causing decreased tumor-supportive functions of macrophages. Considering these results, PPP inhibition might also be a promising target in the conventional chemotherapeutic treatment of cancer. Studies on the therapeutic benefit of addition of PPP inhibitors to conventional chemotherapy should be performed and are planned on cell culture and *in vivo* level in our laboratory.

5.6 PPP inhibition in primary human cells also increases macrophage phagocytic function and pro-inflammatory polarization

As we primarily analyzed the consequences of metabolic regulation on macrophages to elucidate its role in human therapy regimens, we attempted to mimic human conditions by using CLL patient cells and primary human macrophages from healthy donors. A highly significant increase of phagocytosis also was achieved in these primary human cell condition. Furthermore, the macrophages showed the same switch toward pro-inflammatory cytokine secretion under PPP inhibition as seen in cell line experiments before. These results indicate an effectiveness of PPP inhibition in human organism and clinical use. However, this experimental approach has a restriction. Macrophages of healthy donors and not of CLL patients has been used (because of their availability). Macrophages of CLL patients have a polarization toward the TAM-like phenotype and thereby might show other changes in phenotype and activity than macrophages from healthy donors under PPP inhibition. Because of that the efficacy of the treatment might be lower than in our approach. Experiments with CLL cells and macrophages from the same donor should be performed to prove the efficacy of PPP inhibitor treatment. Moreover, we analyzed the effects only in a co-culture setting of two cell

types. This does not reflect the whole TME, in which several other cell types and milieu factors could have an influence on the CLL cell and macrophage behavior.

5.7 PPP inhibition leads to significant prolonged overall survival in a lymphoma mouse model and potentiates macrophage function *in vivo*

To model a more precise microenvironment of lymphoma in patients, we performed *in vivo* experiments. Therefor mice got intravenous injection of hMB cells and afterwards were treated with the CD52-antibody alemtuzumab and the physcion derivate S3, whose low toxicity and high effectiveness in treatment of other tumor entities were demonstrated before.[137,181] In the aggressive lymphoma mouse model,[38] PPP inhibition has an amplification effect on the antibody therapy leading to a significantly prolonged overall survival in comparison to antibody treatment only. This was associated with an increased macrophage infiltration into lymphoma sites and decreased lymphoma cell infiltration of spleen at day of sacrifice. The PPP inhibition *in vivo* increased the myelopoiesis and gave rise to progenitor cell expansion, indicating increased provision of a variety of immune cells, pointing again toward potent multicellular effects of PPP inhibition. The macrophages displayed a pro-inflammatory polarization and a significantly increased phagocytic capacity after PPP inhibition *in vivo*.

With this approach and analyzes, we have proven the *in vivo* efficacy of PPP inhibition leading to macrophage activation, immune cell expansion, and improved therapy response by antibody-mediated phagocytic clearance of lymphoma cells with prolongation of overall survival. This strengthens the feasibility of efficacy of PPP inhibition in clinical use to improve lymphoma chemo-immunotherapy efficacy and patients´ outcome.

5.8 PPP inhibition - a promising target to improve cancer therapy

Taken together, our work opens up a new promising therapeutic concept to improve immunotherapy effects exerted by macrophages. PPP inhibition acts as a robust influencer of macrophage function. We were able to demonstrate a new connection between metabolic modulation and immune response and introduced this link as a key mechanism of macrophage polarization and activation regulation. Thereby we could implement a new treatment strategy acting on multicellular level, which has positive effects on effector immune cells and impairs cancer cell viability, causing promising anti-tumor activity. Previous *in vivo* experiments with the used PPP inhibitors have shown a good effectiveness against cancer cells without any severe side effects,[137,181] promising a low-toxic therapy targeting cancer cells and their microenvironment simultaneously. We have confirmed these observations in the context of antibody-based therapy regimes. Further experiments have to be done to explore therapy effectiveness in different cancer entities, *in vivo*, and in the human organism.

5.9 PPP inhibition – its possible side effects on patients

Beside these demonstrated positive effects further analysis should be done for possible negative effects of PPP inhibition on the macrophage function and the human organism. The here observed positive effect of macrophage activation can also cause negative consequences. As macrophages´ over-activation can have severe side effects in the context of sepsis or auto-inflammation, and the role of itaconate is describes as a central antagonist against it,[167] these aspects have to be investigated with particular thoughtfulness. Sepsis or auto-inflammation can have far-reaching harm for a patients live, can lead to high therapeutic costs and possibly cause patients´ death.

Moreover, the consequences of PPP inhibition for different cell types and organs should be further investigated. The PPP is the major source of different metabolites needed for other anabolic cellular processes and cell proliferation. The NADPH produced in PPP is central for the production of anti-oxidative glutathione needed to rescue the cell against ROS and cellular stress. On the other hand, defects of PPP enzymes are not generally severe or shortening lifetime. For example, G6PD-deficiency can cause hemolytic anemia due to infection, intake of fava beans or some medication, but for most of the individuals there are no constraints in daily life, life quality or life expectation. Moreover, G6PD-deficiency is more prevalent in malaria endemic areas, causing lower incidence of malaria infections in these individuals.[182,183]

These different aspects of PPP inhibition and its consequences underline the need of further research in the context of clinical use, potential and safety.

6. REFERENCES

1 Beekhof R, Alphen C, Henneman AA, *et al.* INKA , an integrative data analysis pipeline for phosphoproteomic inference of active kinases . *Mol Syst Biol* 2019; **15**. DOI:10.15252/msb.20188250.

2 Fernández-García M, Mesquita I, Ferreira C, *et al.* Leishmania donovani Induces Multiple Dynamic Responses in the Metabolome Associated with Amastigote Differentiation and Maturation Inside the Human Macrophage. *J Proteome Res* 2023; **22**: 2256–70.

3 Beielstein AC, Izquierdo E, Blakemore S, *et al.* Macrophages are activated toward phagocytic lymphoma cell clearance by pentose phosphate pathway inhibition. *Cell reports Med* 2024; : 101830.

4 Hanahan D, Weinberg RA. Hallmarks of cancer: the next generation. *Cell* 2011. DOI:10.1016/j.cell.2011.02.013.

5 Beielstein AC, Pallasch CP. Tumor Metabolism as a Regulator of Tumor-Host Interactions in the B-Cell Lymphoma Microenvironment-Fueling Progression and Novel Brakes for Therapy. *Int J Mol Sci* 2019; **20**: 4158.

6 Cassetta L, Pollard JW. Targeting macrophages: Therapeutic approaches in cancer. Nat. Rev. Drug Discov. 2018; **17**: 887–904.

7 Yang L, Zhang Y. Tumor-associated macrophages: from basic research to clinical application. *J Hematol Oncol* 2017; **10**: 58.

8 Pallasch CP, Leskov I, Braun CJ, *et al.* Sensitizing protective tumor microenvironments to antibody-mediated therapy. *Cell* 2014. DOI:10.1016/j.cell.2013.12.041.

9 Pallasch CP, Leskov I, Braun CJ, *et al.* Sensitizing protective tumor microenvironments to antibody-mediated therapy. *Cell* 2014; **156**. DOI:10.1016/j.cell.2013.12.041.

10 Biswas SK, Gangi L, Paul S, *et al.* A distinct and unique transcriptional program expressed by tumor-associated macrophages (defective NF-κB and enhanced IRF-3/STAT1 activation). *Blood* 2006; **107**: 2112–22.

11 Gallina G, Dolcetti L, Serafini P, *et al.* Tumors induce a subset of inflammatory monocytes with immunosuppressive activity on CD8+ T cells. *J Clin Invest* 2006; **116**: 2777.

12 Pittet MJ, Michielin O, Migliorini D. Clinical relevance of tumour-associated macrophages. *Nat Rev Clin Oncol 2022 196* 2022; **19**: 402–21.

13 Jha AK, Huang SCC, Sergushichev A, *et al.* Network integration of parallel metabolic and transcriptional data reveals metabolic modules that regulate macrophage polarization. *Immunity* 2015; **42**: 419–30.

14 Diskin C, Pålsson-McDermott EM. Metabolic modulation in macrophage effector

function. Front. Immunol. 2018; **9**. DOI:10.3389/fimmu.2018.00270.

15 M. de-Brito N, Duncan-Moretti J, C. da-Costa H, *et al.* Aerobic glycolysis is a metabolic requirement to maintain the M2-like polarization of tumor-associated macrophages. *Biochim Biophys Acta - Mol Cell Res* 2020; **1867**: 118604.

16 Hörhold F, Eisel D, Oswald M, *et al.* Reprogramming of macrophages employing gene regulatory and metabolic network models. *PLoS Comput Biol* 2020; **16**: 683–96.

17 Simões RL, De-Brito NM, Cunha-Costa H, *et al.* Lipoxin A4 selectively programs the profile of M2 tumor-associated macrophages which favour control of tumor progression. *Int J Cancer* 2017; **140**: 346–57.

18 Coiffier B, Thieblemont C, Van Den Neste E, *et al.* Long-term outcome of patients in the LNH-98.5 trial, the first randomized study comparing rituximab-CHOP to standard CHOP chemotherapy in DLBCL patients: a study by the Groupe d'Etudes des Lymphomes de l'Adulte. *Blood* 2010; **116**: 2040.

19 Poletto S, Novo M, Paruzzo L, Frascione PMM, Vitolo U. Treatment strategies for patients with diffuse large B-cell lymphoma. *Cancer Treat Rev* 2022; **110**: 102443.

20 Schuster SJ, Bishop MR, Tam CS, *et al.* Tisagenlecleucel in Adult Relapsed or Refractory Diffuse Large B-Cell Lymphoma. *N Engl J Med* 2019; **380**: 45–56.

21 Beekhof R, Alphen C, Henneman AA, *et al.* INKA , an integrative data analysis pipeline for phosphoproteomic inference of active kinases . *Mol Syst Biol* 2019. DOI:10.15252/msb.20198981.

22 Ma J, Wei K, Liu J, *et al.* Glycogen metabolism regulates macrophage-mediated acute inflammatory responses. *Nat Commun* 2020; **11**. DOI:10.1038/s41467-020-15636-8.

23 Taniguchi T, Ogasawara K, Takaoka A, Tanaka N. IRF family of transcription factors as regulators of host defense. Annu. Rev. Immunol. 2001; **19**: 623–55.

24 Tallam A, Perumal TM, Antony PM, *et al.* Gene Regulatory Network Inference of Immunoresponsive Gene 1 (IRG1) Identifies Interferon Regulatory Factor 1 (IRF1) as Its Transcriptional Regulator in Mammalian Macrophages. *PLoS One* 2016; **11**. DOI:10.1371/journal.pone.0149050.

25 O'Neill LAJ, Artyomov MN. Itaconate: the poster child of metabolic reprogramming in macrophage function. Nat. Rev. Immunol. 2019; **19**: 273–81.

26 Burger JA, Tsukada N, Burger M, Zvaifler NJ, Dell'Aquila M, Kipps TJ. Blood-derived nurse-like cells protect chronic lymphocytic leukemia B cells from spontaneous apoptosis through stromal cell-derived factor-1. *Blood* 2000; **96**: 2655–63.

27 Schmitz R, Stanelle J, Hansmann M-L, Uppers RK¨. Pathogenesis of Classical and Lymphocyte-Predominant Hodgkin Lymphoma. 2008. DOI:10.1146/annurev.pathol.4.110807.092209.

28 Burger JA, Ghia P, Rosenwald A, Caligaris-Cappio F. The microenvironment in mature

B-cell malignancies: a target for new treatment strategies. *Blood* 2009; **114**: 3367–75.

29 Scott DW, Gascoyne RD. The tumour microenvironment in B cell lymphomas. *Nat Rev Cancer 2014 148* 2014; **14**: 517–34.

30 Wyckoff J, Wang W, Lin EY, *et al.* A paracrine loop between tumor cells and macrophages is required for tumor cell migration in mammary tumors. *Cancer Res* 2004; **64**: 7022–9.

31 Gordon SR, Maute RL, Dulken BW, *et al.* PD-1 expression by tumour-associated macrophages inhibits phagocytosis and tumour immunity. Nature. 2017; **545**: 495–9.

32 Ruffell B, Coussens LM. Macrophages and therapeutic resistance in cancer. Cancer Cell. 2015; **27**: 462–72.

33 Falchi L, Vardhana SA, Salles GA. Bispecific antibodies for the treatment of B-cell lymphoma: promises, unknowns, and opportunities. *Blood* 2023; **141**: 467–80.

34 Tilly H, Morschhauser F, Sehn LH, *et al.* Polatuzumab Vedotin in Previously Untreated Diffuse Large B-Cell Lymphoma. *N Engl J Med* 2022; **386**: 351–63.

35 Sehn LH, Herrera AF, Flowers CR, *et al.* Polatuzumab vedotin in relapsed or refractory diffuse large B-cell lymphoma. *J Clin Oncol* 2020; **38**: 155–65.

36 Caimi PF, Ai W, Alderuccio JP, *et al.* Loncastuximab tesirine in relapsed or refractory diffuse large B-cell lymphoma (LOTIS-2): a multicentre, open-label, single-arm, phase 2 trial. *Lancet Oncol* 2021; **22**: 790–800.

37 Skłodowska-Curie M, Salles G, Duell J, *et al.* Tafasitamab plus lenalidomide in relapsed or refractory diffuse large B-cell lymphoma (L-MIND): a multicentre, prospective, single-arm, phase 2 study. *Artic Lancet Oncol* 2020; **21**: 978–88.

38 Leskov I, Pallasch CP, Drake A, *et al.* Rapid generation of human B-cell lymphomas via combined expression of Myc and Bcl2 and their use as a preclinical model for biological therapies. *Oncogene* 2013; **32**: 1066–72.

39 Shapouri-Moghaddam A, Mohammadian S, Vazini H, *et al.* Macrophage plasticity, polarization, and function in health and disease. *J Cell Physiol* 2018; **233**: 6425–40.

40 Gordon S, Plüddemann A, Martinez Estrada F. Macrophage heterogeneity in tissues: phenotypic diversity and functions. *Immunol Rev* 2014; **262**: 36.

41 Weiss G, Schaible UE. Macrophage defense mechanisms against intracellular bacteria. *Immunol Rev* 2015; **264**: 182–203.

42 Iwasaki A, Medzhitov R. Control of adaptive immunity by the innate immune system. *Nat Immunol* 2015; **16**: 343–53.

43 Yatim KM, Lakkis FG. A brief journey through the immune system. *Clin J Am Soc Nephrol* 2015; **10**: 1274–81.

44 Murray PJ, Wynn TA. Protective and pathogenic functions of macrophage subsets. *Nat Rev Immunol* 2011; **11**: 723.

45 Tsou CL, Peters W, Si Y, *et al.* Critical roles for CCR2 and MCP-3 in monocyte mobilization from bone marrow and recruitment to inflammatory sites. *J Clin Invest* 2007; **117**: 902–9.

46 Mills CD, Kincaid K, Alt JM, Heilman MJ, Hill AM. M-1/M-2 macrophages and the Th1/Th2 paradigm. *J Immunol* 2000; **164**: 6166–73.

47 Mills CD. Anatomy of a Discovery: M1 and M2 Macrophages. *Front Immunol* 2015; **6**. DOI:10.3389/FIMMU.2015.00212.

48 Mosser DM, Edwards JP. Exploring the full spectrum of macrophage activation. *Nat Rev Immunol 2008 812* 2008; **8**: 958–69.

49 Murray PJ, Allen JE, Biswas SK, *et al.* Macrophage Activation and Polarization: Nomenclature and Experimental Guidelines. *Immunity* 2014; **41**: 14–20.

50 Martinez FO, Gordon S. The M1 and M2 paradigm of macrophage activation: time for reassessment. *F1000Prime Rep* 2014; **6**. DOI:10.12703/P6-13.

51 Biswas SK, Gangi L, Paul S, *et al.* A distinct and unique transcriptional program expressed by tumor-associated macrophages (defective NF-κB and enhanced IRF-3/STAT1 activation). *Blood* 2006; **107**: 2112–22.

52 Colegio OR, Chu N-Q, Szabo AL, *et al.* Functional polarization of tumour-associated macrophages by tumour-derived lactic acid. *Nature* 2014; **513**: 559–63.

53 Bohn T, Rapp S, Luther N, *et al.* Tumor immunoevasion via acidosis-dependent induction of regulatory tumor-associated macrophages. *Nat Immunol* 2018; **19**: 1319–29.

54 Liu D, Chang C, Lu N, *et al.* Comprehensive Proteomics Analysis Reveals Metabolic Reprogramming of Tumor-Associated Macrophages Stimulated by the Tumor Microenvironment. *J Proteome Res* 2017; **16**: 288–97.

55 Stout RD, Suttles J. Functional plasticity of macrophages: reversible adaptation to changing microenvironments. *J Leukoc Biol* 2004; **76**: 509.

56 Stout RD, Jiang C, Matta B, Tietzel I, Watkins SK, Suttles J. Macrophages Sequentially Change Their Functional Phenotype in Response to Changes in Microenvironmental Influences. *J Immunol* 2005; **175**: 342–9.

57 Liao ZX, Fa YC, Kempson IM, Tseng SJ. Repolarization of M2 to M1 Macrophages Triggered by Lactate Oxidase Released from Methylcellulose Hydrogel. *Bioconjug Chem* 2019; **30**: 2697–702.

58 Biswas SK, Mantovani A. Macrophage plasticity and interaction with lymphocyte subsets: cancer as a paradigm. *Nat Immunol 2010 1110* 2010; **11**: 889–96.

59 Oyarce C, Vizcaino-Castro A, Chen S, Boerma A, Daemen T. Re-polarization of immunosuppressive macrophages to tumor-cytotoxic macrophages by repurposed metabolic drugs. *Oncoimmunology* 2021; **10**. DOI:10.1080/2162402X.2021.1898753.

60 Rodríguez-Prados J-C, Través PG, Cuenca J, *et al.* Substrate Fate in Activated Macrophages: A Comparison between Innate, Classic, and Alternative Activation. *J Immunol* 2010; **185**: 605–14.

61 Huang SCC, Smith AM, Everts B, *et al.* Metabolic Reprogramming Mediated by the mTORC2-IRF4 Signaling Axis Is Essential for Macrophage Alternative Activation. *Immunity* 2016; **45**: 817–30.

62 Michl J, Ohlbaum DJ, Silverstein SC. 2-Deoxyglucose selectively inhibits fc and complement receptor-mediated phagocytosis in mouse peritoneal macrophages: I. Description of the inhibitory effect*. *J Exp Med* 1976; **144**: 1465–83.

63 Izquierdo E, Cuevas VD, Fernández-Arroyo S, *et al.* Reshaping of Human Macrophage Polarization through Modulation of Glucose Catabolic Pathways. *J Immunol* 2015; **195**: 2442–51.

64 Freemerman AJ, Johnson AR, Sacks GN, *et al.* Metabolic reprogramming of macrophages: glucose transporter 1 (GLUT1)-mediated glucose metabolism drives a proinflammatory phenotype. *J Biol Chem* 2014; **289**: 7884–96.

65 Arts RJW, Plantinga TS, Tuit S, *et al.* Transcriptional and metabolic reprogramming induce an inflammatory phenotype in non-medullary thyroid carcinoma-induced macrophages. *Oncoimmunology* 2016; **5**. DOI:10.1080/2162402X.2016.1229725.

66 EM P-M, L D, Z Z, *et al.* Pyruvate Kinase M2 Is Required for the Expression of the Immune Checkpoint PD-L1 in Immune Cells and Tumors. *Front Immunol* 2017; **8**. DOI:10.3389/FIMMU.2017.01300.

67 Haschemi A, Kosma P, Gille L, *et al.* The sedoheptulose kinase CARKL directs macrophage polarization through control of glucose metabolism. *Cell Metab* 2012; **15**: 813–26.

68 Infantino V, Convertini P, Cucci L, *et al.* The mitochondrial citrate carrier: A new player in inflammation. *Biochem J* 2011; **438**: 433–6.

69 Infantino V, Iacobazzi V, Palmieri F, Menga A. ATP-citrate lyase is essential for macrophage inflammatory response. *Biochem Biophys Res Commun* 2013; **440**: 105–11.

70 Strelko CL, Lu W, Dufort FJ, *et al.* Itaconic acid is a mammalian metabolite induced during macrophage activation. *J Am Chem Soc* 2011; **133**: 16386–9.

71 Cordes T, Wallace M, Michelucci A, *et al.* Immunoresponsive gene 1 and itaconate inhibit succinate dehydrogenase to modulate intracellular succinate levels. *J Biol Chem* 2016; **291**: 14274–84.

72 Tannahill GM, Curtis AM, Adamik J, *et al.* Succinate is an inflammatory signal that induces IL-1β through HIF-1α. *Nature* 2013; **496**: 238–42.

73 Artyomov MN, Sergushichev A, Schilling JD. Integrating immunometabolism and

macrophage diversity. *Semin Immunol* 2016; **28**: 417–24.

74 Rabold K, Netea MG, Adema GJ, Netea-Maier RT. Cellular metabolism of tumor-associated macrophages – functional impact and consequences. FEBS Lett. 2017; **591**: 3022–41.

75 Weiss JM, Davies LC, Karwan M, *et al.* Itaconic acid mediates crosstalk between macrophage metabolism and peritoneal tumors. *J Clin Invest* 2018; **128**: 3794–805.

76 Arsenijevic D, Onuma H, Pecqueur C, *et al.* Disruption of the uncoupling protein-2 gene in mice reveals a role in immunity and reactive oxygen species production. *Nat Genet* 2000; **26**: 435–9.

77 Feng J, Li L, Ou Z, *et al.* IL-25 stimulates M2 macrophage polarization and thereby promotes mitochondrial respiratory capacity and lipolysis in adipose tissues against obesity. *Cell Mol Immunol* 2018; **15**: 493–505.

78 Vats D, Mukundan L, Odegaard JI, *et al.* Oxidative metabolism and PGC-1beta attenuate macrophage-mediated inflammation. *Cell Metab* 2006; **4**: 13–24.

79 O'Neill LAJ, Kishton RJ, Rathmell J. A guide to immunometabolism for immunologists. Nat. Rev. Immunol. 2016; **16**: 553–65.

80 Posokhova EN, Khoshchenko OM, Chasovskikh MI, Pivovarova EN, Dushkin MI. Lipid synthesis in macrophages during inflammation in vivo: effect of agonists of peroxisome proliferator activated receptors alpha and gamma and of retinoid X receptors. *Biochemistry (Mosc)* 2008; **73**: 296–304.

81 Feingold KR, Shigenaga JK, Kazemi MR, *et al.* Mechanisms of triglyceride accumulation in activated macrophages. *J Leukoc Biol* 2012; **92**: 829–39.

82 Moon JS, Lee S, Park MA, *et al.* UCP2-induced fatty acid synthase promotes NLRP3 inflammasome activation during sepsis. *J Clin Invest* 2015; **125**: 665–80.

83 Ecker J, Liebisch G, Englmaier M, Grandl M, Robenek H, Schmitz G. Induction of fatty acid synthesis is a key requirement for phagocytic differentiation of human monocytes. *Proc Natl Acad Sci U S A* 2010; **107**: 7817–22.

84 Lee JY, Sohn KH, Rhee SH, Hwang D. Saturated fatty acids, but not unsaturated fatty acids, induce the expression of cyclooxygenase-2 mediated through Toll-like receptor 4. *J Biol Chem* 2001; **276**: 16683–9.

85 Oh DY, Talukdar S, Bae EJ, *et al.* GPR120 is an omega-3 fatty acid receptor mediating potent anti-inflammatory and insulin-sensitizing effects. *Cell* 2010; **142**: 687–98.

86 Kliewer SA, Sundseth SS, Jones SA, *et al.* Fatty acids and eicosanoids regulate gene expression through direct interactions with peroxisome proliferator-activated receptors alpha and gamma. *Proc Natl Acad Sci U S A* 1997; **94**: 4318–23.

87 Im SS, Yousef L, Blaschitz C, *et al.* Linking lipid metabolism to the innate immune response in macrophages through sterol regulatory element binding protein-1a. *Cell*

Metab 2011; **13**: 540–9.

88 Covarrubias AJ, Aksoylar HI, Horng T. Control of macrophage metabolism and activation by mTOR and Akt signaling. *Semin Immunol* 2015; **27**: 286–96.

89 Kang K, Reilly SM, Karabacak V, *et al.* Adipocyte-derived Th2 cytokines and myeloid PPARdelta regulate macrophage polarization and insulin sensitivity. *Cell Metab* 2008; **7**: 485–95.

90 Odegaard JI, Ricardo-Gonzalez RR, Red Eagle A, *et al.* Alternative M2 activation of Kupffer cells by PPARdelta ameliorates obesity-induced insulin resistance. *Cell Metab* 2008; **7**: 496–507.

91 Mukundan L, Odegaard JI, Morel CR, *et al.* PPAR-delta senses and orchestrates clearance of apoptotic cells to promote tolerance. *Nat Med* 2009; **15**: 1266–72.

92 Rao E, Singh P, Zhai X, *et al.* Inhibition of tumor growth by a newly-identified activator for epidermal fatty acid binding protein. *Oncotarget* 2015; **6**: 7815–27.

93 Schumann T, Adhikary T, Wortmann A, *et al.* Deregulation of PPARβ/δ target genes in tumor-associated macrophages by fatty acid ligands in the ovarian cancer microenvironment. *Oncotarget* 2015; **6**: 13416–33.

94 Xiang W, Shi R, Kang X, *et al.* Monoacylglycerol lipase regulates cannabinoid receptor 2-dependent macrophage activation and cancer progression. *Nat Commun* 2018; **9**. DOI:10.1038/s41467-018-04999-8.

95 Rath M, Müller I, Kropf P, Closs EI, Munder M. Metabolism via Arginase or Nitric Oxide Synthase: Two Competing Arginine Pathways in Macrophages. *Front Immunol* 2014; **5**. DOI:10.3389/FIMMU.2014.00532.

96 MacMicking J, Xie QW, Nathan C. Nitric oxide and macrophage function. *Annu Rev Immunol* 1997; **15**: 323–50.

97 Clementi E, Brown GC, Feelisch M, Moncada S. Persistent inhibition of cell respiration by nitric oxide: Crucial role of S-nitrosylation of mitochondrial complex I and protective action of glutathione. *Proc Natl Acad Sci U S A* 1998; **95**: 7631–6.

98 Albina JE, Mastrofrancesco B. Modulation of glucose metabolism in macrophages by products of nitric oxide synthase. *Am J Physiol* 1993; **264**. DOI:10.1152/AJPCELL.1993.264.6.C1594.

99 Hu X, Liu G, Hou Y, *et al.* Induction of M2-like macrophages in recipient NOD-scid mice by allogeneic donor CD4(+)CD25(+) regulatory T cells. *Cell Mol Immunol* 2012; **9**: 464–72.

100 Hardbower DM, Asim M, Luis PB, *et al.* Ornithine decarboxylase regulates M1 macrophage activation and mucosal inflammation via histone modifications. *Proc Natl Acad Sci U S A* 2017; **114**: E751–60.

101 Rodriguez PC, Zea AH, DeSalvo J, *et al.* L-arginine consumption by macrophages

modulates the expression of CD3 zeta chain in T lymphocytes. *J Immunol* 2003; **171**: 1232–9.

102 Van den Bossche J, Baardman J, Otto NA, *et al.* Mitochondrial Dysfunction Prevents Repolarization of Inflammatory Macrophages. *Cell Rep* 2016; **17**: 684–96.

103 Choi J, Stradmann-Bellinghausen B, Yakubov E, Savaskan NE, Regnier-Vigouroux A. Glioblastoma cells induce differential glutamatergic gene expressions in human tumor-associated microglia/macrophages and monocyte-derived macrophages. *Cancer Biol Ther* 2015; **16**: 1205–13.

104 Klimp AH, Hollema H, Kempinga C, van der Zee AGJ, de Vries EGE, Daemen T. Expression of cyclooxygenase-2 and inducible nitric oxide synthase in human ovarian tumors and tumor-associated macrophages. *Cancer Res* 2001; **61**: 7305–9.

105 DiNapoli MR, Calderon CL, Lopez DM. The altered tumoricidal capacity of macrophages isolated from tumor-bearing mice is related to reduce expression of the inducible nitric oxide synthase gene. *J Exp Med* 1996; **183**: 1323–9.

106 Ghassabeh GH, De Baetselier P, Brys L, *et al.* Identification of a common gene signature for type II cytokine-associated myeloid cells elicited in vivo in different pathologic conditions. *Blood* 2006; **108**: 575–83.

107 Sharda DR, Yu S, Ray M, *et al.* Regulation of macrophage arginase expression and tumor growth by the Ron receptor tyrosine kinase. *J Immunol* 2011; **187**: 2181–92.

108 Chang CI, Liao JC, Kuo L. Macrophage arginase promotes tumor cell growth and suppresses nitric oxide-mediated tumor cytotoxicity. *Cancer Res* 2001; **61**: 1100–6.

109 Van den Bossche J, Lamers WH, Koehler ES, *et al.* Pivotal Advance: Arginase-1-independent polyamine production stimulates the expression of IL-4-induced alternatively activated macrophage markers while inhibiting LPS-induced expression of inflammatory genes. *J Leukoc Biol* 2012; **91**: 685–99.

110 Mills CD, Shearer J, Evans R, Caldwell MD. MACROPHAGE ARGININE METABOLISM AND THE INHIBITION OR STIMULATION OF CANCER'. http://journals.aai.org/jimmunol/article-pdf/149/8/2709/1056963/2709.pdf (accessed Feb 16, 2024).

111 Zhao Q, Kuang D-M, Wu Y, *et al.* Activated CD69+ T cells foster immune privilege by regulating IDO expression in tumor-associated macrophages. *J Immunol* 2012; **188**: 1117–24.

112 He D, Mao Q, Jia J, *et al.* Pentose Phosphate Pathway Regulates Tolerogenic Apoptotic Cell Clearance and Immune Tolerance. *Front Immunol* 2022; **12**. DOI:10.3389/FIMMU.2021.797091.

113 Nakamizo S, Sugiura Y, Ishida Y, *et al.* Activation of the pentose phosphate pathway in macrophages is crucial for granuloma formation in sarcoidosis. *J Clin Invest* 2023; **133**.

DOI:10.1172/JCI171088.

114 Moreton P, Hillmen P. Alemtuzumab therapy in B-cell lymphoproliferative disorders. *Semin Oncol* 2003; **30**: 493–501.

115 Geskin LJ. Monoclonal Antibodies. *Dermatol Clin* 2015; **33**: 777–86.

116 Warburg O. Über den Stoffwechsel der Carcinomzelle. *Naturwissenschaften* 1924. DOI:10.1007/BF01504608.

117 Caldwell CC, Kojima H, Lukashev D, *et al.* Differential Effects of Physiologically Relevant Hypoxic Conditions on T Lymphocyte Development and Effector Functions. *J Immunol* 2001; **167**: 6140–9.

118 Spencer JA, Ferraro F, Roussakis E, *et al.* Direct measurement of local oxygen concentration in the bone marrow of live animals. *Nature* 2014; **508**: 269–73.

119 Stincone A, Prigione A, Cramer T, *et al.* The return of metabolism: Biochemistry and physiology of the pentose phosphate pathway. *Biol Rev* 2015; **90**: 927–63.

120 Chen H, Wu D, Bao L, *et al.* 6PGD inhibition sensitizes hepatocellular carcinoma to chemotherapy via AMPK activation and metabolic reprogramming. *Biomed Pharmacother* 2019; **111**: 1353–8.

121 Liu H, Huang D, McArthur DL, Boros LG, Nissen N, Heaney AP. Fructose induces transketolase flux to promote pancreatic cancer growth. *Cancer Res* 2010; **70**: 6368–76.

122 Bravard A, Luccioni C, Muleris M, Lefrancois D, Dutrillaux B. Relationships between UMPK and PGD activities and deletions of chromosome 1p in colorectal cancers. *Cancer Genet Cytogenet* 1991; **56**: 45–56.

123 Zheng W, Feng Q, Liu J, *et al.* Inhibition of 6-phosphogluconate dehydrogenase reverses cisplatin resistance in ovarian and lung cancer. *Front Pharmacol* 2017; **8**. DOI:10.3389/fphar.2017.00421.

124 Giusti L, Iacconi P, Ciregia F, *et al.* Fine-needle aspiration of thyroid nodules: Proteomic analysis to identify cancer biomarkers. *J Proteome Res* 2008; **7**: 4079–88.

125 Bhanot H, Weisberg EL, Reddy MM, *et al.* Acute myeloid leukemia cells require 6-phosphogluconate dehydrogenase for cell growth and NADPH-dependent metabolic reprogramming. *Oncotarget* 2017; **8**: 67639–50.

126 Ge T, Yang J, Zhou S, Wang Y, Li Y, Tong X. The Role of the Pentose Phosphate Pathway in Diabetes and Cancer. Front. Endocrinol. (Lausanne). 2020; **11**. DOI:10.3389/fendo.2020.00365.

127 Mitsuishi Y, Taguchi K, Kawatani Y, *et al.* Nrf2 Redirects Glucose and Glutamine into Anabolic Pathways in Metabolic Reprogramming. *Cancer Cell* 2012; **22**: 66–79.

128 Zhao F, Mancuso A, Bui T V., *et al.* Imatinib resistance associated with BCR-ABL upregulation is dependent on HIF-1α-induced metabolic reprograming. *Oncogene* 2010;

29: 2962–72.

129 Liu R, Li W, Tao B, *et al.* Tyrosine phosphorylation activates 6-phosphogluconate dehydrogenase and promotes tumor growth and radiation resistance. *Nat Commun* 2019; **10**. DOI:10.1038/s41467-019-08921-8.

130 Qin Z, Xiang C, Zhong F, *et al.* Transketolase (TKT) activity and nuclear localization promote hepatocellular carcinoma in a metabolic and a non-metabolic manner. *J Exp Clin Cancer Res* 2019; **38**. DOI:10.1186/s13046-019-1131-1.

131 Shukla SK, Purohit V, Mehla K, *et al.* MUC1 and HIF-1alpha Signaling Crosstalk Induces Anabolic Glucose Metabolism to Impart Gemcitabine Resistance to Pancreatic Cancer. *Cancer Cell* 2017; **32**: 71-87.e7.

132 Bensaad K, Tsuruta A, Selak MA, *et al.* TIGAR, a p53-Inducible Regulator of Glycolysis and Apoptosis. *Cell* 2006; **126**: 107–20.

133 Düvel K, Yecies JL, Menon S, *et al.* Activation of a Metabolic Gene Regulatory Network Downstream of mTOR Complex 1. *Mol Cell* 2010; **39**: 171–83.

134 Xu IMJ, Lai RKH, Lin SH, *et al.* Transketolase counteracts oxidative stress to drive cancer development. *Proc Natl Acad Sci U S A* 2016; **113**: E725–34.

135 Chan B, VanderLaan PA, Sukhatme VP. 6-Phosphogluconate dehydrogenase regulates tumor cell migration in vitro by regulating receptor tyrosine kinase c-Met. *Biochem Biophys Res Commun* 2013; **439**: 247–51.

136 Zhang H, Zhang H, Wang S, Ni Z, Wang T. 1-Hydroxy-8-methoxy-anthraquinon reverses cisplatin resistance by inhibiting 6PGD in cancer cells. *Open Life Sci* 2019; **14**: 454–61.

137 Lin R, Elf S, Shan C, *et al.* 6-Phosphogluconate dehydrogenase links oxidative PPP, lipogenesis and tumour growth by inhibiting LKB1–AMPK signalling. *Nat Cell Biol* 2015; **17**: 1484–96.

138 Gao F, Liu W, Guo Q, Bai Y, Yang H, Chen H. Physcion blocks cell cycle and induces apoptosis in human B cell precursor acute lymphoblastic leukemia cells by downregulating HOXA5. *Biomed Pharmacother* 2017; **94**: 850–7.

139 Budihardjo II, Walker DL, Svingen PA, *et al.* 6-Aminonicotinamide sensitizes human tumor cell lines to cisplatin. *Clin Cancer Res* 1998; **4**.

140 Sukhatme VP, Chan B. Glycolytic cancer cells lacking 6-phosphogluconate dehydrogenase metabolize glucose to induce senescence. *FEBS Lett* 2012; **586**: 2389–95.

141 Daneshmandi S, Cassel T, Lin P, *et al.* Blockade of 6-phosphogluconate dehydrogenase generates CD8+ effector T cells with enhanced anti-tumor function. *Cell Rep* 2021; **34**. DOI:10.1016/j.celrep.2021.108831.

142 Bronte V, Brandau S, Chen SH, *et al.* Recommendations for myeloid-derived

suppressor cell nomenclature and characterization standards. Nat. Commun. 2016; **7**: 1–10.

143 Solinas G, Schiarea S, Liguori M, *et al.* Tumor-Conditioned Macrophages Secrete Migration-Stimulating Factor: A New Marker for M2-Polarization, Influencing Tumor Cell Motility. *J Immunol* 2010; **185**: 642–52.

144 Hesketh M, Sahin KB, West ZE, Murray RZ. Macrophage Phenotypes Regulate Scar Formation and Chronic Wound Healing. *Int J Mol Sci 2017, Vol 18, Page 1545* 2017; **18**: 1545.

145 Woo M-S, Yang J, Beltran C, Cho S. Cell Surface CD36 Protein in Monocyte/Macrophage Contributes to Phagocytosis during the Resolution Phase of Ischemic Stroke in Mice. *J Biol Chem* 2016; **291**: 23654.

146 Kwiecień I, Polubiec-Kownacka M, Dziedzic D, Wołosz D, Rzepecki P, Domagała-Kulawik J. CD163 and CCR7 as markers for macrophage polarization in lung cancer microenvironment. *Cent Eur J Immunol* 2019; **44**: 395–402.

147 Jablonski KA, Amici SA, Webb LM, *et al.* Novel markers to delineate murine M1 and M2 macrophages. *PLoS One* 2015; **10**. DOI:10.1371/journal.pone.0145342.

148 Davidson AJ, Wood W. Macrophages Use Distinct Actin Regulators to Switch Engulfment Strategies and Ensure Phagocytic Plasticity In Vivo. *Cell Rep* 2020; **31**. DOI:10.1016/J.CELREP.2020.107692.

149 DeBerardinis RJ, Chandel NS. Fundamentals of cancer metabolism. *Sci Adv* 2016; **2**: e1600200.

150 Moore KJ, Tabas I. The Cellular Biology of Macrophages in Atherosclerosis. *Cell* 2011; **145**: 341.

151 Moore KJ, Sheedy FJ, Fisher EA. Macrophages in atherosclerosis: a dynamic balance. *Nat Rev Immunol* 2013; **13**: 709.

152 Otero K, Turnbull IR, Poliani PL, *et al.* Macrophage colony-stimulating factor induces the proliferation and survival of macrophages via a pathway involving DAP12 and β-catenin. *Nat Immunol* 2009; **10**: 734–43.

153 Lin CC, Hsiao L Der, Cho RL, Yang CM. Carbon monoxide releasing molecule-2-upregulated ROS-dependent heme oxygenase-1 axis suppresses lipopolysaccharide-induced airway inflammation. *Int J Mol Sci* 2019; **20**. DOI:10.3390/ijms20133157.

154 Uddin MJ, Joe Y, Kim SK, *et al.* IRG1 induced by heme oxygenase-1/carbon monoxide inhibits LPS-mediated sepsis and pro-inflammatory cytokine production. *Cell Mol Immunol* 2016; **13**: 170–9.

155 Fleetwood AJ, Lawrence T, Hamilton JA, Cook AD. Granulocyte-Macrophage Colony-Stimulating Factor (CSF) and Macrophage CSF-Dependent Macrophage Phenotypes Display Differences in Cytokine Profiles and Transcription Factor Activities: Implications

for CSF Blockade in Inflammation. *J Immunol* 2007; **178**: 5245–52.

156 Foucher ED, Blanchard S, Preisser L, *et al.* IL-34 Induces the Differentiation of Human Monocytes into Immunosuppressive Macrophages. Antagonistic Effects of GM-CSF and IFNγ. *PLoS One* 2013; **8**. DOI:10.1371/journal.pone.0056045.

157 Poh AR, Love CG, Masson F, *et al.* Inhibition of Hematopoietic Cell Kinase Activity Suppresses Myeloid Cell-Mediated Colon Cancer Progression. *Cancer Cell* 2017; **31**: 563-575.e5.

158 Dwyer AR, Mouchemore KA, Steer JH, *et al.* Src family kinase expression and subcellular localization in macrophages: implications for their role in CSF-1-induced macrophage migration. *J Leukoc Biol* 2016; **100**: 163–75.

159 Cai T-T, Ye S-B, Liu Y-N, *et al.* LMP1-mediated glycolysis induces myeloid-derived suppressor cell expansion in nasopharyngeal carcinoma. *PLoS Pathog* 2017; **13**: e1006503.

160 Stanley ER, Chitu V. CSF-1 receptor signaling in myeloid cells. Cold Spring Harb. Perspect. Biol. 2014; **6**. DOI:10.1101/cshperspect.a021857.

161 Poh AR, O'Donoghue RJJ, Ernst M. Hematopoietic cell kinase (HCK) as a therapeutic target in immune and cancer cells. Oncotarget. 2015; **6**: 15752–71.

162 Rojo R, Pridans C, Langlais D, Hume DA. Transcriptional mechanisms that control expression of the macrophage colony-stimulating factor receptor locus. Clin. Sci. 2017; **131**: 2161–82.

163 Novak U, Harpur AG, Paradiso L, *et al.* Colony-stimulating factor 1-induced STAT1 and STAT3 activation is accompanied by phosphorylation of Tyk2 in macrophages and Tyk2 and JAK1 in fibroblasts. *Blood* 1995; **86**: 2948–56.

164 Sauter KA, Pridans C, Sehgal A, *et al.* Pleiotropic effects of extended blockade of CSF1R signaling in adult mice. *J Leukoc Biol* 2014; **96**: 265–74.

165 Cannarile MA, Weisser M, Jacob W, Jegg AM, Ries CH, Rüttinger D. Colony-stimulating factor 1 receptor (CSF1R) inhibitors in cancer therapy. J. Immunother. Cancer. 2017; **5**. DOI:10.1186/s40425-017-0257-y.

166 Lazarowski ER, Harden TK. UDP-sugars as extracellular signaling molecules: Cellular and physiologic consequences of P2Y14 receptor activation. Mol. Pharmacol. 2015; **88**: 151–60.

167 O'Neill LAJ, Artyomov MN. Itaconate: the poster child of metabolic reprogramming in macrophage function. Nat. Rev. Immunol. 2019; **19**: 273–81.

168 Sakai A, Kusumoto A, Kiso Y, Furuya E. Itaconate reduces visceral fat by inhibiting fructose 2,6-bisphosphate synthesis in rat liver. *Nutrition* 2004; **20**: 997–1002.

169 Lampropoulou V, Sergushichev A, Bambouskova M, *et al.* Itaconate Links Inhibition of Succinate Dehydrogenase with Macrophage Metabolic Remodeling and Regulation of

Inflammation. *Cell Metab* 2016; **24**: 158–66.

170 Mills EL, Ryan DG, Prag HA, *et al.* Itaconate is an anti-inflammatory metabolite that activates Nrf2 via alkylation of KEAP1. *Nature* 2018; **556**: 113–7.

171 Weiss JM, Davies LC, Karwan M, *et al.* Itaconic acid mediates crosstalk between macrophage metabolism and peritoneal tumors. *J Clin Invest* 2018; **128**: 3794–805.

172 Kobayashi EH, Suzuki T, Funayama R, *et al.* Nrf2 suppresses macrophage inflammatory response by blocking proinflammatory cytokine transcription. *Nat Commun* 2016; **7**. DOI:10.1038/NCOMMS11624.

173 Freigang S, Ampenberger F, Spohn G, *et al.* Nrf2 is essential for cholesterol crystal-induced inflammasome activation and exacerbation of atherosclerosis. *Eur J Immunol* 2011; **41**: 2040–51.

174 Wu WL, Papagiannakopoulos T. The Pleiotropic Role of the KEAP1/NRF2 Pathway in Cancer. *Annu Rev Cancer Biol* 2020; **4**: 413–35.

175 Garcia-Diaz A, Shin DS, Moreno BH, *et al.* Interferon Receptor Signaling Pathways Regulating PD-L1 and PD-L2 Expression. *Cell Rep* 2017; **19**: 1189–201.

176 Liu Y, Huang Z, Wei Y, *et al.* Identification of STXBP6-IRF1 positive feedback loop in regulation of PD-L1 in cancer. *Cancer Immunol Immunother* 2021; **70**: 275–87.

177 Nath N, Kashfi K. Tumor associated macrophages and 'NO'. Biochem. Pharmacol. 2020; **176**. DOI:10.1016/j.bcp.2020.113899.

178 Scrivens M, Dickenson JM. Functional expression of the P2Y 14 receptor in murine T-lymphocytes. *Br J Pharmacol* 2005; **146**: 435–44.

179 Van Ginderachter JA, Movahedi K, Hassanzadeh Ghassabeh G, *et al.* Classical and alternative activation of mononuclear phagocytes: Picking the best of both worlds for tumor promotion. *Immunobiology* 2006; **211**: 487–501.

180 Zenke K, Muroi M, Tanamoto K ichi. IRF1 supports DNA binding of STAT1 by promoting its phosphorylation. *Immunol Cell Biol* 2018; **96**: 1095–103.

181 Elf S, Lin R, Xia S, *et al.* Targeting 6-phosphogluconate dehydrogenase in the oxidative PPP sensitizes leukemia cells to antimalarial agent dihydroartemisinin. *Oncogene* 2017; **36**: 254–62.

182 Garcia AA, Koperniku A, Ferreira JCB, Mochly-Rosen D. Treatment strategies for glucose-6-phosphate dehydrogenase deficiency: past and future perspectives. *Trends Pharmacol Sci* 2021; **42**: 829–44.

183 Luzzatto L, Ally M, Notaro R. Glucose-6-phosphate dehydrogenase deficiency. *Blood* 2020; **136**: 1225–40.

7. APPENDIX

7.1 List of figures

7.2 List of supplemental figures

7.3 List of tables

7.4 List of supplemental tables

Online availability of supplemental figures: https://www.sciencedirect.com/science/article/pii/S2666379124006013?via%3Dihub#appsec2 (assessed 11.12.2024)[3]

8. PRIOR PRINTED PUBLICATION OF RESULTS

1 Beielstein AC, Izquierdo E, Blakemore S, *et al.* Macrophages are activated toward phagocytic lymphoma cell clearance by pentose phosphate pathway inhibition. *Cell reports Med* 2024; : 101830.